

**UNIVERSIDADE FEDERAL DE MINAS GERAIS
ESCOLA DE ENGENHARIA
PROGRAMA DE PÓS-GRADUAÇÃO EM ENGENHARIA QUÍMICA**

RICARDO ADRIANO DORLEDO DE FARIA

**DEVELOPMENT OF IMPEDIMETRIC SENSORS AND BIOSENSORS BASED ON
SCREEN-PRINTED CARBON ELECTRODES FOR DETECTION OF ANALYTES
OF MEDICAL, ENVIRONMENTAL AND INDUSTRIAL INTERESTS**

**BELO HORIZONTE - MG
2020**

RICARDO ADRIANO DORLEDO DE FARIA

**DEVELOPMENT OF IMPEDIMETRIC SENSORS AND BIOSENSORS BASED ON
SCREEN-PRINTED CARBON ELECTRODES FOR DETECTION OF ANALYTES
OF MEDICAL, ENVIRONMENTAL AND INDUSTRIAL INTERESTS**

Thesis presented to the Department of
Chemical Engineering of the Engineering
School of Universidade Federal de Minas
Gerais as a partial requirement to obtain the
Doctorate Degree in Chemical Engineering.
Research field: Green technologies,
materials and nanotechnology

Advisor: Tulio Matencio

Co-advisor: Luiz Guilherme Dias Heneine

BELO HORIZONTE – MG
2020

F224d	<p>Faria, Ricardo Adriano Dorledo de. Development of impedimetric sensors and biosensors based on screen-printed carbon electrodes for detection of analytes of medical, environmental and industrial interests [recurso eletrônico] / Ricardo Adriano Dorledo de Faria. - 2020. 1 recurso online (xxii, 164f. : il., color.) : pdf.</p> <p>Orientador: Tulio Matencio. Coorientador: Luiz Guilherme Dias Heneine.</p> <p>Tese (doutorado) - Universidade Federal de Minas Gerais, Escola de Engenharia.</p> <p>Inclui bibliografia.</p> <p>Exigências do sistema: Adobe Acrobat Reader.</p> <p>1. Engenharia química - Teses. 2. Cobra venenosa – Venenos - Teses. 3. Glicose - Teses. 4. Alimentos – Adulteração e inspeção - Teses. 5. Biosensores – Teses. 6. Espectroscopia de impedância – Teses. I. Matencio, Tulio. II. Heneine, Luiz Guilherme Dias. III. Universidade Federal de Minas Gerais. Escola de Engenharia. IV. Título.</p>
	CDU: 66.0(043)


UNIVERSIDADE FEDERAL DE MINAS GERAIS
 ESCOLA DE ENGENHARIA
 PROGRAMA DE PÓS-GRADUAÇÃO EM ENGENHARIA QUÍMICA

“Development of impedimetric sensors and biosensors based on screen-printed carbon electrodes for detection of analytes of medical, environmental and industrial interests”

Ricardo Adriano Dorledo de Faria

Tese submetida à Banca Examinadora designada pelo Colegiado do Programa de Pós-Graduação em Engenharia Química da Escola de Engenharia da Universidade Federal de Minas Gerais, como parte dos requisitos à obtenção do título de **DOUTOR EM ENGENHARIA QUÍMICA**.

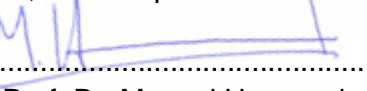
46ª TESE APROVADA EM 3 DE ABRIL DE 2020 POR:



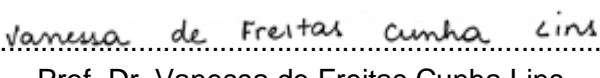
 Prof. Dr. Alan Rodrigues Teixeira Machado
 Universidade do Estado de Minas Gerais (UEMG)



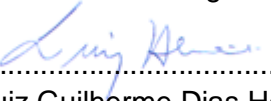
 Dr. Younès Messaddeq
 Centre d'Optique, Photonique et Laser / Université Laval




 Prof. Dr. Manuel Houmard
 Department of Materials and Construction Engineering/ UFMG



 Prof. Dr. Vanessa de Freitas Cunha Lins
 Department of Chemical Engineering / UFMG



 Dr. Luiz Guilherme Dias Heneine
 Co-advisor – Head of Immunology Laboratory / Fundação Ezequiel Dias (FUNED)



 Prof. Dr. Tulio Matencio
 Advisor – Department of Chemical Engineering/ UFMG

ACKNOWLEDGMENTS

I have much to thank many people who played important roles in my personal and professional life during these years as a PhD student. First and foremost, I reiterate in this document my gratitude to God, the only one who was with me all the time. My Father and Lord who, independent of my sins, faults and miseries blessed my thoughts and provided everything and more that I needed to succeed in this journey. To God all praise and glory.

To my advisor professor Dr. Tulio Matencio for the opportunity to learn more in the field of Electrochemistry, for the insightful comments, for the confidence in my work and for always being such a tender figure, respecting my opinions and teaching me with impressive patience.

To my co-advisor Dr. Luiz Heneine for all the support throughout my research besides all these ten years of scientific collaboration. I am also thankful because you believed in my capabilities and invested knowledge and expectations in my formation.

I acknowledge professor Dr. Vanessa Lins for the opportunity to work in the Laboratory of Corrosion and Surface Engineering, which was essential to perform many electrochemical tests and to learn more on the topic of Corrosion. Moreover, I have always felt welcomed and supported by your generous sharing of enormous knowledge.

I am also profoundly grateful to Dr. Younès Messaddeq for the amazing opportunity to have worked in the *Centre d'Optique Photonique et Laser* (COPL) during my research internship in Canada. This experience was not just extremely important to obtain the major portion of the results presented in my thesis, but it also represented an important possibility of personal growth. At COPL, I could improve my language skills, I had the possibility to communicate my science, the opportunity to contribute to other projects and I knew many special people. In light of this context, I would like to offer my special thanks to Dr. Hassan Iden, with whom I worked for months in many researches, to the kind assistance of Michelle Bernier and to the researchers Julie Fréchette, Mourad Roudjane, Yannick Ledemi and Sandra Messaddeq. I extend my sincerest regards to my colleagues Salah, Simon, Alice,

Antisar, Alexandre, Geoffrey, Marie, Long, Olivier and Brice for the special support during my internship year. For all this and more, I would like to express my deep gratitude to professor Younès and to register that you represent now an important reference to my life, since you are not “just” a highlighted professional, but also a very sensible human who is gently attentive even to our interior issues.

Far from my family and long-time friends, I was never unassisted in Quebec and this is the reason for which I am especially grateful to my Canadian family. To my special friends Ismail Ben Amar, Rafaela Lamarca, Douglas Franco, Asma Ben Saad and Camila Ferreira, my sincerest thanks for the wonderful moments we passed together, and for all the aid that you provided me during this period. You were my safe harbor in the middle of the difficulties and I feel deeply proud to call you friends.

Professors Alan Rodrigues Teixeira Machado and Manuel Houmard, please receive my honest acknowledgments not exclusively for accepting my invitation to be members of this jury but especially for representing professional inspiration for me, the main reason for which I chose you for this moment.

At UFMG, my grateful thanks are also extended to Fernanda Abreu, who is a particular professional inspiration for being always very gentle and competent in assisting our needs at the departmental secretary. To my friends of the Department of Chemical Engineering, Renata, Marcelo, Enil, Débora, Daniel and Daniela for all the great moments we shared at and outside the university.

A special thanks goes to my parents for the prayers, their love, for showing me the benefits of hard working and for the sacrifices invested in my formation. Herein, I would like to offer back my infinite gratitude not only in the form of this thesis but mainly in the form of the person I became due to the opportunity of education. It is extended to all my family for the constant encouragement and for always celebrating my achievements with me.

Finally, I would like to thank the *Coordenação de Aperfeiçoamento de Pessoal de Nível Superior* (CAPES), the Natural Sciences and Engineering Research Council of Canada (CRSNG), the Canada Excellence Research Chair in Photonics Innovations (CERCP) and the Canadian Funding for Infrastructure (CFI) for the financial support that I received to develop my researches in Brazil and in Canada.

I dedicate this thesis to my nephews Caio and Maria Laura as well as to my godchildren Thiago and Bárbara as a sign of my real belief in the importance of education in our lives. I hope you all never forget to keep Science in your hearts as one of the seven gifts of the Holy Spirit and one of the most important tools to build a dignified and more egalitarian society.

"Je suis de ceux qui pensent que la science est d'une grande beauté. Un scientifique dans son laboratoire est non seulement un technicien, il est aussi un enfant placé devant des phénomènes naturels qui l'impressionnent comme des contes de fées".

- Marie Curie

RESUMO

O advento da tecnologia de sensores para várias aplicações tem contribuído para a qualidade da vida humana especialmente por prover respostas sensíveis, seletivas e rápidas. Contrariamente, as técnicas analíticas tradicionais ainda enfrentam algumas barreiras principalmente ligadas ao alto custo, não-portabilidade e longos tempos de resposta. Nesse contexto, a presente tese traz os principais aspectos de sensores e biossensores para aplicação na área médica, na indústria alimentícia e no monitoramento ambiental, todos baseados na Espectroscopia de Impedância Eletroquímica (EIE). Devido às suas propriedades eletroquímicas, à facilidade de funcionalização, ao baixo custo e à empregabilidade em sistemas miniaturizados, eletrodos impressos de carbono (EICs) serviram como transdutores em (bios)sensores para o reconhecimento de carne de cavalo, glicose e dimetil sulfeto (DMS). O imunossensor composto por EICs e imunoglobulina G de cavalo foi capaz de detectar seletivamente carne de cavalo em baixas concentrações, com um limite de detecção (LD) igual a 0,004%*m/v*, corroborando sua promissora aplicação como ferramenta para identificação de adulteração de produtos cárneos crus por carne de cavalo. O sensor de glicose contendo ácido 3-aminofenil borônico como unidade de reconhecimento não detectou outros açúcares nem mesmo sofreu influência significativa de interferentes. Pelo contrário, o dispositivo impedimétrico apresentou um LD igual a $8,53 \times 10^{-9}$ M sob tempo de resposta otimizado de $4,0 \pm 0,6$ s. Em apenas três minutos, o sensor de DMS detectou o analito com LD igual a $1,50 \times 10^{-9}$ M e apresentou crescente resposta em tempo real diante do analito diluído em solução simulada de água do mar. Em comum, os (bios)sensores desenvolvidos apresentaram LDs e tempos de resposta condizentes com as aplicações reais.

Palavras-chave: Sensor; biossensor; Espectroscopia de Impedância Eletroquímica; veneno de cobra; fraude alimentar; glicose; dimetil sulfeto

ABSTRACT

The advent of sensing technologies for various applications has increased the quality of human life especially for providing sensitive, selective and fast responses. Contrary, traditional analytical assays still face some shortcomings mainly related to high cost, non-portability and lengthy response time. In this context, the present thesis brings the main aspects of sensors and biosensors for application in the medical field, food industry and environmental monitoring, all of them based on the Electrochemical Impedance Spectroscopy (EIS). Due to their electrochemical properties, easiness of modification, low cost and employability in miniaturized systems, screen-printed carbon electrodes (SPCEs) served as transducers in (bio)sensors devoted to recognize horsemeat for meat authentication, glucose and dymethyl sulfide (DMS). The SPCE-based immunosensor containing horse immunoglobulin G was capable to selectively detect horsemeat at low concentrations, within a limit of detection (LOD) equal to 0.004%w/v, corroborating its promising application as a tool for screening horse adulteration in raw meat products. The glucose sensor consisting of 3-aminophenylboronic acid as unit of recognition did not detect other sugars nor suffered significant influence of interfering species. Instead, the impedimetric device exhibited a LOD equal to 8.53×10^{-9} M under an optimized response time of 4.0 ± 0.6 s. In only three minutes, the DMS sensor detected the analyte at a LOD equal to 1.50×10^{-9} M and provided increasing real-time response towards the target molecule diluted in simulated ocean water. In common, the developed (bio)sensors presented LODs and response times consistent with the real application.

Keywords: Sensor; biosensor; Electrochemical Impedance Spectroscopy; snake venom; food fraud; glucose; dymethyl sulfide

LIST OF FIGURES

Figure 1 – SEM images of the SPCE before (a) and after (b) the activation of the surface using H ₂ SO ₄	53
Figure 2 - Raman spectra of the SPCE sample in the range of 830 - 1900 cm ⁻¹ and their respective deconvolution curves for (a) the bright structures, and (b) the dark structures.....	54
Figure 3 - Raman spectra of the SPCE sample in the range of 2400 - 3100 cm ⁻¹ and their respective deconvolution curves for (a) the bright structures, and (b) the dark structures.....	55
Figure 4 - Topographic image from AFM conductive test referring to the distribution of electrical current over the surface of the SPCE	56
Figure 5 - Cyclic voltammogram of the SPCE immersed in KCl and redox solutions under a potential ranging from -1.0 to 1.0 V vs Ag/AgCl at 50 mV.s ⁻¹	57
Figure 6 - OCP variation as a function of time with respect to the SPCE immersed in KCl and redox solutions.....	59
Figure 7 - Equivalent circuits used to fit EIS data and respective Bode plots referring to the SPCE obtained in KCl (a) and redox solutions (b).....	60
Figure 8 - Polarization plots of the SPCE in KCl and redox solutions.....	62
Figure 9 - Chronoamperometry plots of the SPCEs polarized in KCl and redox solutions. The inset is an amplification of the graphic up to 3.0 μA.cm ⁻²	64
Figure 10 - Evolution of the number of citations of articles containing “food fraud” as a keyword according to the Web of Science database (from 1945 to 2018).....	75
Figure 11 - Influence of the temperature, valence of the target ion and the variation of its activity on the expected potential and sensitivity of potentiometric sensors.....	77
Figure 12 - Cyclic voltammogram of the stepwise functionalization of SPCE to develop the horsemeat biosensor obtained at a scan rate of 50 mV.s ⁻¹ in 0.1 M KCl (pH 7.4).....	93 93 93
Figure 13 - SEM image of the SPCE before (a) and after (b) acid treatment using CV.....	94 94
Figure 14 - EDX spectrum of the SPCE before and after the acid treatment..... using CV. The inset shows the spectrum in the lower energy region (up to	94 94

0.35 keV).....	94
Figure 15 - SEM images of the treated SPCE modified by the deposition of PANI (a), glutaraldehyde (b), anti-horse IgG (c) and casein (d).....	95
Figure 16 - Nyquist plot of the immunosensor before and after the exposure to horse serum at various concentrations in PBS buffer.....	96
Figure 17 - Bode diagram of both experimental and K-K transform plots of the horsemeat biosensor.....	98
Figure 18 - Calibration curve of the immunosensor exposed to horse, swine and bovine serum at various concentrations in PBS buffer.....	99
Figure 19 - Calibration curve of the immunosensor exposed to horsemeat, pork.... and beef solutions diluted 1,000; 10,000 and 100,000 times.....	100
Figure 20 - Functionalization steps to obtain the glucose sensor.....	113
Figure 21 - SEM images of the SPCE before (a) and after (b) functionalization with 3-aminophenylboronic acid and (c) inclined view of the functionalized electrode.....	115
Figure 22 - Impedimetric monitoring of the SPCE before and after functionalization with 3-aminophenylboronic acid.....	116
Figure 23 - Cyclic voltammograms related to the bare (a) and functionalized (b) SPCE under different scan rates (0.1, 0.075, 0.05, 0.02 and 0.01 mV.s ⁻¹) in 0.1 M KCl + 5 mM Fe(CN) ₆ ^{3-/4-} and (c) the relationship between the anodic/cathodic current peaks of the redox species at the electrodes and the square root of corresponding scan rates.....	118
Figure 24 - Nyquist plot of the glucose sensor exposed to the target analyte at various concentrations.....	119
Figure 25 - Scheme of the binding process between the boronic acid immobilized on the SPCE surface and the D-glucose molecule.....	119
Figure 26 - Variation of the charge transfer resistance (ΔR_{ct}) of the glucose sensor exposed to glucose, fructose and sucrose at various concentrations.....	120
Figure 27 - Relative residual errors referring to the impedance of the glucose sensor during 100 consecutive measurements.....	124
Figure 28 - Variation of the R_{ct} of the sensor in function of the period of storage	125

- Figure 29 - Relationship between the time to record $|Z|$, Z' and Z'' at 1000, 100, 10, 1 and 0.1 Hz and the respective correlation coefficient of these impedance parameters and the glucose concentration..... 126
- Figure 30 - Scheme of the relationship among the time response and the impedance parameters as a function of the frequency in the Nyquist plot (a) as a consequence of the interfacial phenomena occurring between the SPCE and the electrolyte (b). In the illustration, the yellow spheres with the signal “+” correspond to the cations solvated by the molecules from the bulk solution (blue spheres) and the signal “-” on the different regions of the SPCE corresponds to the electrons electrostatically attracted toward the interfaces 127
- Figure 31 - Variation of the R_{ct} of the glucose sensor in function of the interference of bovine serum, 0.02 M dopamine and 0.1 M NaCl in the absence and presence of glucose at 10^{-8} M..... 128
- Figure 32 - Scheme of the procedure for the functionalization of SPCE with gold particles (a) and photograph of the finished sensor in the electrochemical cell (b) .139
- Figure 33 - SEM images of the SPCE before (a) and (b) after the deposition of gold and (c) the correspondent EDX spectrum of the clusters of gold on the graphitic flakes..... 142
- Figure 34 - Nyquist plots of the sensor after incubation for 3 min in aqueous solutions of DMS at various concentrations. The inset is the Randles equivalent circuit used to fit the EIS data..... 144
- Figure 35 - Exposition of the gold transducer particles on the SPCE surface before and after the incubation in DMS solutions hindering the electron transfer processes between the Fe^{III} and Fe^{II} ions..... 144
- Figure 36 - Polynomial dependence between the ΔR_{ct} and the concentration of the aqueous DMS solution 145
- Figure 37 - Cyclic voltammogram (a) and Nyquist plot (b) of the bare, regenerated and contaminated sensor with an aqueous solution of DMS at 10^{-8} M..... 149
- Figure 38 - Evolution of the OCP (a), R_e (b) and R_p (c) of the sensor due to the exposure to DMS from 1.0×10^{-11} M to 1.0×10^{-8} M in simulated ocean water 151

LIST OF TABLES

Table 1 - Recent applications of SPCE as electrochemical transducer in biosensors	43
Table 2 - Parameters estimated from the method of potentiodynamic anodic polarization with respect to the SPCE in KCl and redox solutions.....	62
Table 3 - R ² value related to the logarithm fit of the correlation between ΔR_{ct} and concentration of horse, swine and bovine serum diluted in PBS buffer	100
Table 4 - Comparison of the performance of various enzymatic and non-enzymatic glucose sensors with the sensor based on SPCE containing 3-aminophenylboronic acid.....	122
Table 5 - Chemical composition of the artificial solution of ocean water.....	140
Table 6 - LOD of DMS sensors reported in the literature employing various transduction modes	147
Table 7 - Values of E_{pa} , E_{pc} and ΔE_p related to the sensor before and after the exposure to DMS as well as after the regeneration step by CV in 0.05 M H ₂ SO ₄ ...	150

LIST OF ABBREVIATIONS

AC	Alternating current
AFM	Atomic Force Microscopy
BSA	Bovine serum albumin
cAFM	Conductive Atomic Force Microscopy
CPE	Constant Phase Element
CV	Cyclic Voltammetry
DMS	Dimethyl sulfide
DMSP	Dimethyl Sulfopropionate
DC	Direct current
EIS	Electrochemical Impedance Spectroscopy
EIC	Eletrodos impressos de carbono
EDX	Energy Dispersive X-ray Spectroscopy
ELISA	Enzyme-Linked Immunosorbent Assay
FTIR	Fourier Transform Infrared Spectroscopy
GOx	Glucose oxidase
GMA	Grocery Manufacturers Association
IgG	Immunoglobulin G
JEV	Japanese encephalitis virus
K-K	Kramers-Kronig
LOD	Limit of detection
LOQ	Limit of quantification
NP	Nanoparticle
NADH	Nicotinamide-adenine-dinucleotide reduced
OCP	Open Circuit Potential
PBS	Phosphate Buffered Saline
PANI	Polyaniline
SEM	Scanning Electron Microscopy
SPCE	Screen-printed carbon electrode
SPE	Screen-printed electrode
UV-Vis	Ultraviolet-visible Spectroscopy

VOSC Volatile Organic Sulfur Compound

WHO World Health Organization

LIST OF SYMBOLS

a_i	Activity of chemical species	[-]
ω	Angular frequency	[rad]
I_{pa}	Anodic current peak	[A]
Ra	Average roughness	[μm]
\bar{x}_{bl}	Average signal of blank measurements	[$\Omega\cdot\text{cm}^2$]
SD_{bl}	Blank standard deviation	[-]
I_{pc}	Cathodic current peak	[A]
R_{ct}	Charge transfer resistance	[$\Omega\cdot\text{cm}^2$]
χ^2	Chi-squared	[-]
C_r	Concentration of the redox species	[M]
i_{corr}	Corrosion current	[A]
j_{corr}	Corrosion current density	[$\text{A}\cdot\text{cm}^{-2}$]
E_{corr}	Corrosion potential	[V]
Q	CPE capacitance	[$\text{s}^n\cdot\Omega^{-1}$]
Z_{CPE}	CPE impedance	[$\Omega\cdot\text{cm}^2\cdot\text{s}^{-n}$]
i	Current	[A]
D_{ox}	Diffusion coefficient of the oxidized specie	[$\text{m}^2\cdot\text{s}^{-1}$]
D_{red}	Diffusion coefficient of the reduced specie	[$\text{m}^2\cdot\text{s}^{-1}$]
d	Distance	[cm]
C	Double-layer capacitance	[$\text{F}\cdot\text{cm}^2$]
R_e	Electrolyte resistance	[$\Omega\cdot\text{cm}^2$]
E_{ef}	Electromotive force	[V]
Z_e	Electron charge	[C]
F	Faraday constant	[$\text{s}\cdot\text{A}\cdot\text{mol}^{-1}$]
j_i	Flux of electroactive molecules	[$\text{mol}\cdot\text{cm}^{-2}\cdot\text{s}^{-1}$]
ϵ_0	Free space permittivity	[$\text{F}\cdot\text{m}^{-1}$]
f	Frequency	[Hz]
R	Gas constant	[$\text{J}\cdot\text{mol}^{-1}\cdot\text{K}^{-1}$]
S_{horse}	Horse serum concentration	[M]
Z'	Imaginary impedance	[$\Omega\cdot\text{cm}^2$]
j	Imaginary number	[-]

Z	Impedance	[$\Omega \cdot \text{cm}^{-2}$]
L	Inductance	[$\text{H} \cdot \text{cm}^2$]
C_{ox}^0	Initial concentration of oxidized species	[M]
C_{red}^0	Initial concentration of reduced species	[M]
Z_i	Ion valence	[-]
$ Z $	Magnitude of impedance	[$\Omega \cdot \text{cm}^{-2}$]
n	Number of electrons	[-]
ν^*	Overall reaction rate	[$\text{M} \cdot \text{s}^{-1}$]
ΔE_p	Peak-to-peak separation	[V]
ϕ	Phase angle	[$^\circ$]
E	Potential	[V]
E_{pa}	Potential of the anodic peak	[V]
E_{pc}	Potential of the cathodic peak	[V]
p	p-value	[-]
ν_{\leftarrow}^*	Reaction rate in the backward direction	[$\text{M} \cdot \text{s}^{-1}$]
ν_{\rightarrow}^*	Reaction rate in the forward direction	[$\text{M} \cdot \text{s}^{-1}$]
Z''	Real impedance	[$\Omega \cdot \text{cm}^{-2}$]
R^2	Regression coefficient	[-]
ϵ_r	Relative solution permittivity	[-]
τ	Response time	[s]
ν	Scan rate	[$\text{V} \cdot \text{s}^{-1}$]
S	Sensor's sensitivity	[$\Omega \cdot \text{cm}^2 \cdot \text{M}^{-1}$]
x_L	Signal of the sensor exposed to the analyte	[$\Omega \cdot \text{cm}^2$]
SD	Standard deviation	[-]
E_0^*	Standard potential of an electrode	[V]
k	Statistical factor	[-]
A	Surface area	[m^2]
T	Temperature	[K]
t	Time	[s]
$\sigma_{R_{ct}}$	Residual R_{ct} error	[%]

σ_w	Warburg coefficient	[$\Omega \cdot s^{-1/2}$]
Z_W	Warburg impedance	[$\Omega \cdot s^{-1/2} \cdot \text{rad}^{-1/2}$]

SUMÁRIO

CHAPTER 1 - INTRODUCTION	24
1.1 GENERAL ASPECTS OF SENSORS.....	24
1.2 OBJECTIVES.....	27
1.2.1 General objectives.....	27
1.2.2 Specific objectives	27
1.3 THESIS STRUCTURE	29
1.4 REFERENCES.....	30
CHAPTER 2 – FARADAIC AND NON-FARADAIC ELECTROCHEMICAL IMPEDANCE SPECTROSCOPY AS TRANSDUCTION TECHNIQUES FOR SENSING APPLICATIONS.....	34
2.1 ABSTRACT.....	34
2.2 INTRODUCTION.....	35
2.3 EIS THEORY	35
2.4 FARADAIC SENSORS.....	37
2.5 NON-FARADAIC SENSORS.....	38
2.6 CONCLUSION	38
2.7 REFERENCES.....	39
CHAPTER 3 - APPLICATION OF SCREEN-PRINTED CARBON ELECTRODE AS AN ELECTROCHEMICAL TRANSDUCER IN BIOSENSORS	41
3.1 ABSTRACT.....	41
3.2 INTRODUCTION.....	41
3.3 FABRICATION.....	42
3.4 PRE-TREATMENT.....	42
3.5 APPLICATIONS IN ELECTROCHEMICAL BIOSENSING.....	43
3.6 CONCLUSION	43
3.7 REFERENCES.....	44
CHAPTER 4 - ELECTROCHEMICAL BEHAVIOR OF SCREEN-PRINTED CARBON ELECTRODES AS TRANSDUCERS IN BIOSENSORS	46
4.1 ABSTRACT.....	46
4.2 INTRODUCTION.....	47
4.3 MATERIALS AND METHODS.....	49
4.3.1 Chemicals	49
4.3.2 Apparatus.....	50
4.3.3 Test solutions	50

4.3.4 Characterization of the SPCE	50
4.3.5 Electrochemical tests	51
4.4 RESULTS AND DISCUSSION	52
4.4.1 Chemical and morphological characterization of the SPCEs	52
4.4.2 Electrochemical characterization	55
4.4.3 Corrosion tests	62
4.5 CONCLUSIONS.....	64
4.6 REFERENCES.....	65
CHAPTER 5 - RECENT TRENDS IN THE ELECTROANALYTICAL DETECTION OF FOOD FRAUD	73
5.1 ABSTRACT.....	73
5.2 INTRODUCTION.....	74
5.3 POTENTIOMETRIC SENSORS	76
5.4 AMPEROMETRIC SENSORS.....	78
5.5 IMPEDIMETRIC SENSORS.....	80
5.6 CONCLUSION	81
5.7 REFERENCES.....	82
CHAPTER 6 - A NEW TOOL FOR THE DETECTION OF HORSEMEAT ADULTERATION IN RAW MEAT	86
6.1 ABSTRACT.....	86
6.2 INTRODUCTION.....	87
6.3 MATERIALS AND METHODS.....	88
6.3.1 Apparatus and chemicals	88
6.3.2 Functionalization of the SPCEs for recognition of horse IgG	89
6.3.3 Characterization of the biosensor	90
6.3.4 Electrochemical sensing of horse IgG	90
6.4 RESULTS AND DISCUSSION	91
6.4.1 Characterization of the immunosensor by CV	91
6.4.2 Characterization of the immunosensor by SEM-EDX	93
6.4.3 Immunosensor padronization: horse serum IgG detection	96
6.4.4 Validation of impedance data by Kramer's-Kronig transform	97
6.4.5 Analysis of the sensitivity and selectivity of the biosensor towards horse serum in buffer solution	98
6.4.6 Analysis of commercial meat samples	100
6.4.7 Limit of detection (LOD) of the proposed immunosensor	101

6.5 CONCLUSIONS.....	102
6.6 REFERENCES.....	103
CHAPTER 7 – NON-ENZYMATIC IMPEDIMETRIC SENSOR BASED ON 3-AMINOPHENYLBORONIC ACID FUNCTIONALIZED SCREEN-PRINTED CARBON ELECTRODE FOR HIGHLY SENSITIVE GLUCOSE DETECTION	109
7.1 ABSTRACT.....	109
7.2 INTRODUCTION.....	110
7.3 MATERIALS AND METHODS.....	112
7.3.1 Materials and chemicals	112
7.3.2. Instrumentation and apparatus	113
7.3.3. Functionalization and characterization of the SPCE	113
7.3.4. Selective detection of glucose by EIS	114
7.3.5. Evaluation of the sensor’s stability	114
7.4 RESULTS AND DISCUSSION	115
7.4.1. Characterization of the functionalized SPCE	115
7.4.2 Detection of glucose in aqueous solution by EIS.....	118
7.4.3 Repeatability and reproducibility analysis	123
7.4.4. Response time	125
7.4.5 Investigation of the effect of dopamine, NaCl and serum on the performance of the glucose sensor.....	127
7.5 CONCLUSIONS.....	129
7.6 REFERENCES.....	130
CHAPTER 8 - A NOVEL IMPEDIMETRIC SENSOR FOR TRACE LEVEL DETECTION OF DIMETHYL SULFIDE (DMS).....	135
8.1 ABSTRACT.....	135
8.2 INTRODUCTION.....	136
8.3 MATERIALS AND METHODS.....	137
8.3.1 Apparatus and chemicals	137
8.3.2 Functionalization of the SPCE with gold particles	138
8.3.3 EIS as a transduction technique for DMS sensing	139
8.3.4 Electrochemical regeneration of the sensor	141
8.4 RESULTS AND DISCUSSION	141
8.4.1 Morphological and chemical characterization of the Au-modified electrode.....	141
8.4.2 Electrochemical detection of DMS.....	142

8.4.3 Reusability of the sensor	148
8.4.4 DMS sensing in artificial ocean water	150
8.5 CONCLUSIONS.....	152
8.6 REFERENCES.....	152
CHAPTER 9 – GENERAL CONCLUSIONS AND FUTURE PERSPECTIVES.....	159
9.1 THESIS FINDINGS AND SUGGESTIONS FOR FUTURE WORKS	159
9.2 RESULTADOS DA TESE E SUGESTÕES PARA TRABALHOS FUTUROS.....	162

CHAPTER 1 - INTRODUCTION

1.1 GENERAL ASPECTS OF SENSORS

According to the International Union of Pure and Applied Chemistry (IUPAC), a sensor is a device capable to convert an input signal related to the presence of a target analyte into a measurable output signal [1]. Typically, the foremost concept associated to the word “sensor” is that of our human senses, by which the organism receive an external stimulus, processes this data in the brain as neurological impulses and respond with an output signal referring to an information of sound, image, taste, sense of touch or smell [2].

Depending on the agent responsible for sensing a target analyte or on the mechanism to convert the information into an analytical signal, sensors can be classified in several categories. Accordingly, a sensor whose detection mechanism consists of biochemical reactions between a recognition receptor and an analyte of interest is named biosensor [1]. The first reports of the term “biosensor” dates from the 1960s by Clark and Lyons and its development has since required multidisciplinary knowledge in the areas of chemistry, biology and engineering [3]. Its working mechanism is based on the interaction between its reactive sites and the analyte of interest present in a given medium, stimulating the beginning of a reaction that will be converted by a transduction element into a measurable analytical signal and that can be analyzed electronically [2].

Bhalla *et al.* [4] pointed out the following main attributes of (bio)sensors and highlighted that the optimization of these characteristics are directly related to their performance:

- **Sensitivity:** is the minimum analyte concentration capable to generate a significant signal from the sensor. In the medical field, for example, very low values of limit of detection (LOD) are required in the diagnosis of Prostatic Specific Antigen (PSA), which in concentrations above 4 ng.mL^{-1} in the blood may indicate the presence of prostate cancer [4];
- **Selectivity:** one of the main properties of a (bio)sensor, is the ability of the biological recognition element to specifically detect an analyte of interest

among other substances and/or interfering species commonly present in the context of application;

- **Reproducibility:** the ability of generating identical responses when the device is exposed to identical conditions. It is closely linked to the characteristics of the transducer and the electronic system;
- **Stability:** the ability to remain unaltered when exposed to the adversities of an environment. Generally, these external stimuli cause disturbances in the output signal of the (bio)sensor during the measurements, which can affect its accuracy. The stability is especially important in situations that require long device incubation times or continuous monitoring;
- **Linearity:** corresponds to the range at which the sensor's output signal is proportional to the analyte concentration. The quality of the corresponding mathematical model, which can be linear or polynomial, is normally assessed by a coefficient of correlation [5-8].

Biosensors are typically classified according to the transduction mechanism or to the biological recognition element. In the first group, there are optical, gravimetric, magnetic, electrochemical and thermal biosensors, while in the second one there are those based on enzymes, microorganisms, antibodies / antigens, nucleic and biomimetic acids [9].

Amongst the biosensors possibilities, the electrochemical immunosensors represent a special group because they combine the advantages of high specificity of the interactions between antibodies and antigens with the high sensitivity of electrochemical techniques [10]. Bhalla *et al.* [4] pointed out that the reactions between antigen and antibody are the best example of selectivity of a biosensor, which is the main characteristic to be considered in the development of this type of device. In addition, according to the Markets and Markets group [11], based on the rise of immunological techniques, experts estimate a market reach of US\$ 25.45 billion for the year 2021 compared to the US\$ 17.16 billion already reached in 2016, which represents an average growth of 8.6% per year.

In the context of the electrochemical immunosensors, those based on the Electrochemical Impedance Spectroscopy (EIS) technique, called "impedimetric", figure among the most promising and currently studied types of biosensors [12]. This

is due to the combination of characteristics such as the low cost of producing electrodes, instrumentation with also relatively low cost, the possibility of miniaturization and possibility of obtaining processing signals by remote control, which makes it amenable for *in-situ* applications [13].

Ali *et al.* [2], who studied the recent biosensor impact applications, point out that the biggest progresses in the field of analytical sensors have been in the areas of biomedicine, agriculture, food and environmental.

In the food industry, efforts have been made to ensure product safety and quality. However, the traditional techniques used for chemical and spectroscopic experimentation have presented some limitations mainly related to the high cost of instrumentation and the long time required to perform the tests [14]. Hideshima *et al.* [15] reported the detection of allergens in food products using field effect transistors. Castillo *et al.* [16] developed an aptamer-based sensor for aflatoxin B1 detection, a mycotoxin identified as a food contaminant with carcinogenic potential present in corn, peanuts and milk. Gaudin [17] portrayed advances in the development of biosensors for the detection of antibiotics in foods of animal origin, also emphasizing the importance of simpler, cheaper and faster methods for this purpose.

In the medicine field, the application of biosensing technologies has rapidly grown due to the increase in the population contingent and consequently the number of people affected by various diseases [18]. In this context, for example, the detection of glucose levels in the blood has gained great space for the diagnosis of diabetes, representing 85% of the market of biosensors [19,20].

The diagnosis of other various diseases has also been reported in the literature in recent years with the application of biosensors, such as anemia [21], malaria [22], tuberculosis [23] and Zika virus [24]. However, as highlighted by Bhalla *et al.* [4], in addition to glucose biosensors and pregnancy tests, few other sensors have reached visible commercialization. The authors reported that this challenge is due to several factors, such as the difficulty of transforming academic developments into commercially viable prototypes for the industry, the complicated regulatory barrier in the clinical area and the natural difficulty in managing the multidisciplinary knowledge involved in the fields of biological sciences and engineering for developing these devices for plural applications.

In this context of vast possibilities, it is therefore necessary to develop scientific and technological sensors and biosensors with faster, cheaper, simpler and more precise performances, aiming to support safety in the areas of health, environmental protection and industrial quality.

1.2 OBJECTIVES

1.2.1 General objectives

The objective of this thesis was to describe the development of impedimetric (bio)sensors for application in the detection of analytes of medical, industrial and environmental interests reaching high performances with respect to sensitivity, selectivity, linearity, fast response time and lower cost in comparison to traditional analytical techniques. To achieve these desirable characteristics, the developed sensors were fabricated with screen-printed carbon electrodes (SPCEs) as transducer substrates. The screen-printing technology has revolutionized the field of electrochemical sensors because it is capable to produce very reproducible electrodes with good sensitivity and selectivity with low manufacturing cost [25]. Combined to the ease modification of SPCEs in special, several researches have exploited these materials as an electrochemical matrix for miniaturized sensing platforms in several applications [26-30].

1.2.2 Specific objectives

For the consolidation of the general objective, the specific objectives of this work were:

- To review the literature on the EIS technique to serve as the transduction mechanisms for the proposed sensors of this research;
- To differentiate the Faradaic and non-Faradaic mechanisms of EIS in order to evaluate the key advantages and important limitations of each technique;

- To review the recent studies employing SPCEs as electrochemical transducers;
- To evaluate SPCEs regarding their chemical composition, stability, electrochemical behavior and corrosion resistance in electrolytic solutions that simulate the application as Faradaic and non-Faradaic sensors;
- To review the electroanalytical techniques traditionally employed to identify fraud in food products;
- To develop an impedimetric immunosensor for recognition of horsemeat as a fraudulent element in raw meat and to characterize the proposed device with respect to its morphology, electrochemical behavior, sensitivity, selectivity against pork and beef and analytical response towards horse serum diluted in buffered solution and towards horsemeat commercial samples;
- To fabricate and to characterize a non-enzymatic impedimetric sensor for recognition of glucose, studying its LOD, selectivity against other sugars (fructose and sucrose) and common interfering species for medical application of the sensor (dopamine, NaCl and animal serum), morphological structure of the functionalized SPCE, electroactivity, linearity, repeatability, reproducibility, transduction mechanism and response time under optimal operational conditions;
- To prepare a dimethyl sulfide (DMS) sensor based on the modification of SPCE with gold particles and to evaluate its performance at nanomolar analyte concentration, to assess its morphology, LOD, limit of quantification (LOQ), linearity, reusability, capability of recognizing the analyte in simulated ocean water and capability of providing real-time impedimetric sensing.

1.3 THESIS STRUCTURE

The present thesis is divided into eight chapters. This first chapter lays out an overview about the sensors technology and use of SPCEs as electrochemical transducers.

Chapter 2, entitled “Faradaic and non-faradaic electrochemical impedance spectroscopy as transduction techniques for sensing applications”, builds on a mini review published by Faria *et al.* [31] on the *International Journal of Biosensors & Bioelectronics* bringing the theory of the EIS technique with a focus on the Faradaic and non-Faradaic mechanisms of transduction.

Chapter 3 (Application of screen-printed carbon electrode as an electrochemical transducer in biosensors) introduces the main characteristics of SPCEs with respect to fabrication, pre-treatments for improving their electroactivity and current applications in electrochemical sensing platforms. This section is adaption from the published mini review of Faria *et al.* [32].

Chapter 4 (Electrochemical behavior of screen-printed carbon electrodes as transducers in biosensors) deals with the characteristics of SPCEs for application in electrochemical (bio)sensors. The original text was adapted from the manuscript by Faria *et al.* [33].

”Recent trends in the electroanalytical detection of food fraud” is the title of the Chapter 5, which provides a comprehensive review on the electrochemical techniques recently employed for the identification of food fraud, highlighting the importance of these analytical methods in the work of preventing and inspecting these criminal act. This section was adapted from the review published by Faria *et al.* [34].

Complementarily to the information raised in the fifth chapter of this thesis with respect to the importance of screening food fraud, Chapter 6 refers to the article “A new tool for the detection of horsemeat adulteration in raw meat” published in the *Journal of Biosensors & Bioelectronics* [35]. This chapter describes the development of an impedimetric sensor using anti-horse antibodies for the detection of horsemeat.

The article “Non-enzymatic impedimetric sensor based on 3-aminophenylboronic acid functionalized screen-printed carbon electrode for highly sensitive glucose

detection” [36] published in the *Sensors* journal was adapted to Chapter 7. This work describes the development, characterization and application of a high sensitive glucose sensor based on the EIS technique.

Finally, Chapter 8 reports the fabrication of a DMS sensor based on the modification of SPCEs with gold particles to detect the molecule at nanomolar level. This text is an adaptation of the manuscript “A novel impedimetric sensor for trace level detection of dimethyl sulfide (DMS)” accepted for publication by the *Journal of Materials Science: Materials in Electronics* (ISSN: 0957-4522; DOI: 10.1007/s10854-020-03588-0).

1.4 REFERENCES

- [1] INTERNATIONAL UNION OF PURE AND APPLIED CHEMISTRY, IUPAC. Electrochemical Biosensors: recommended definitions and classification. Technical report. **Pure and Applied Chemistry**, 71(12), p. 2333-2348, 1999.
- [2] ALI, J.; NAJEEB, J.; ALI, M.A.; ASLAM, M.F.; RAZA, A. Biosensors: their fundamentals, designs, types and most recent impactful applications: a review. **Journal of Biosensors and Bioelectronics**, 8, p. 1, 2017.
- [3] MEHROTRA, P. Biosensors and their applications – a review. **Journal of oral biology and craniofacial research**, 6, p. 153-159, 2016.
- [4] BHALLA, N.; JOLLY, P.; FORMISANO, N.; ESTRELA, P. Introduction to Biosensors. **Essays in Biochemistry**, 60, p. 1-8, 2016.
- [5] SOLER, M.; MESA-ANTUNEZ, P.; ESTEVEZ, M-C.; RUIZ-SANCHEZ, A.J.; OTTE, M.A.; SEPULVEDA, B.; COLLADO, D.; MAYORGA, C.; TORRES, M.; PEREZ-INESTROSA, E.; LECHUGA, L.M. Highly sensitive dendrimer-based nanoplasmonic biosensor for drug allergy diagnosis. **Biosensors and Bioelectronics**, 66, p. 115-123, 2015.
- [6] ANDERSON, D.E.; BALAPANGU, S.; FLEISCHER, H.N.A.; VIADÉ, R.A.; KRAMPA, F.D.; KANYONG, P.; AWANDARE, G.A.; TIBURU, E.K. Investigating the Influence of Temperature on the Kaolinite-Base Synthesis of Zeolite and Urease Immobilization for the Potential Fabrication of Electrochemical Urea Biosensors. **Sensors**, 17(8), p. 1831, 2017.
- [7] DELUTHAULT, A., KERZÉHO, V., BERNARD, S., SOULIER, F., CAUVET, P. New calibration technique of contact-less resonant biosensor. **Journal of Electronic Test**, 3, p. 365-375, 2017.

- [8] THOMAS, E.M.; TESTA, S.M. The colorimetric determination of selectively cleaved adenosines and guanosines in DNA oligomers using bicinchoninic acid and copper. **Journal of Biological Inorganic Chemistry**, 22(1), p. 31-46, 2017.
- [9] CHAUDHARY, D.A.; UPADHYAY, J.B.; KOSHTA, V. Application of biosensors in dairy-food industry. **The Asian Journal of Animal Science**, 9(1), p. 92-96, 2014.
- [10] WEN, W.; YAN, X.; ZHU, C.; DU, D.; LIN, Y. Recent advances on Electrochemical immunosensors. **Analytical Chemistry**, 89, p. 138-156, 2016.
- [11] MARKETS AND MARKETS. **Immunoassay Market by Technology (ELISA, Fluorescence, Colorimetric, Chemiluminescence, Rapid Test, Western Blot, ELISPOT, PCR), Application (Infectious Disease, Endocrinology, Cardiology, Oncology, Hematology) & End User - Global Forecast to 2021**. Disponível em: <https://www.marketsandmarkets.com/Market-Reports/immunoassay-market-436.html>. Acesso em 4 fev. 2018.
- [12] KOKKINOS, C.; ECONOMOU, A.; PRODRMIDIS, M.I. Electrochemical immunosensors: critical survey of different architectures and transduction strategies. **Trends in Analytical Chemistry**, 79, p. 88-105, 2016.
- [13] PRODRMIDIS, M.I. Impedimetric immunosensors – a review. **Electrochimica Acta**, 55, p. 4227-4233, 2010.
- [14] SCOGNAMIGLIO, V.; ARDUINI, F.; PALLESCHI, G.; REA, G. Biosensing technology for sustainable food safety. **Trends in Analytical Chemistry**, 62, p. 1-10, 2014.
- [15] HIDESHIMA, S.; SAITO, M.; FUJITA, K.; HARADA, Y.; TSUNA, M.; SEKIGUCHI, S.; KUROIWA, S.; NAKANISHI, T.; OSAKA, T. Label-free detection of allergens in food via surfactant-induced signal amplification using a field effect transistor-based biosensor. **Sensors and Actuators B: Chemical**, 254, p. 1011-1016, 2018.
- [16] CASTILLO, G.; SPINELLA, K.; POTURNAYOVÁ, A.; SNEJDÁRKOVÁ, M.; MOSIELLO, L.; HIANIK, T. Detection of aflatoxin B1 by aptamer-based biosensor using PAMAM dendrimers as immobilization platform. **Food Control**, 52, p. 9-18, 2015.
- [17] GAUDIN, V. Advances in biosensor development for the screening of antibiotic residues in food products of animal origin – a comprehensive review. **Biosensors and Bioelectronics**, 90, p. 363-377, 2017.
- [18] BAHADIR, E.B.; SEZGINTÜRK, M.K. Applications of commercial biosensors in clinical, food, environmental, and biothreat/biowarfare analyses. **Analytical Biochemistry**, 478, p. 107-120.

- [19] SCOGNAMIGLIO, V.; PEZZOTTI, G.; PEZZOTTI, I.; CANO, J.; BUONASERA, K.; GIANNINI, D.; GIARDI, M.T. Biosensors for effective environmental and agrifood protection and commercialization: from research to market. **Microchimica Acta**, 170, p. 215-225, 2010.
- [20] REA, G.; POLTICELLI, F.; ANTONACCI, A.; SCOGNAMIGLIO, V.; KATIVAR, P.; KULKARNI, S.A.; JOHANNINGMEIER, U.; GIARDI, M.T. Structure-based design of novel *Chlamydomonas reinhardtii* D1-D2 photosynthetic proteins for herbicide monitoring. **Protein Science**, 18, p. 2139-2151, 2009.
- [21] PETERSON, R.D.; WILUND, K.R.; CHUNNINGHAM, B.T.; ANDRADE, J.E. Comparison of methods study between a photonic crystal biosensor and certified ELISA to measure biomarkers of iron deficiency in chronic kidney disease patients. **Sensors**, 17, p. 2203, 2017.
- [22] FRASER, L.A.; KINGHORN, A.B.; DIRKZWAGER, R.M.; LIANG, S.; CHEUNG, Y-W.; LIM, B.; SHIU, S.C-C.; TANG, M.S.L.; ANDREW, D.; MANITTA, J.; RICHARDS, J.S.; TANNER, J.A. A portable microfluidic Aptamer-Tethered Enzyme Capture (APTEC) biosensor for malaria diagnosis. **Biosensors and Bioelectronics**, 100, p. 591-596, 2018.
- [23] SUN, W.; YUAN, S.; HUANG, H.; LIU, N.; TAN, Y. A label-free biosensor based on localized surface plasmon resonance for diagnosis of tuberculosis. **Journal of Microbiological Methods**, 142, p. 41-45, 2017.
- [24] JIANG, Q.; YATIN, J.C.; CAO, S.; KHARASCH, E.D.; SINGAMANENI, S.; MORRISSEY, J.J. Rapid, point-of-care, paper-based plasmonic biosensor for Zika virus diagnosis. **Advanced biosystems**, 1, 1-8, 2017.
- [25] THIYAGARAJAN, N.; CHANG, J.L.; SENTHILKUMAR, K.; ZEN, J.M. Disposable electrochemical sensors: A mini review. **Electrochemistry Communications**, 38, p. 86-90, 2014.
- [26] CARDOSO, A.R.; SÁ, M.H.; SALES, M.G.F. An impedimetric molecularly-imprinted biosensor for Interleukin-1 β determination, prepared by in-situ electropolymerization on carbon screen-printed electrodes. **Bioelectrochemistry**, 130, p. 107287, 2019.
- [27] GETO, A.; NOORI, J.S.; MORTENSEN, J.; SVENDSEN, W.E.; DIMAKI, M. Electrochemical determination of bentazone using simple screen-printed carbon electrodes. **Environment International**, 129, p. 400-407, 2019.
- [28] SASAL, A.; TYSZCZUK-ROTKO, K.; WÓJCIAK, M.; SOWA, I. First electrochemical sensor (screen-printed carbon electrode modified with carboxyl functionalized multiwalled carbon nanotubes) for ultratrace determination of diclofenac. **Materials**, 13(3), p. 781, 2020.

- [29] HUANG, Y.; CUI, L.; XUE, Y.; ZHANG, S. ; ZHU, N. ; LIANG, J. ; LI, G. Ultrasensitive cholesterol biosensor based on enzymatic silver deposition on gold nanoparticles modified screen-printed carbon electrode. **Materials Science and Engineering C**, 77, p. 1-8, 2017.
- [30] DECHTRIRAT, D.; SOOKCHAROENPINYO, B.; PRAJONGTAT, P.; SRIPRACHUABWONG, C.; SANGUANKIAT, A.; TUANTRANONT, A.; HANNONGBUA, S. An electrochemical MIP sensor for selective detection of salbutamol based on a graphene/PEDOT:PSS modified screen printed carbon electrode. **RSC Advances**, 8, p. 206-212, 2018.
- [31] FARIA, R. A. D.; HENEINE, L. G. D.; MATENCIO, T.; MESSADDEQ, Y. Faradaic and non-faradaic electrochemical impedance spectroscopy as transduction techniques for sensing applications. **International Journal of Biosensors & Bioelectronics**, 5, p. 29–31, 2019.
- [32] FARIA, R. A. D.; MESSADDEQ, Y.; HENEINE, L. G. D.; MATENCIO, T. Application of screen-printed carbon electrode as an electrochemical transducer in biosensors. **International Journal of Biosensors & Bioelectronics**. 5, p. 1–2, 2019.
- [33] FARIA, R. A. D.; DOUAD, A.; SOARES, R. B.; HENEINE, L. G. D.; MATENCIO, T.; LINS, V. F. C.; MESSADDEQ, Y. Electrochemical behavior of screen-printed carbon electrodes as transducers in biosensors. **Corrosion**, 76(6), 2020.
- [34] FARIA, R. A. D.; HENEINE, L. G. D.; MATENCIO, T.; MESSADDEQ, Y. Recent trends in the electroanalytical detection of food fraud. **International Journal of Biosensors & Bioelectronics**, 5, p. 63–67, 2019.
- [35] FARIA, R. A. D.; IDEN, H.; BHARUCHA, E.; LINS, V. F. C.; MESSADDEQ, Y.; MATENCIO, T.; HENEINE, L. G. D. A new tool for the detection of horsemeat adulteration in raw meat. **Journal of Biosensors and Bioelectronics**, 9, p. 1-7, 2018.
- [36] FARIA, R. A. D.; IDEN, H.; HENEINE, L. G. D.; MATENCIO, T.; MESSADDEQ, Y. Non-enzymatic impedimetric sensor based on 3-aminophenylboronic acid functionalized screen-printed carbon electrode for highly sensitive glucose detection. **Sensors**, 19, p. 1686, 2019.

CHAPTER 2 – FARADAIC AND NON-FARADAIC ELECTROCHEMICAL IMPEDANCE SPECTROSCOPY AS TRANSDUCTION TECHNIQUES FOR SENSING APPLICATIONS

*Adapted text from: FARIA, R. A. D.; HENEINE, L. G. D.; MATENCIO, T.; MESSADDEQ, Y. Faradaic and non-faradaic electrochemical impedance spectroscopy as transduction techniques for sensing applications. **International Journal of Biosensors & Bioelectronics**, 5(1), p. 29–31, 2019.*

Ricardo Adriano Dorledo de Faria^{1,2}, Luiz Guilherme Dias Heneine³, Tulio Matencio^{1,4}, Younès Messaddeq^{2,5}

¹Department of Chemical Engineering, Universidade Federal de Minas Gerais, Brazil

²Université Laval, Canada

³Department of Applied Immunology, Fundação Ezequiel Dias, Brazil

⁴Department of Chemistry, Universidade Federal de Minas Gerais, Brazil

⁵Institute of Chemistry, UNESP, Brazil

2.1 ABSTRACT

Electrochemical Impedance Spectroscopy (EIS) stands out as a powerful technique for application in electroanalytical devices. Especially due to the possibility of label-free performance, use of miniaturized systems, in situ measurements and the relative low cost, impedimetric sensors have attracted particular attention in the recognition of analytes of medical, environmental and industrial interests. Depending on the presence or absence of redox species in the electrode or in the electrolyte, the technique can be categorized as faradaic or non-faradaic EIS respectively. The choice of the most suitable sensing method relies mainly on the expected application. Despite the non-faradaic methods presents the advantages of the application in point-of-care devices due to the possibility of miniaturization of the electrodes and the absence of redox couple, the faradaic sensors tends to be more sensitive.

Keywords: electrochemical impedance spectroscopy, sensor, faradaic EIS, non-faradaic EIS

2.2 INTRODUCTION

Electrochemical techniques have been widely employed to detect and/or quantify molecules of medical, environmental and industrial interests. Among traditional techniques such as potentiometry, amperometry and conductometry, the EIS has gained great attention as an analytical tool for a broad range of analytes, mainly because it can be performed as a non-destructive method and it enables *in situ* measurements [1,2]. Moreover, EIS exempt the use of special reagents, which makes it suitable for label-free applications, which significantly diminishes its cost in relation to other techniques and makes it easier to perform [3]. In common, all the electrochemical sensors consist on relating a measurable output electrical signal to the changes in the structure (usually the surface) of an electrode because of the recognition of a target analyte. The in-depth understanding of the mechanisms and fundamentals involving the sensing phenomena is a challenge in electroanalytical techniques and can lead to the improvement of the main desirable characteristics of a sensor: the selectivity, stability and sensibility [4]. In this sense, this minireview presents the main aspects regarding the EIS as a technique for application in sensors based on its two categories of performance: the faradaic and non-faradaic EIS.

2.3 EIS THEORY

The EIS basis lies on the development of multiple microscopic processes when an electrode/electrolyte system suffers from an electrical stimulus. This small perturbation can provoke the transfer of electrons in electronic conductors and the transport of charged species from the electrode to the electrolyte (and *vice-versa*) due to the occurrence of oxidation and reduction reactions. Accordingly, the resultant flow rate of electrons and charges is a function of the resistance of both electrode and electrolyte as well as it depends on the reaction rates that take place on the interface [5].

Basically, a sinusoidal AC potential (potentiostatic EIS) or current (galvanostatic EIS) is applied to an electrochemical system under study and the resultant AC current or potential is measured as a frequency-dependent parameter. The ratio between the applied potential $E(\omega, t)$, which can also be superimposed by a constant DC potential, and the current $I(\omega, t)$ is the impedance $Z(\omega, t)$ (Equations 1, 2 and 3). Herein, ω is the angular frequency ($\omega = 2\pi f$, where f is the variable frequency), t is the time, $|Z|$ is the magnitude of impedance, Z' is the real impedance, Z'' is the imaginary impedance, in which j is the imaginary number $\sqrt{-1}$, and ϕ is the phase angle between the potential and current signals [6,7].

$$Z(\omega, t) = \frac{E(\omega, t)}{I(\omega, t)} = |Z(\omega, t)| e^{j\phi} \quad (1)$$

$$|Z(\omega, t)| = (\cos\phi + j\sin\phi) \quad (2)$$

$$Z(\omega, t) = Z'(\omega) + jZ''(\omega) \quad (3)$$

Typically, impedance data are represented as a function of Z' and Z'' (Nyquist diagram) or drawing $|Z|$ and/or ϕ as a function of the frequency (Bode diagram). By exploiting these graphical representations in certain frequency ranges, it is possible to assess some interfacial characteristics of an electrode as well as the conductive features of the electrolyte. However, due to the complex composition of the global impedance from an electrochemical cell, the EIS data is commonly modeled to an electrical equivalent circuit in order to further analyze the inductive, capacitive and resistive components [8].

EIS comprises two groups: the faradaic and non-faradaic EIS. The use of one or the other terminology is associated to the occurrence of electrical charge transfer across an interface due to the presence or absence of redox species [3]. Based mainly on the characteristics of the transducer substrate, the electrolyte and the application of interest, one can elect the most appropriate technique to develop an electrochemical sensor.

2.4 FARADAIC SENSORS

In faradaic EIS, reduction and/or oxidation reactions among electroactive species take place at the electrode leading to the generation of an electrical current [3]. Thus, the faradaic sensors require the presence of redox probes and the application of DC conditions to promote the development of the electrochemical reactions. This type of EIS receives this name because the generated current obeys the Ohm's Law (Equation 4), which means that the faradaic current is related to the number of electrons transferred in the redox reactions (n), to the Faraday constant (F), the surface area of the electrode (A) and the flux of electroactive molecules at the interface boundary (j_i) [9].

$$I = nFAj_i$$

(4)

By means of the current generated from the redox reactions, the faradaic sensors can achieve higher sensitivity in comparison to the non-faradaic devices [2].

To model the appropriate equivalent circuit associated to faradaic sensors, besides the electrolyte resistance and the capacitance (that is usually replaced by a constant phase element – CPE), it must take in account the effect of a charge transfer resistance (R_{ct}) and a Warburg impedance (Z_w). The R_{ct} is a consequence of the potential generated by the oxidative and reductive phenomena at the electrode as well as of the repulsion or steric effect caused by the charged species that arrives to the conductive surface [3]. Accordingly, the Z_w results from the diffusion of the electroactive species from the bulk solution to the electrode. Graphically, R_{ct} can be determined by the diameter of a semicircle in the Nyquist plot and Z_w can be deduced from a 45° inclined straight line at low frequencies [10].

Despite the reduction and oxidation reactions are often associated to the presence of a redox couple in the electrolyte ($\text{Fe}(\text{CN})_6^{3-/4-}$ is commonly employed as a redox pair in the literature), the redox phenomena can also occur in the structure of the electrode. For example, some conductive polymers such as polyaniline, polypyrrole

and polythiophene possess the ability of conduct charge along their chain due to doping mechanisms [11].

2.5 NON-FARADAIC SENSORS

Contrary to the faradaic EIS, the non-faradaic method does not demand the use of redox couples and, consequently, no reference electrode is necessary, because no DC potential is required [2]. These features make this kind of sensors more amenable to miniaturization and to online/real-time applications. In this kind of technique, by charging and discharging the double-layer capacitance, it is possible to assess the dielectric changes on the electrode. Thus, the impedance of a non-faradaic sensor arises from the effect caused by the insulating characteristics of the target analyte bond to the conductive substrate [12]. Typically, the most valuable impedance parameter in this case is the double layer capacitance and it is only limited by the nature of the charge carriers and their concentration at the boundary layer of the transducer substrate [3]. Nonetheless, the $|Z|$ and ϕ components are adequate transducer parameters [13]. In this case, the equivalent circuit consists of a combination of resistors and capacitors. The double layer capacitance (C) is described by the Helmholtz model (Equation 5) as a function of the free space permittivity (ϵ_0), the relative solution permittivity (ϵ_r), the distance (d) of the Helmholtz layer and the surface area of the electrode (A) [14].

$$C = \frac{\epsilon_0 \epsilon_r}{d} A \quad (5)$$

2.6 CONCLUSION

Both faradaic and non-faradaic EIS present relevant advantages as transducer techniques in electrochemical sensors for various applications. In the faradaic mode, the R_{ct} is the impedance component correlated to the concentration of an analyte of interest and it is a result of the current generated from the reduction and oxidation

reactions among electroactive species. On the other hand, the capacitance is generally the most important transducer term to interpret the recognition of a certain analyte in non-faradaic EIS. Despite less sensitive, the non-faradaic sensor is a promising candidate for real-time applications because it does not require the presence of redox couples.

2.7 REFERENCES

- [1] BAHADIR, E. B.; SEZGINTÜRK, M. K. A review on impedimetric biosensors. **Artificial Cells, Nanomedicine, and Biotechnology**, 44(1), p. 248-262, 2016.
- [2] PARK, J. S.; KIM, H. J. ; LEE, J. H.; PARK, J. H.; KIM, J.; HWANG, K. S.; LEE, B. C. Amyloid beta detection by faradaic electrochemical impedance spectroscopy using interdigitated microelectrodes. **Sensors**, 18(2), p. 426, 2018.
- [3] DANIELS, J. S.; POURMAND, N. Label-free impedance biosensors: opportunities and challenges. **Electroanalysis**, 19(12). p. 1239-1257, 2007.
- [4] PEJCIC, B., MARCO, R. Impedance spectroscopy: over 35 years of electrochemical sensor optimization. **Electrochimica Acta**, p. 5217-6229, 2006.
- [5] MACDONALD, J. R.; JOHNSON, W. B. Fundamentals of Impedance Spectroscopy. In: Barsoukov E, Macdonald JR. **Impedance Spectroscopy – theory, experiment and applications**. Hoboken, NJ: Willey-Interscience; 2018:1-20.
- [6] SACCO, A. Electrochemical impedance spectroscopy as a tool to investigate the electroreduction of carbon dioxide: a short review. **Journal of CO₂ Utilization**, 27, p. 22-31, 2018.
- [7] SACCO, A. Electrochemical impedance spectroscopy: fundamentals and application in dye-sensitized solar cells. **Renewable and Sustainable Energy Reviews**, 79, p. 814-829, 2017.
- [8] ATES, M. Review study of electrochemical impedance spectroscopy and equivalent electrical circuits of conducting polymers on carbon surfaces. **Progress in Organic Coatings**, 71, p. 1-10, 2011.
- [9] HAMMOND, J. L.; FORMISANO, N.; ESTRELA, P.; CARRARA, S.; TKAC, J. Electrochemical biosensors and nanobiosensors. **Essays in Biochemistry**, 60(1), p. 69-80, 2016.

- [10] BARAI, A.; CHOUCHELAMANE, G. H.; GUO, Y.; MCGORDON, A.; JENNINGS, P. A study on the impact of lithium-ion cell relaxation on electrochemical impedance spectroscopy. **Journal of Power Sources**, 280, p. 74-80, 2015.
- [11] JR, A. R.; SOTO, A. M. G.; MELLO, S. V.; BONE, S.; TAYLOR, D. M.; MATTOSO, L. H. C. An electronic tongue using polypyrrole and polyaniline. **Synthetic Metals**, 132, p. 109-116, 2003.
- [12] LIN, S. P.; VINZONS, L. U.; KANG, Y. S.; LAI, T. S.; Non-faradaic electrical impedimetric investigation of the interfacial effects of neuronal cell growth and differentiation on silicon nanowire transistors. **ACS Applied Materials Interfaces**, 7, p. 9866-9878, 2015.
- [13] CECCHETTO, J.; FERNANDES, F. C. B.; LOPES, R.; BUENO, P. R. The capacitive sensing of NS1 Flavivirus biomarker. **Biosensors and Bioelectronics**, 87, p. 949-956, 2017.
- [14] KANG, J.; WEN, J.; JAYARAM, S. H.; AIPING, Y.; WANG, X. Development of an equivalent circuit model for electrochemical double layer capacitors (EDLCs) with distinct electrolytes. **Electrochimica Acta**, 115, p. 587-598, 2014.

CHAPTER 3 - APPLICATION OF SCREEN-PRINTED CARBON ELECTRODE AS AN ELECTROCHEMICAL TRANSDUCER IN BIOSENSORS

*Text adapted from: FARIA, R. A. D.; MESSADDEQ, Y.; HENEINE, L. G. D.; MATENCIO, T. Application of screen-printed carbon electrode as an electrochemical transducer in biosensors. **International Journal of Biosensors & Bioelectronics**. 5(1), p. 1–2, 2019.*

Ricardo Adriano Dorledo de Faria,^{1,2} Younès Messaddeq,^{2,3} Luiz Guilherme Dias Heneine,⁴ Tulio Matencio⁵

¹Department of Chemical Engineering, Universidade Federal de Minas Gerais, Brazil

²Center for Optics, Photonics and Lasers (COPL), Université Laval, Canada

³Institute of Chemistry, Brazil

⁴Department of Applied Immunology, Fundação Ezequiel Dias, Brazil

⁵Department of Chemistry, Universidade Federal de Minas Gerais, Brazil

3.1 ABSTRACT

Screen-printed electrodes have been extensively employed as an economical transducer substrate for electrochemical biosensing applications due to their small size, easiness of mass production and the possibility of use with portable devices which facilitates in situ applications. Carbon inks can be widely modified by the addition of materials and/or molecules and this versatility confers the capacity to be used for the purposes of food, agricultural, environmental and biomedical analyses.

Keywords: screen printed electrode, carbon, biosensing

3.2 INTRODUCTION

Great interest has been directed to the screen printing technology for biosensing applications. Screen-printed electrodes (SPEs) possess as major advantage over the traditional electrodes the possibility of use in miniaturized systems, whose

applications demand portable devices. Besides the possibility to perform *in situ* analyses, the easiness of mass production makes these electrodes very interesting for the market.

3.3 FABRICATION

Usually, the SPEs consist of a three-electrode configuration (working, counter and reference electrodes). Carbon ink is painted onto one extremity of the conductive tracks to form the working and counter electrodes, and the reference electrode is commonly based on silver electroactive tracts. An insulating film is glued to the exposed tracts and between the electrodes to avoid short-circuit. The screen-printed carbon electrodes (SPCEs) contain a chemically inert carbon conductive ink, organic solvents, additives and some binding components [1,2].

3.4 PRE-TREATMENT

Since the SPCE possess insulator additives to improve the adhesion of carbon ink on the support, the pre-treatment of these electrodes is considered a key point to overcome its limited electron transfer kinetics at the interface with the electrolyte. In order to activate the edge planes of the SPCE, many techniques have been considered to enhance the carbon electroactivity (e.g. thermal, chemical and mechanical treatments), although the electrochemical processes are the most commonly used. Sundaresan *et al.* [3] performed 10 cycles of Cyclic Voltammetry (CV) in 0.05 M phosphate buffer in a potential range from -0.5 to 2.0 V vs Ag/AgCl. Pan *et al.* [4] applied a fixed -1.2 V vs Ag/AgCl potential during 20 s to an electrode containing a drop of 0.1 M NaOH.

3.5 APPLICATIONS IN ELECTROCHEMICAL BIOSENSING

The final step to produce an SPCE for a specific purpose is the modification (functionalization) of the working electrode surface. The target analyte drives the choice of molecules or biomolecules with specific reactivity towards it to be attached. Table 1 shows some recent applications of SPCEs regarding the biosensing of molecules of medical, environmental and food interests.

Table 1 - Recent applications of SPCE as electrochemical transducer in biosensors

Application	Target analyte	Molecule of recognition	Detection technique	Ref.
Medical diagnosis	Cardiac troponin I	5'-amine modified Tro4 aptamer	Chronoamperometry	[5]
	Japanese encephalitis virus (JEV)	Anti-JEV antibodies	EIS	[6]
Environment monitoring	Cathecol	Laccase	Chronopotentiometry	[7]
	Bisphenol A	Dendritic platinum NPs	CV	[8]
Food analysis	Fructose	Graphite NPs	Chronoamperometry	[9]
	Ethyl carbamate	O-aminophenol	CV	[10]

*NPs = nanoparticles

3.6 CONCLUSION

The possibility of SPCE functionalization to detect various molecules associated to its miniaturized dimensions and low cost of production has been extensively exploited, as reported in the literature, for the development of versatile electrochemical biosensors. The electroactivity of carbon has been improved by

different treatments making it suitable for application as a transducer in electroanalysis mainly towards the detection of biological molecules.

3.7 REFERENCES

- [1] GONZÁLEZ-SANCHEZ, M.I.; GÓMEZ-MONEDERO, B.; AGRISUELAS, J.; INIESTA, J.; VALERO, E. Highly activated screen-printed carbon electrodes by electrochemical treatment with hydrogen peroxide. **Electrochemistry Communications**, 91, p. 36-40, 2018.
- [2] TUDORACHE, M.; BALA, C. Biosensors based on screen-printing technology, and their applications in environmental and food analysis. **Analytical and Bioanalytical Chemistry**, 388(3), p. 565-578, 2007.
- [3] SUNDARESAN, P.; CHEN, T. W.; CHEN, S. M.; TSENG, T. W.; LIU, X. Electrochemical activation of screen printed carbon electrode for the determination of antibiotic drug metronidazole. **International Journal of Electrochemical Science**, 13, p. 1441-1451, 2018.
- [4] PAN, D.; RONG, S.; ZHANG, G.; ZHANG, Y.; ZHOU, Q.; LIU, F.; LI, M.; CHANG, D.; PAN, H. Amperometric determination of dopamine using activated screen-printed carbon electrodes. **Electrochemistry**, 83(9), p. 725-729, 2015.
- [5] JO, H.; HER, J.; LEE, H.; SHIM, Y. B.; BAN, C. Highly sensitive amperometric detection of cardiac troponin I using sandwich aptamers and screen-printed carbon electrodes. **Talanta**, 165, p. 442-448, 2017.
- [6] CHIN, S. K.; LIM, L. S.; PANG, S. C.; SUN, M. S. H.; PERERA, D. Carbon nanoparticle modified screen printed carbon electrode as a disposable electrochemical immunosensor strip for the detection of Japanese encephalitis virus. **Microchimica Acta**, 184(2), p. 491-497, 2016.
- [7] PALANISAMY, S.; RAMARAJ, S. K.; CHEN, S. M.; YANG, T. C. K.; FAN, P. Y.; CHEN, T. W.; VELUSAMY, V.; SELVAM, V. A novel laccase biosensor based on laccase immobilized graphene-cellulose microfiber composite modified screen-printed carbon electrode for sensitive determination of catechol. **Nature**, 7, p. 1-12, 2017.
- [8] SHIM, K.; KIM, J.; SHAHABUDDIN, M.; YAMAUCHI, Y.; HOSSAIN, M. S. A.; KIM, J. H. Efficient wide range electrochemical bisphenol-A sensor by self-supported dendritic platinum nanoparticles on screen-printed carbon electrode. **Sensors and Actuators B: Chemical**, 255, p. 2800-2808, 2018.

[9] NICHOLAS, P.; PITTSOON, R.; HART, J. P. Development of a simple, low cost chronoamperometric assay for fructose based on a commercial graphite-nanoparticle modified screen-printed carbon electrode. **Food Chemistry**, 241, p. 122-126, 2018.

[10] ZHAO, X.; ZUO, J.; QIU, S.; HU, W.; WANG, Y.; ZHANG, J. Reduced graphene oxide-modified screen-printed carbon (rgo-spce)-based disposable electrochemical sensor for sensitive and selective determination of ethyl carbamate. **Food Analytical Methods**, 10(10), p. 3329-3337, 2017.

CHAPTER 4 - ELECTROCHEMICAL BEHAVIOR OF SCREEN-PRINTED CARBON ELECTRODES AS TRANSDUCERS IN BIOSENSORS

*Text adapted from: FARIA, R. A. D.; DOUAUD, A.; SOARES, R. B.; HENEINE, L. G. D.; MATENCIO, T.; LINS, V. F. C.; MESSADDEQ, Y. Electrochemical behavior of screen-printed carbon electrodes as transducers in biosensors. **Corrosion**, 76(6), 553-561, 2020.*

Ricardo Adriano Dorledo de Faria,^{1,2} Alexandre Douaud², Renata Braga Soares¹,
Luiz Guilherme Dias Heneine³, Tulio Matencio¹, Vanessa de Freitas Cunha Lins¹,
Younès Messaddeq^{2,5}

¹Department of Chemical Engineering, Universidade Federal de Minas Gerais (UFMG), Minas Gerais, 30270-901, Brazil

²Center for Optics, Photonics and Lasers (COPL), Université Laval, Quebec, QC G1V 0A6, Canada

³Department of Applied Immunology, Fundação Ezequiel Dias (FUNED), Minas Gerais, 30510-010, Brazil

⁴Department of Chemistry, Universidade Federal de Minas Gerais (UFMG), Minas Gerais, 30270-901, Brazil

⁵Institute of Chemistry, UNESP, Araraquara, São Paulo, 14800-060, Brazil

4.1 ABSTRACT

Screen-printed carbon electrode (SPCE) was examined as a transducer substrate for application in electrochemical sensors. Aqueous solutions of 0.1 M KCl and 0.1 M KCl + 5 mM $K_3[Fe(CN)_6]/K_4[Fe(CN)_6]$ (redox solution) were prepared to simulate the environment of faradaic and non-faradaic sensing respectively. The SPCE presented an irregular surface composed by two main carbon phases. Raman spectroscopy results revealed the presence of peaks around 1580 cm^{-1} and 1334 cm^{-1} related to the G and D bands corresponding to sp^2 carbon atoms (graphite flakes) and a multitude of broad bands associable to amorphous sp^3 carbon in the ink matrix. Conductive Atomic Force Microscopy indicated that the irregular structure of the SPCE led to the heterogeneous distribution of the current over the surface and the electroactivity of this material was mainly attributed to the presence of graphite.

Polarization curves and Electrochemical Impedance Spectroscopy revealed that the redox solution was more aggressive to the SPCE, despite this electrode was achieved a quasi-steady state for one hour under the effect of a polarization potential in both electrolytes. Such result justifies its use as an electrochemical transducer in faradaic and non-faradaic devices.

Keywords: carbon, corrosion resistance, electrochemical impedance spectroscopy, polarization

4.2 INTRODUCTION

Electrochemical sensors have been widely exploited as a powerful device to detect the presence and/or the concentration of substances of public interest. These devices attract great attention because they usually comply the key aspects of a sensor: the accuracy of the measurement, sensitivity, sensibility and reproducibility [1]. Traditionally, an electrochemical sensor consists of a three-configuration electrode system (two-configuration is also possible) immersed in an electrolyte: a reference, a counter-electrode (as called “auxiliary”) and a working electrode. In the latter, some modifications can be performed in order to make it capable to recognize an analyte of interest [2]. As a result of the interaction between the sensitive working electrode and a molecule of interest, an electrical signal is produced on the interface electrode-electrolyte, providing useful information about the detection phenomenon [3]. In a group of electrochemical devices comprising classical techniques such as the amperometry [4-6], potentiometry [7-9] and conductometry [10-12], the impedimetric sensors possess single prominence. EIS is based on the analysis of an electrochemical system in which an AC potential is applied and the resultant AC current (or *vice-versa* in case of galvanostatic EIS) is analyzed under a frequency range that can varies from high down to very low values (i.e. from MHz to mHz) [13]. The main advantages of using EIS as a transduction technique for sensing applications are the fact that it is a non-destructive method since a small perturbation around the equilibrium is imposed to the system; the facility of using in

miniaturized/portable systems for *in situ* analysis and its low cost if compared with other techniques [14-16].

EIS is categorized into two groups with respect to the charge transfer across the interface electrode/electrolyte. The faradaic EIS is the technique in which the presence of a redox couple generates the development of a current due to oxidative and reductive reactions. In case of sensing applications, it is possible to correlate the concentration of a target analyte with the faradaic current resultant from the redox reactions according to the Faraday's Law [16,17]. On the other hand, the non-faradaic EIS does not require the addition of redox species nor the use of a reference electrode. The non-faradaic impedance arises from the ionic species present on the interface electrode/electrolyte causing alterations in the double layer capacitance [18,19].

Employing both faradaic and non-faradaic EIS, many authors have been studied different materials to use as an electrochemical transducer in electrochemical sensors, such as stainless steel [20,21] indium tin oxide [22] and conducting polymers [23-25].

The transducer is a key point in the development of sensors because it converts the energy resultant from the recognition of the analyte on its surface into a measurable electrical output signal that correlates the presence/concentration of this analyte [26]. A special point in using a certain transducer matrix to develop a sensor is the stability of the electrode components. Zhao *et al.* [27] pointed out many advantages of employing porous silicon as a substrate for biosensors (such as its large surface area and the easiness of functionalization) but recognized that this material was unstable in water and other electrolytes due to oxidative and reductive reactions. Similarly, Glogener *et al.* [28] investigated the corrosion of microelectronic chips used as sensors for glucose detection for *in situ* application and Beltrami *et al.* [29] inspected the deposition of protective films in magnetoelastic alloys in order to prevent the corrosion of the material in a sensor since the corrosion products arises to the decrease of the device's sensitivity.

In the recent years one of the most employed electrochemical substrates for sensing applications has been the screen-printed carbon electrodes (SPCE) [30-33]. The increasing use of SPCE as an electrochemical transducer arises from the

presence of a carbon conductive ink that can be easily modified for the recognition of various analytes, besides its easiness of fabrication, minimal dimensions and low cost [34]. Despite the precise composition of this carbon ink kept as a proprietary information by the manufacturers, it is known that it contains graphite particles (responsible for enhancing the electroactivity of the SPCE), polymeric binders, solvents and some additives to improve its dispersion, adhesion and printing properties [35,36]. Traditionally, the carbon ink is printed on plastic or ceramic materials in order to allow the fabrication of the SPCE at higher curing temperatures and to make it more cost-effective [36].

Although several authors have focused on both the characterization and optimization of the carbon ink mainly with respect to its electrochemical properties [37-40], there is still an important gap in the literature regarding the effect of the electrolytes in which the SPCE are in contact in the electroanalytical platforms and the electroactivity of the electrode. The interference of these solutions merits special attention because they can allow the development of redox reactions on the electrode's surface and negatively affects the performance of the SPCE-based sensors. Thus, the electrochemical mechanisms of charge transfer occurring at the interface electrode-electrolyte must be known in order to verify the possibility of using a SPCE for biosensing applications. In this work we evaluated the corrosion resistance of this material in electrolytic media representative of non-faradaic (0.1M KCl) and faradaic (0.1 M KCl containing 5 mM $K_3[Fe(CN)_6]/K_4[Fe(CN)_6]$) sensors.

4.3 MATERIALS AND METHODS

4.3.1 Chemicals

Potassium chloride was purchased from Fisher Chemical, sulfuric acid (98%) was acquired from Anachemia and both potassium ferricyanide and potassium ferrocyanide were purchased from Sigma Aldrich. All chemicals were of analytical grade and used as received with no additional purification. The solutions were prepared using ultrapure water (18.2 M Ω .cm resistivity at 20°C).

4.3.2 Apparatus

The SPCE (Pine Research Instruments, model RRPE1002C) consisted of a polyethylene terephthalate plastic base with dimensions of 15 mm x 61 mm x 0.36 mm, on which the working (4 mm x 5 mm) and auxiliary electrodes were made by carbon ink and the reference electrode was a deposit of Ag/AgCl.

4.3.3 Test solutions

The solutions were prepared with ultrapure deionized water. The corrosion media consisted of an aqueous solution of KCl at 0.1 M as supporting electrolyte and an aqueous solution of 0.1 M KCl containing 5 mM of $K_3[Fe(CN)_6]/K_4[Fe(CN)_6]$ as redox couple (herein named "redox solution"). The pH of both solutions was equal to 7.4 at 25°C and the tests were performed under air atmosphere with no stirring.

4.3.4 Characterization of the SPCE

Prior to any characterization, the SPCE was activated by cycling the potential from -2.5 to 2.5 V vs Ag/AgCl at $100 \text{ mV}\cdot\text{s}^{-1}$ in an aqueous solution of 0.05M H_2SO_4 as recommended by the manufacturer [41]. The combination of the cycled potential and the acidic medium is responsible for altering the chemical and morphological structure of the carbon ink. With this procedure, the electron transfer kinetics of the carbon in the matrix is accelerated because some organic binders are removed from the electrode surface during the pretreatment. Hence, this removal enhances the roughness of the SPCE surface, exposing more active carbon area to the electrolyte [38,41].

The surface morphology of the SPCE was characterized by Scanning Electron Microscopy (SEM) with a 5 kV acceleration voltage. Conductive Atomic Force Microscopy (CAFM) was carried out with a Tunneling AFM (TUNA) module and a tip covered with Pt/Ir to assess both topography and electrical conductance of the

electrode. Different test measurements were performed to define a threshold at which the spectra did not vary independently of the laser power. Moreover, a good indication of the non-alteration of the sample was the absence of visual modification on the surface after exposure to the laser beam.

Raman Spectroscopy was performed in a microscope equipped with a 50x objective (NA 0.75), giving an estimated laser spot of 1 μm in diameter. A backscattering geometry was used in the 830-1920 cm^{-1} and 2250-3100 cm^{-1} ranges, using an 1800 $\text{l}\cdot\text{mm}^{-1}$ grating. The spectra are the sum of five consecutive acquisitions of 5 s, and were acquired with a 633 nm (He-Ne) laser, using a power of 0.54 mW. Such a low power was necessary in order to obtain quality spectra without altering the sensitive sample.

4.3.5 Electrochemical tests

All the electrochemical measurements were carried out using a Princeton Applied Research VersaSTAT 3 potentiostat (Ametek Scientific Instruments) equipped with a frequency response analyzer module. The electrochemical stability of the SPCE immersed in the different media was inspected by monitoring the open circuit potential (OCP) during 1800 s at room temperature in the freely aerated media.

4.3.5.1 Cyclic Voltammetry (CV)

The electroactivity of the SPCE was examined by CV by scanning the potential from -1.0 to 1.0 V vs Ag/AgCl at 50 $\text{mV}\cdot\text{s}^{-1}$ in both KCl and redox solutions.

4.3.5.2 EIS characterization

EIS was performed over a frequency range from 100,000 to 0.025 Hz using a 10 mV rms potential amplitude. EIS data was recorded and modelled to an electrical

equivalent circuit using the ZView version 2.9b software from Scribner and Associates.

4.3.5.3 Potentiodynamic anodic polarization

Potentiodynamic anodic polarization was carried out to obtain polarization curves by scanning the potential from -20 mV to 250 mV vs OCP at a scan rate of 1 mV.s⁻¹.

4.3.5.4 Chronoamperometry

The evolution of the electrical current on the SPCE under a fixed potential was monitored over 60 min in both electrolyte conditions in order to accomplish a comprehensive analysis of the corrosion process involved at the interface of the electrode immersed in the different media. The above-mentioned monitoring time was determined based on the achievement of an equilibrium state, condition at which there was a negligible variation of the current in the first few minutes.

To perform the Chronoamperometry tests, the value of the applied potential was defined by means of the polarization plots as an intermediary value at the anodic branch in which the electrode was not active.

4.4 RESULTS AND DISCUSSION

4.4.1 Chemical and morphological characterization of the SPCEs

Figure 1 depicts the superficial structure of the SPCEs before and after treatment by CV. The electrochemical treatment in H₂SO₄ aqueous solution improves the electroactivity of the working electrode by removing non-conductive components from the ink without removing the graphite flakes from the surface [41]. The use of this

method is a recommendation of the manufacturer of the SPCE, which reported the previously mentioned effects of the CV treatment are reported [41].

The as-received electrode contained a disordered rough surface with notable wrinkles, in which the graphite flakes seemed to be covered by the polymeric ink as also reported in the literature [42,43]. After treating the electrode, the surface was rougher and more electroactive because of the activation of the graphite edge planes [41,44]. Fanjul-Bolado *et al.* [36], which studied the morphological and electrochemical characteristics of screen-printed and conventional carbon paste electrodes, found a similar structure in a commercial SPCE from DropSens. The authors reported that the randomly distributed graphite flakes into the ink matrix led to an arithmetic mean deviation of the average roughness profile (Ra) equal to 1.14 μm .

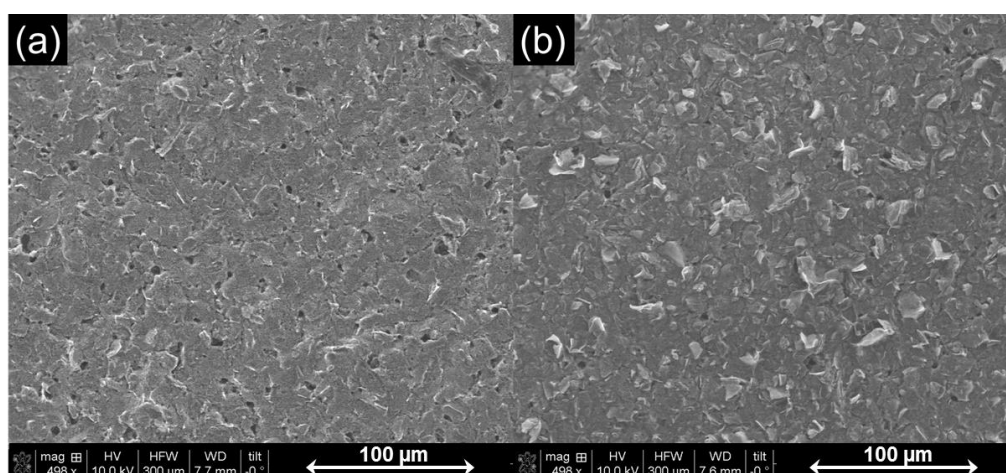


Figure 1 – SEM images of the SPCE before (a) and after (b) the activation of the surface using H_2SO_4

As it can be seen on the Figure 1b, the SPCE is composed of two distinct types of structures: one is bright composed of large crystals, and the other one is dark with respect to the ink matrix. To carefully analyze the surface of the electrode, Raman Spectroscopy technique have been used.

As the SPCE is made of carbon ink, we focused our study on the two principal carbon Raman regions: the first one ranging from 830 to 1900 cm^{-1} , and the second one in the 2400 to 3100 cm^{-1} spectral range. Figure 2 presents the Raman spectra of the bright (Figure 2a) and dark (Figure 2b) regions. The bright structures present an intense peak around 1580 cm^{-1} , called the G band which corresponds to the

stretching bond of rings and chains of sp^2 carbon atoms. The peak located at 1334 cm^{-1} is the D band corresponding to the breathing mode of rings [45]. By having a narrow and intense G band, and a rather small D band, we can safely assume that the bright structures are composed of graphite. Furthermore, Figure 3a indicates the presence of a sharp peak located at 2687 cm^{-1} and at 2466 cm^{-1} [46], confirming the presence of graphite.

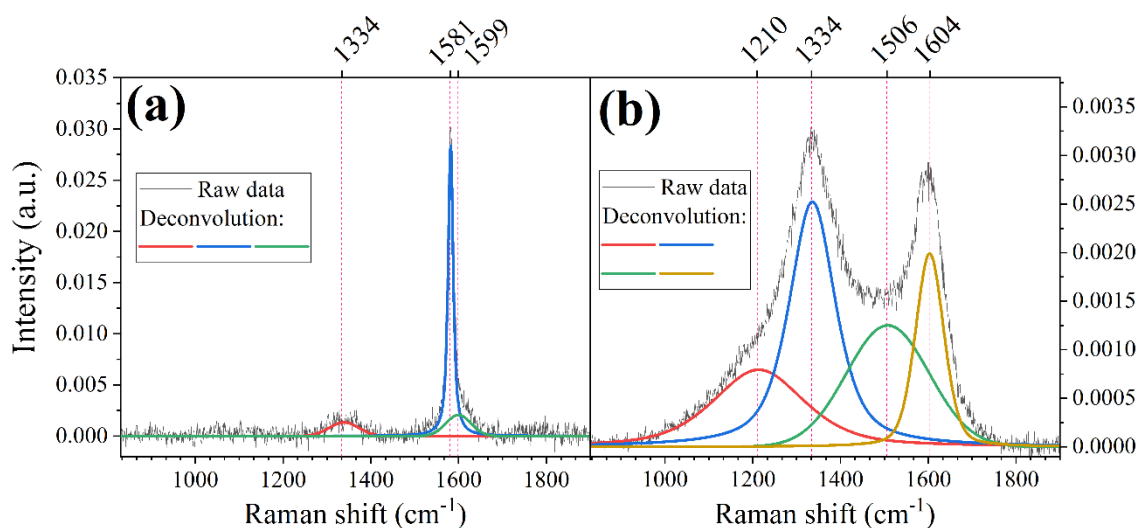


Figure 2 - Raman spectra of the SPCE sample in the range of $830 - 1900\text{ cm}^{-1}$ and their respective deconvolution curves for (a) the bright structures, and (b) the dark structures

Concerning the dark regions, Figure 2b presents a multitude of broad bands located at 1210 , 1334 , 1506 and 1604 cm^{-1} which are indicative of disorder amongst the sp^2 carbons. This disorder can be characteristic of quasi-amorphous sp^3 carbon. Another indication of the amorphous state of the dark region is the very low Raman signal of Figure 3b and the presence of a broad band located at 2918 cm^{-1} . Due to the presence of peaks at 2654 and 2689 cm^{-1} , we cannot dismiss the presence of sp^2 graphite carbon. Therefore, we can assume that the dark structures are composed of a mixture of two phases: sp^2 graphitic carbon and sp^3 amorphous carbon.

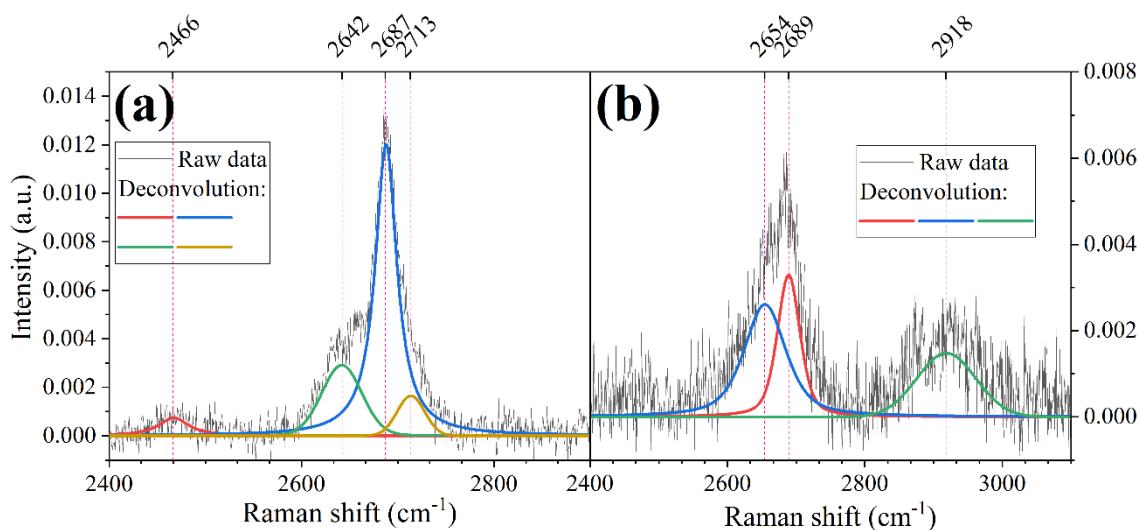


Figure 3 - Raman spectra of the SPCE sample in the range of 2400 - 3100 cm⁻¹ and their respective deconvolution curves for (a) the bright structures, and (b) the dark structures.

4.4.2 Electrochemical characterization

By applying the bias voltage between the SPCE and the conducting cantilever, it was possible to obtain the AFM images presented in Figure 4. The presence of graphite flakes previously observed in the SEM images corroborates the irregular topography of the SPCE revealed by AFM. As expected, the size scale of the regions identified as graphite flakes in Figure 1 (which was proved by Raman Spectroscopy) was different from the colored irregularities in Figure 4. This is because the current distribution on the surface is not restricted to the graphite particles. These flakes are the most (but not exclusive) conductive component in the SPCE, which implicates on the current flow along the whole surface. For the same reason and because of the qualitative character of the technique, it is not possible to precisely annotate the regions referring exclusively to the graphite flakes in the cAFM image. Thus, the cAFM result was not expected to reveal well limited regions arising from the graphite or any other component, but some with highlighted values of current due to the presence of graphite flakes (mainly due to the uncovered edges) and a less conductive matrix composed by the other ink components.

The rough surface of the electrode comprised spots with significant difference of current. This fact was likely due to the presence of ink binder that was not completely removed during the acid treatment. Moreover, the analysis of the current map in the same Figure 4 reiterate that the electroactivity of the SPCE arises from its graphite flakes, since the higher current values (around 4.1 nA) results from very localized spots in the higher regions. However, it is also notable the presence of regions with intermediary values of conductivity (represented in yellow) in a significant portion of the surface, possibly due to the conductive contribution of the amorphous sp^3 carbon phase recognized by Raman spectroscopy.

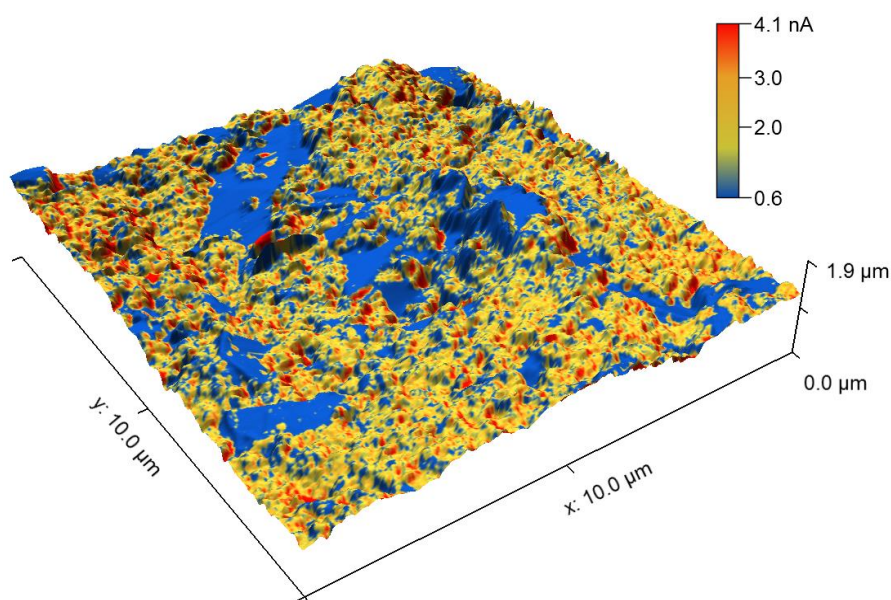


Figure 4 - Topographic image from AFM conductive test referring to the distribution of electrical current over the surface of the SPCE

Regarding to the electroactivity of the SPCE, the cyclic voltammogram presented in Figure 5 shows the presence of an irreversible cathodic peak at -0.44 V vs Ag/AgCl related to the exposure to KCl. An electrochemical system is called irreversible when the reaction rate in the forward direction (ν_{\rightarrow}^*) is negligible compared to the backward direction (ν_{\leftarrow}^*) or *vice-versa* [47]. Accordingly and as shown in Figure 5, since one can assume the validity of the relation $\nu_{\rightarrow}^* \gg \nu_{\leftarrow}^*$, the overall reaction rate (ν^*) is practically equal to the rate of the anodic direction (

$v^* \approx v_{\rightarrow}^*$), which causes the development of an asymmetric plot in the cyclic voltammogram. Considering the results obtained by Slate *et al.* [48] that indicated the absence of observable redox peaks of different graphitic electrodes immersed in 0.1M KCl, the presence of the mentioned cathodic peak possibly arises from the irreversible reduction of the oxygen atoms from functional groups of graphene oxide [49,50].

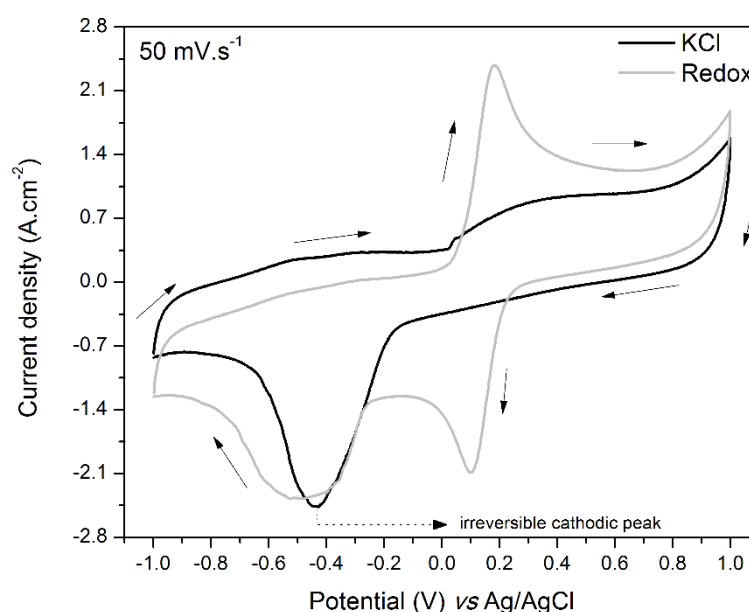
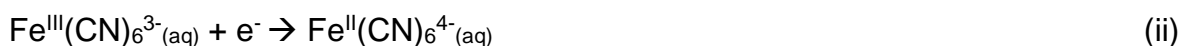


Figure 5 - Cyclic voltammogram of the SPCE immersed in KCl and redox solutions under a potential ranging from -1.0 to 1.0 V vs Ag/AgCl at 50 mV.s⁻¹

The slow charge transfer kinetics of the electrode in KCl solution restricts the use of the SPCE in sensing platforms in the absence of a redox pair. Accordingly, this material seems to be more amenable for non-faradaic sensors or in platforms where the electro active species are present in the electrolyte. Concerning to its potential window though, Morrin *et al.* [51] cited that the narrow potential presented by carbon inks is not necessarily a determinant point to avoid the use of these material in electrochemical sensing, because amperometric measurements are usually performed after achieving the steady state condition, which means that the sensing is not significantly affected by transient currents. Contrarily, the presence of potassium ferrocyanide and potassium ferricyanide led to the development of a faradaic current responsible for the formation of the additional anodic (at 0.18 V vs Ag/AgCl) and

cathodic (at 0.10 V vs Ag/AgCl) peaks relative to the respective half-reactions (i) and (ii) as follows [52-54]:



The peak-to-peak separation (ΔE_p), which is defined as the difference between the potential of the anodic peak (E_{pa}) and the potential of the cathodic peak (E_{pc}) [54], was equal to 80 mV in the presence of the redox couple. According to the literature [36,54,55] the ΔE_p is equal to 57 mV at 298 K for electrochemically reversible processes. Elgrish *et al.* [54] describe the reversibility as an indicative of the capability of the electro active species to reduce at the electrode and be subsequently reoxidized. In case of high barrier to the electron transfer, the process is irreversible and demands higher energy (potential) to suffer the reverse electrochemical reaction, enlarging the ΔE_p . Accordingly, there is a difference between the observed ΔE_p in figure 5 and 57 mV expected from a reversible fast one-electron reaction according to the Nernst equation. Furthermore, the ratio between the modulus of the anodic current peak (I_{pa}) and cathodic current peak (I_{pc}) was 1.1, which indicates a quasireversible behavior [55]. Despite close to the unity, the fact that it did not completely follow the Nernstian condition, as expected from a redox $\text{Fe}^{\text{III}}/\text{Fe}^{\text{II}}$ couple at the equilibrium, is associated to heterogeneous process of electron transfer due to the presence of the binder in the SPCE, which hinders the electron transfer and, consequently, impacts on its electroactivity [36,56-58].

Before performing the EIS tests to further characterize the electrode, the variation of the OCP was monitored owing to an Ag/AgCl reference during 1800 s in order to monitor the electrochemical stability of the electrolyte immersed in KCl and redox solutions. Another reason for monitoring the OCP was the achievement of the equilibrium before performing the EIS aiming to evaluate the changes in the impedance spectra exclusively around the equilibrium potential. As a criterion to achieve this condition, the EIS was performed only after the electrode presented a variation of OCP less than 10 mV in 300 s. As seen in Figure 6, in the last 300 s of

the monitoring, the SPCE exhibited a variation of OCP equal to 3 mV when immersed in KCl and 7 mV in the redox solution.

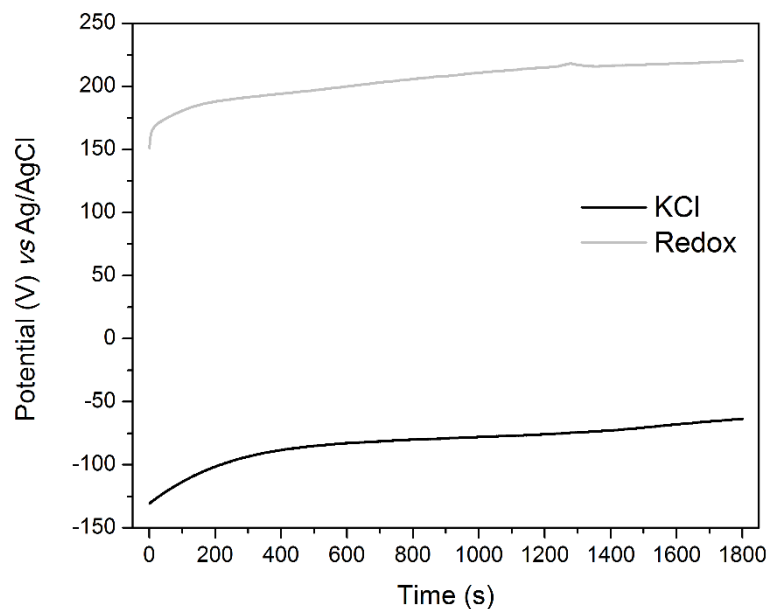


Figure 6 - OCP variation as a function of time with respect to the SPCE immersed in KCl and redox solutions

Afterwards, the recorded EIS data was modelled to an electrical equivalent circuit in order to better interpret the characteristics of the SPCE immersed in the different media. According to the spectra presented in Figure 7, the KCl was less aggressive to the carbon than the redox solution. This fact is notable due to the higher magnitude of impedance ($|Z|$) and phase angle ($-\phi$) related to the KCl in Figure 7a in comparison to both parameters referring to the redox plot in Figure 7b.

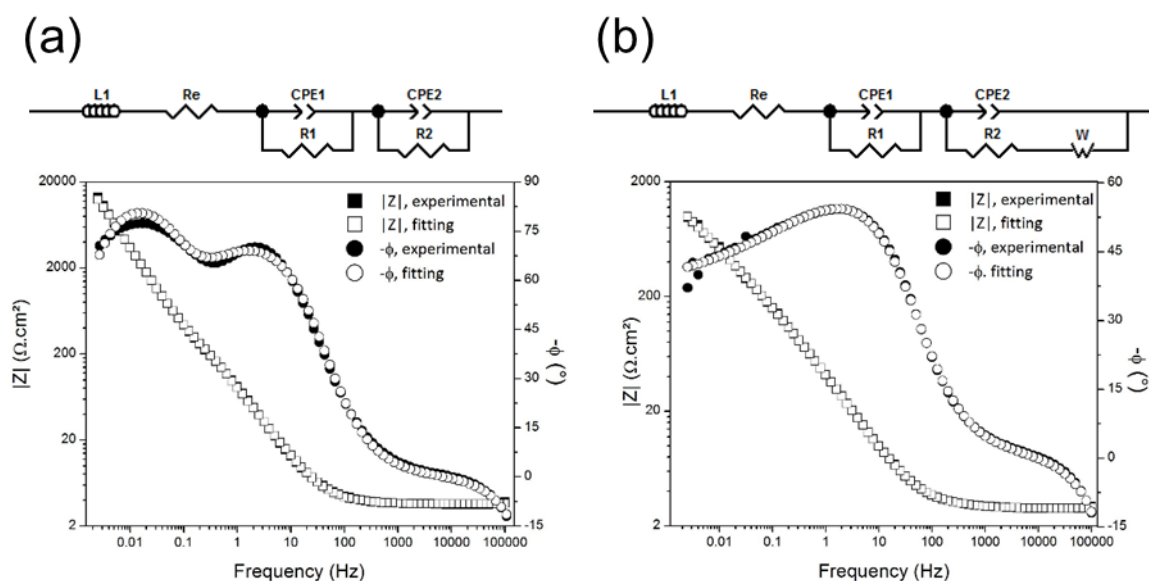


Figure 7 - Equivalent circuits used to fit EIS data and respective Bode plots referring to the SPCE obtained in KCl (a) and redox solutions (b)

The equivalent circuit consisted of an arrangement of resistive, capacitive and inductive elements as seen in Figure 7. The fitting quality was ensured by the low values of the statistical parameter chi-squared (χ^2) which was approximately equal to 10^{-4} in agreement with the criterion adopted in the literature [59-62]. In the Bode plots of the same figure, it is possible to verify that the experimental and fitting curves are practically superimposed, corroborating the equivalence of the proposed electrical circuit to the electrochemical system under investigation. A Warburg impedance (Z_W) was included in Figure 7b to represent the impedance to the diffusion of the electroactive probe from the bulk solution to the interface with the electrode. The Warburg element represents the resistance to the mass transfer process associated to the diffusion layer of the ions $[\text{Fe}(\text{CN})_6]^{3-/4-}$ from the bulk solution to the electrode surface [62]. This special type of impedance is expressed as a function of the radial frequency (ω) and the Warburg coefficient (σ_W), which is related to the initial concentrations of the oxidized (c_{ox}^0) and reduced (c_{red}^0) species as well as their respective diffusion coefficients D_{ox} and D_{red} according to Equations 6 and 7 [63]. In the equation, T is the temperature, R is the universal gas constant, z_e is the electron charge and F is the Faraday constant.

$$Z_W = \sigma \omega^{-0.5} - j\sigma \omega^{-0.5} \quad (6)$$

$$\sigma = \left(\frac{1}{2^{0.5}} \right) \left[\frac{RT}{z_e F} \right]^2 \left(\frac{1}{C_{ox}^0 D_{ox}^{0.5}} + \frac{1}{C_{red}^0 D_{red}^{0.5}} \right) \quad (7)$$

In the circuit, the inductor represents the effect of wires/cables of the equipment at high frequencies as commonly observed in the literature [64,65]. The constant phase element (CPE) corresponds to the double layer capacitance on the interface electrode/electrolyte and its use instead a capacitor refers to the non-ideality of the surface. This behavior occurs due to the electrode roughness and/or the dispersion of the capacitance because of the presence of ions slowly adsorbed on the surface as well as its heterogeneous chemical composition [66]. The CPE is related to the depression of the semicircle in the Nyquist plot and its impedance (Z_{CPE}) is described by Equation 8, in which Q arises from the magnitude of Z_{CPE} in $\Omega \cdot \text{cm}^2 \cdot \text{s}^{-n}$, j is the imaginary number $\sqrt{-1}$ and “ n ” is the constant phase whose value can vary from 0 to -1 [67].

$$Z_{CPE} = \frac{1}{Q(j\omega)^n} \quad (8)$$

Independently of the evaluated medium, the SPCE presented two time constants one at high frequencies represents the pair R1/CPE1 and the other at low frequencies (R2/CPE2). The use of these two resistor-capacitor pairs to model the EIS data consider the two regions with different current distribution verified in the conductive AFM images. The first time constant perhaps refers to the ink portion of the SPCE containing the amorphous sp^3 carbon atoms and the second one is probably related to the interface with the conductive graphite flakes.

4.4.3 Corrosion tests

Polarization plots referring to the SPCE exposed to the KCl and redox media are presented in Figure 8 and Table 2 contains the values related to the E_{corr} and j_{corr} parameters. Overall, despite the redox solution shifted the E_{corr} (parameter that indicates the corrosion insusceptibility) to nobler potentials, the tests conducted in KCl represented a shift of j_{corr} to lower values indicating that the SPCE is less affected by this electrolyte than by the redox solution in agreement with the EIS results. One attributes this behavior to the development of the oxidation and reduction reactions throwing electrons from the conductive electrode surface and, thus, increase the current density on the interface with the electrolyte.

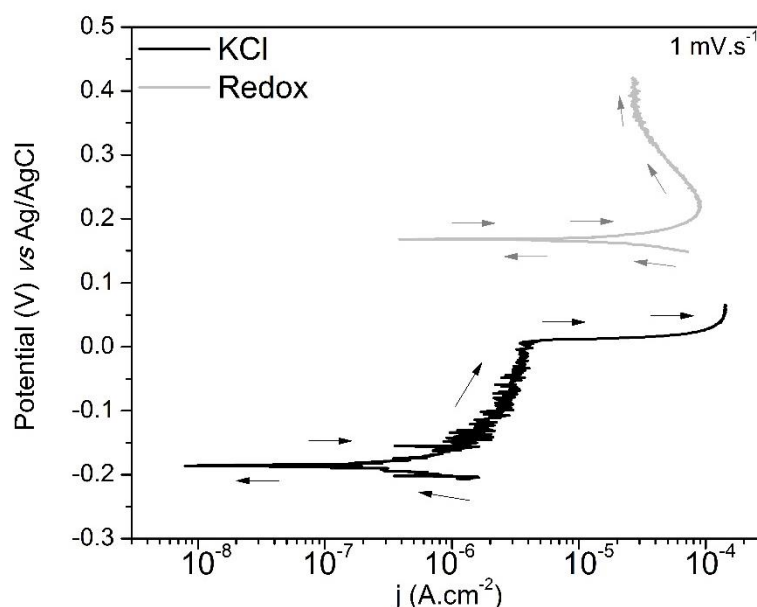


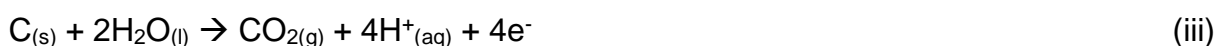
Figure 8 - Polarization plots of the SPCE in KCl and redox solutions

Table 2 - Parameters estimated from the method of potentiodynamic anodic polarization with respect to the SPCE in KCl and redox solutions

Parameter	KCl	Redox
E_{corr} (mV) vs Ag/AgCl	-167.7 ± 25.1	151.7 ± 18.0
j_{corr} ($\mu\text{A}\cdot\text{cm}^{-2}$)	1.5 ± 0.4	147.9 ± 17.2

The corrosion mechanism seemed to be different in each medium. In KCl, a sudden increase of the potential at approximately 10^{-6} A.cm⁻² suggests the passivation of graphite extending from -0.173 to 0.01 V vs Ag/AgCl. Then, the further increase of the potential caused an abrupt increase of the current probably in reason of the attack of chloride ions in defective areas of the passive film leading to the breakdown of this layer and occurrence of pitting corrosion. In contrast, the passive region is not clearly observable in redox solution probably because the carbon suffered continuous oxidation in the presence of the active redox species with the increasing potential, leading to a mechanism of generalized corrosion.

According to its Pourbaix Diagram [68], carbon is thermodynamically stable in an aqueous medium at pH 7.4. However, the scanning of the potential toward higher values provokes the oxidation of carbon to form carbon dioxide as described in the reaction iii [69].



In an aerated near-neutral pH medium, the cathodic reaction takes place on the edges of the graphite structure, on its defects and grain boundaries causing the reduction of dissolved O₂ gas [67] according to reaction iv:



The stability of the SPCE was examined during 60 min by Chronoamperometry under a fix polarization potential related to the middle of the passive region for KCl (-77.6 mV vs Ag/AgCl) and the middle of the anodic branch for the redox solution (349.6 mV vs Ag/AgCl). The chemical stability of a material is a crucial feature to elect an electrochemical transducer for sensors because the occurrence of certain redox reactions can affect its performance, sensibility, reproducibility and service life [70].

Figure 9 exhibits the variation of the current density of the electrode immersed in each medium as a function of the time. In both conditions, there was a rapid and sharp decrease of the current in few seconds followed by the achievement of a

quasi-steady state. The higher current density with respect to the redox solution indicates the occurrence of a large amount of charge transfer processes at the interface electrode/electrolyte. These reactions occurs because of the $\text{Fe}(\text{CN})_6^{3-}$ and $\text{Fe}(\text{CN})_6^{4-}$ ions from the solution that interact with the SPCE in a mechanism of electron transfer owing to the enhancement of the overall current. The chronoamperometric plot related to the redox solution experimented later stabilization (the KCl plot reached the current stabilization after approximately 3 minutes, and the redox plot after 45 minutes). Accordingly, the chronoamperometry results indicated that, despite the redox solution presented a higher impact on the electrochemical behavior of the SPCE, in both electrolytes the electrode achieved an equilibrium state. Thus, it is possible to presume that the SPCE is a promising candidate as an electrochemical matrix to both faradaic and non-faradaic sensors

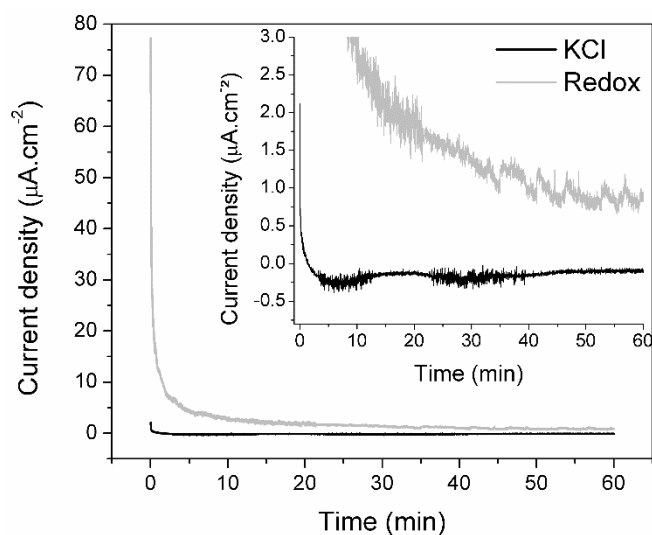


Figure 9 - Chronoamperometry plots of the SPCEs polarized in KCl and redox solutions. The inset is an amplification of the graphic up to $3.0 \mu\text{A}\cdot\text{cm}^{-2}$

4.5 CONCLUSIONS

The chemical, morphological and electrical characteristics of SPCE were studied in order to evaluate its employability as a transducer material in electrochemical sensors. To simulate the environment referring to faradaic and non-faradaic sensors,

solutions of 0.1 M KCl and 0.1 M KCl + 5 mM $K_3[Fe(CN)_6]/K_4[Fe(CN)_6]$ were prepared. The corrosion mechanism of the SPCE in both solutions was elucidated in order to evaluate the impact of these electrolytes in the electrochemical behavior of the transducer electrode. The SPCE contained an irregular surface comprised of a carbon ink with local dispersions of graphite flakes. The Raman spectra of the SPCE indicate the presence of graphite in the bright flakes observed by SEM, containing peaks referring to the G band (1580 cm^{-1}) of sp^2 carbon atoms and the D band (1334 cm^{-1}) concerning its breathing mode of rings. The multiple peaks associated to the dark region of the SEM image indicated the major presence of disordered amorphous structure of sp^3 carbon but also the presence of the sp^2 graphitic phase. The graphitic regions represented the most conductive area of the surface, which presupposes the possibility of its use in electrochemical devices. Regarding the evaluated electrolytes, EIS and potentiodynamic anodic polarization indicated the KCl as the less aggressive medium to the electrode. Under the influence of this solution, the SPCE experimented localized corrosion passing through the growing of a protective passive layer and a subsequent breakdown point at high anodic potentials in comparison with its E_{corr} . Contrary, the additional presence of $K_3[Fe(CN)_6]/K_4[Fe(CN)_6]$ caused the development of the redox reactions of the iron from the solution by means of the electron availability on the carbon matrix leading to a condition of generalized corrosion. Finally, Chronoamperometry tests suggested the great stability of the SPCE in both electrolytic media up to 60 minutes, when low variation of the current density was observed. Therefore, we credited the increasing use of SPCE as an electrochemical transducer substrate in faradaic and non-faradaic sensors not simply to its low cost, miniaturized dimensions and easiness of fabrication as reported in the literature but mainly to the features inspected in this work (great current distribution on its surface, composition and stability in both KCl and redox solution).

4.6 REFERENCES

[1] JADON, N; JAIN, R.; SHARMA, S.; SINGH, K. Recent trends in electrochemical sensors for multianalyte detection - a review. **Talanta**, 161, p. 894-916, 2016.

- [2] GRIESHABER, D.; MACKENZIE, R.; VÖRÖS, J.; REIMHULT, E. Electrochemical biosensors - sensor principles and architectures. **Sensors**, 8, p. 1400-1458, 2008.
- [3] ROTARIU, L.; LAGARDE, F.; JAFFREZIC-RENAULT, N.; BALA, C. Electrochemical biosensors for fast detection of food contaminants - trends and perspective. **Trends in Analytical Chemistry**, 79, p. 80-87, 2016.
- [4] HARRAZ, F. A.; FAISAL, M.; ISMAIL, A. A.; AL-SAYARI, S. A.; AL-SALAMI, A. E.; AL-HAKRY, A.; AL-ASSIRI, M. S. TiO₂/reduced graphene oxide nanocomposite as efficient ascorbic acid amperometric sensor. **Journal of Electroanalytical Chemistry**, 832, p. 225-232, 2019.
- [5] MACCAFERRI, G.; TERZI, F.; XIA, Z.; VULCANO, F.; LISCIIO, A.; PALERMO, V.; ZANARDI, C. Highly sensitive amperometric sensor for morphine detection based on electrochemically exfoliated graphene oxide. Application in screening tests of urine samples. **Sensors and Actuators B: Chemical**, 281, p. 139-745, 2019.
- [6] PANRAKSA, Y.; SIANGPROH, W.; KHAMPIENG, T.; CHAILAPAKUL, O.; APILUX, A. Paper-based amperometric sensor for determination of acetylcholinesterase using screen-printed graphene electrode. **Talanta**, 178, p. 1017-1023, 2018.
- [7] ALIZADEH, T.; NAYERI, S.; MIRZAEI, S. A high performance potentiometric sensor for lactic acid determination based on molecularly imprinted polymer/MWCNTs/PVC nanocomposite film covered carbon rod electrode. **Talanta**, 192, p. 103-111, 2019.
- [8] BELIKOVA, V.; PANCHUK, V.; LEGIN, E.; MELENTEVA, A.; KIRSANOV, D.; LEGIN, A. Continuous monitoring of water quality at aeration plant with potentiometric sensor array. **Sensors and Actuators B: Chemical**, 282, p. 854-860, 2019.
- [9] ELBAKINY, H. T.; YEHIA, A. M.; RIAD, S. M.; ELSAHARTY, Y. S. Potentiometric diclofenac detection in wastewater using functionalized nanoparticles. **Microchemical Journal**, 145, p. 90-95, 2019.
- [10] LI, Y.; SONG, Z.; LI, Y.; CHEN, S.; LI, S.; LI, Y.; WANG, H.; WANG, Z. Hierarchical hollow MoS₂ microspheres as materials for conductometric NO₂ gas sensors. **Sensors and Actuators B: Chemical**, 282, p. 259-267, 2019.
- [11] LIANG, J.; WANG, J.; ZHANG, L.; WANG, S.; YAO, C.; ZHANG, Z. Conductometric immunoassay of alpha-fetoprotein in sera of liver cancer patients using bienzyme-functionalized nanometer-sized silica beads. **Analyst**, 144, p. 265-273, 2019.
- [12] LATIF, U.; PING, L.; DICKERT, F. L. Conductometric sensor for PAH detection with molecularly imprinted polymer as recognition layer. **Sensors**, 18, p. 767, 2018.

- [13] SACCO, A. Electrochemical impedance spectroscopy: fundamentals and application in dye-sensitized solar cells. **Renewable and sustainable energy reviews**, 79, p. 814-829, 2017.
- [14] BAHADIR, E. B.; SEZGINTÜRK, M. K. A review on impedimetric biosensors. *Artificial Cells. Nanomedicine. and Biotechnology*, 44, p. 248-262, 2016.
- [15] PARK, J. S.; KIM, H. J.; LEE, J. H.; PARK, J. H.; KIM, J.; HWANG, K. S.; LEE, B. C. Amyloid beta detection by faradaic electrochemical impedance spectroscopy using interdigitated microelectrodes. **Sensors**, 18, p. 426, 2018.
- [16] HAMMOND, J. L.; FORMISANO, N.; ESTRELA, P.; CARRARA, S.; TKAC, J. Electrochemical biosensors and nanobiosensors. **Essays in Biochemistry**, 60, p. 69-80, 2016.
- [17] DANIELS, J. S.; POURMAND, N. Label-free impedance biosensors: opportunities and challenges. **Electroanalysis**, 19, p. 1239-1257, 2007.
- [18] POSSECKARDT, J.; SCHIRMER, C.; KICK, A.; REBATSCHKE, K.; LAMZ, T.; MERTIG, M. Monitoring of *Saccharomyces cerevisiae* viability by non-Faradaic impedance spectroscopy using interdigitated screen-printed platinum electrodes. **Sensors and Actuators B: Chemical**, 255, p. 3417-3424, 2018.
- [19] KASHYAP, D.; DWIVEDI, P. K.; PANDEY, J. K.; KIM, Y. H.; SHARMA, A.; GOEL, S. Application of electrochemical impedance spectroscopy in bio-fuel cell characterization: a review. **Journal of Hydrogen Energy**, 39, p. 20159-20170, 2014.
- [20] FARIA, R. A. D.; LINS, V. F. C.; NAPPI, G. U.; MATENCIO, T.; HENEINE, L. G. D. Development of an impedimetric immunosensor for specific detection of snake venom. **BioNanoScience**, 8, p. 988-996, 2018.
- [21] KITTE, S. A.; GAO, W.; ZHOLUDOV, Y. T.; QI, L.; NSABIMANA, A.; LIU, Z.; XU, G. Stainless steel electrode for sensitive luminol electrochemiluminescent detection of H₂O₂ glucose and glucose oxidase activity. **Analytical Chemistry**, 89, p. 9864-9869, 2017.
- [22] CANBAZ, M. Ç.; SEZGINTÜRK, M. K. Fabrication of a highly sensitive disposable immunosensor based on indium tin oxide substrates for cancer biomarker detection. **Analytical Biochemistry**, 446, p. 9-18, 2013.
- [23] TURCO, A.; CORVAGLIA, S.; MAZZOTTA, E. Electrochemical sensor for sulfadimethoxine based on molecularly imprinted polypyrrole: study of imprinting parameters. **Biosensors and Bioelectronics**, 63, p. 240-247, 2015.
- [24] WANG, Y.; JIN, J.; YUAN, C.; ZHANG, F.; MA, L.; QIN, D.; SHAN, D.; LU, X. A novel electrochemical sensors based on zirconia/ordered macroporous polyaniline for ultrasensitive detection of pesticides. **Analyst**, 140, p. 560-566, 2015.

- [25] FAISAL, M.; HARRAZ, F. A.; AL-SALAMI, A. E.; AL-SAYARI, S. A.; AL-HAJRY, S. A.; AL-ASSIRI, A. Polythiophene/ZnO nanocomposite-modified glassy carbon electrode as efficient electrochemical hydrazine sensor. **Materials Chemistry and Physics**, 214, p. 126-134, 2018.
- [26] BHALLA, N.; JOLLY, P.; FORMISANO, N.; ESTRELA, P. Introduction to biosensors. **Essays in Biochemistry**, 60, p. 1-8, 2016.
- [27] ZHAO, Y.; LAWRIE, J. L.; BEAVERS, K. R.; LAIBINIS, P. E.; WEISS, S. M. Effect of DNA-induced corrosion on passivated porous silicon biosensors. **ACS Applied Materials & Interfaces**, 6, p. 13510-13519, 2014.
- [28] GLOGENER, P.; KRAUSE, M.; KATZER, J.; SCHUBERT, M. A.; BIRKHOLZ, M.; BELLMANN, O.; KRÖGER-KOCH, C.; HAMMON, H. M.; METGES, C. C.; WELSCH, C.; RUFF, R.; HOFFMANN, K. P. Prolonged corrosion stability of a microchip sensor implant during in vivo exposure. **Biosensors**, 8, p. 1-11, 2018.
- [29] BELTRAMI, L. V. R.; KUNST, S. R.; BIRRIEL, E. J.; Malfatti, C. F. Magnetoelastic biosensors: corrosion protection of an FeNiMoB alloy from alkoxide precursors. **Thin Solid Films**, 624, p. 83-94, 2017.
- [30] CHAIYO, S.; MEHMETI, E.; ZAGAR, K.; SIANGPROH, W.; CHAILAPAKUL, O.; KALCHER, K. Electrochemical sensors for the simultaneous determination of zinc, cadmium and lead using a Nafion/ionic liquid/graphene composite modified screen-printed carbon electrode. **Analytica Chimica Acta**, 918, p. 26-34, 2016.
- [31] MURTADA, K.; JODEH, S.; ZOUGAGH, M.; RÍOS, Á. Development of an Aluminium Doped TiO₂ Nanoparticles-modified Screen Printed Carbon Electrode for Electrochemical Sensing of Vanillin in Food Samples. **Electroanalysis**, 30, p. 969-974, 2018.
- [32] NICHOLAS, P.; PITTSOON, R.; HART, J. P. Development of a simple low cost chronoamperometric assay for fructose based on a commercial graphite-nanoparticle modified screen-printed carbon electrode. **Food Chemistry**, 241, p. 122-126, 2018.
- [33] SHIM, K.; KIM, J.; SHAHABUDDIN, M.; YAMAUCHI, Y.; HOSSAIN, M. S. A.; KIM, J. H. Efficient wide range electrochemical bisphenol-A sensor by self-supported dendritic platinum nanoparticles on screen-printed carbon electrode. **Sensors and Actuators B: Chemical**, 255, p. 2800-2808, 2018.
- [34] FARIA, R. A. D.; MESSADDEQ, Y.; HENEINE, L. G. D.; MATENCIO, T. Application of screen-printed carbon electrode as an electrochemical transducer in biosensors. **International Journal of Biosensors & Bioelectronics**, 5, p. 1-2, 2019.
- [35] TALEAT, Z.; KHOSHROO, A.; MAZLOUM-ARDAKANI, M. Screen-printed electrodes for biosensing: a review (2008-2013). **Microchimica Acta**, 181, p.865-891, 2014.

[36] FANJUL-BOLADO, P.; HERNÁNDEZ-SANTOS, D.; LAMAS-ARDISANA, P. J.; MARTÍN-PERNÍA, A.; COSTA-GARCÍA, A. Electrochemical characterization of screen-printed and conventional carbon paste electrodes. **Electrochimica Acta**, 53, p. 3635-3642, 2008.

[37] SÝS, M.; KHALED, E.; METELKA, R.; VYTRÁS, K. Electrochemical characterization of novel screen-printed carbon paste electrodes for voltammetric measurements. **Journal of the Serbian Chemical Society**, 82, p. 865-877, 2017.

[38] FARIA, R. A. D.; IDEN, H.; BHARUCHA, E.; LINS, V. F. C.; MESSADDEQ, Y.; MATENCIO, T.; HENEINE, L. G. D. A new tool for the detection of horsemeat adulteration in raw meat. **Journal of Biosensors and Bioelectronics**, 9, p. 1-7, 2018.

[39] MAZZARACCHIO, V.; TOMEI, M. R.; CACCIOTTI, I.; CACCIOTTI, I.; CHIODONI, A.; NOVARA, C.; CASTELLINO, M.; SCORDO, G.; AMINE, A.; MOSCONE, D.; ARDUINI, F. Inside the different types of carbon black as nanomodifiers for screen-printed electrodes. **Electrochimica Acta**, 317, p. 673-683, 2019.

[40] WANG, J.; XU, Z.; ZHANG, M.; LIU, J.; ZOU, H.; WANG, L. Improvement of electrochemical performance of screen-printed carbon electrodes by UV/ozone modification. **Talanta**, 192, p. 40-45, 2019.

[41] PINE RESEARCH. **Screen-printed electrode information**. Carbon and ceramic electrode information, pine research, 2016, document DRP 10036, <https://www.pineresearch.com/shop/wp-content/uploads/sites/2/2016/10/DRP10036-Screen-Printed-ElectrodesOverview REV001>, accessed in Jan. 2019.

[42] RANDVIIR, E. P.; BROWNSON, D. A. C.; METTERS, J. P.; KADARA, R. O.; BANKS, C. E. The fabrication, characterization and electrochemical investigation of screen-printed grapheme electrodes. **Physical Chemistry Chemical Physics**, 16, p. 4598-4611, 2014.

[43] YANG, X.; WU, F.; CHEN, D. Z.; LIN, H. W. An electrochemical immunosensor for rapid determination of clenbuterol by using magnetic nanocomposites to modify screen printed carbon electrode based on competitive immunoassay mode. **Sensors and Actuators B: Chemical**, 192, p. 529-535, 2014.

[44] MARTÍN-YERGA, D.; RAMA, E. C.; COSTA-GARCÍA, A. Electrochemical characterization of ordered mesoporous carbon screen-printed electrodes. **Journal of the Electrochemical Society**, 163, p. 176-179, 2016.

[45] FERRARI, A. C. Raman spectroscopy of graphene and graphite: Disorder, electron-phonon coupling, doping and nonadiabatic effects. **Solid State Communications**, 143, 2007.

[46] SHIMADA, T.; SUGAI, T.; FANTINI, C.; SOUZA, M.; CANÇADO, L. G.; JORIO, A.; PIMENTA, M. A.; SAITO, R.; GRÜNEIS, A.; DRESSELHAUS, G.;

DRESSELHAUS, M. S.; OHNO, Y.; MIZUTANI, T.; SHINOHARA, H. Origin of the 2450 cm^{-1} Raman bands in HOPG, single-wall and double-wall carbon nanotubes. **Carbon**, 43, p. 1049-1054, 2005.

[47] LEFROU, C.; FABRY, P.; POIGNET, J. C. **L'électrochimie – Fondamentaux avec exercices corrigés**. EDP Sciences, Grenoble Sciences' collection, 2009. ISBN 978-3-642-30249-7.

[48] SLATE, A. J.; BROWNSON, D. A. C.; DENA, A. S. A.; SMITH, G. C.; WHITEHEAD, K. A.; BANKS, C. E. Exploring the electrochemical performance of graphite and graphene paste electrodes composed of varying lateral flake sizes. **Physical Chemistry Chemical Physics**, 20, p. 20010-20022, 2018.

[49] AMBROSI, A.; CHUA, C. K.; BONANNI, A.; PUMERA, M. Electrochemistry of graphene and related materials. **Chemical Reviews**, 114, p. 7150-7188, 2014.

[50] QIAO, M. X.; ZHANG, Y.; ZHAI, L. F.; SUN, M. Corrosion of graphite electrode in electrochemical advanced oxidation processes: degradation protocol and environmental implication. **Chemical Engineering Journal**, 344, p. 410-418, 2018.

[51] MORRIN, A.; KILLARD, A. J.; SMYTH, M. R. Electrochemical characterization of commercial and home-made screen-printed carbon electrodes. **Analytical Letters**, 36, p. 2021-2039, 2003.

[52] HUANG, B.; MUY, S.; FENG, S.; KATAYAMA, Y.; LU, Y. C.; CHEN, G.; SHAO-HORN, Y. Non-covalent interactions in electrochemical reactions and implications in clean energy applications. **Physical Chemistry Chemical Physics**, 20, p.15680-15686, 2018.

[53] NIU, W. J.; ZHU, R. H.; COSNIER, S.; ZHANG, X. J.; SHAN, D. Ferrocyanide-ferricyanide redox couple induced electrochemiluminescence amplification of carbon dots for ultrasensitive sensing of glutathione. **Analytical Chemistry**, 87, p.11150-11156, 2015.

[54] ELGRISHI, N.; ROUNTREE, K. J.; MCCARTHY, B. D.; ROUNTREE, E. S.; EISENHART, T. T.; DEMPSEY, J. L. A practical beginner's guide to cyclic voltammetry. **Journal of Chemical Education**, 95, p.197-206, 2018.

[55] VRANOVIČOVÁ, B.; VATRÁL, J.; BOČA, R. Correlation of electrochemical parameters for the redox couple Fe(III)/Fe(II) in the presence of amino acids and catecholamines. **Journal of Electroanalytical Chemistry**, 860, p. 113920, 2020.

[56] WANG, J.; TIAN, B.; NASCIMENTO, V. B.; ANGNES, L. Performance of screen-printed carbon electrodes fabricated from different carbon inks. *Electrochimica Acta*, 43, p. 3459-3465, 1998.

[57] KLINGLER, R.J.; KOCHI, J.K. Electron-transfer kinetics from cyclic voltammetry. Quantitative description of electrochemical reversibility. **The Journal of Physical**

Chemistry, 85, p. 1731–1741, 1981.

[58] SANDFORD, C.; EDWARDS, M.A.; KLUNDER, K.; HICKEY, D.P.; LI, M.; BARMAN, K.; SIGMAN, M.S.; WHITE, H.S.; MINTEER, S. A Synthetic Chemist's Guide to Electroanalytical Tools for Studying Reaction Mechanisms. *Chemical Science*, 10, p. 6404-6422, 2019.

[59] FAN, L.; TANG, F.; REIS, S. T.; CHEN, G.; KOENIGSTEIN, M. L. Corrosion resistances of steel pipes internally coated with enamel. *Corrosion*, 73, p. 1335-1345, 2017.

[60] GARCIA-CABEZON, C.; MARTIN-PEDROSA, F.; BLANCO-VAL, Y.; RODRIGUEZ-MENDEZ, M. L. Corrosion properties of a low-nickel austenitic porous stainless steel in simulated body fluids. *Corrosion*, 74, p.683-693, 2018.

[61] FARIA, R. A. D.; IDEN, H.; HENEINE, L. G. D.; MATENCIO, T.; MESSADDEQ, Y. Non-enzymatic impedimetric sensor based on 3-aminophenylboronic acid functionalized screen-printed carbon electrode for highly sensitive glucose detection. *Sensors*, 19, p. 1686, 2019.

[62] HELALI, S.; ALATAWI, A. S.; ABDELGHANI, A. Pathogenic *Escherichia coli* biosensor detection on chicken food samples. *Journal of Food Safety*, e12510, 2018.

[63] WOLYNEC, S. **Técnicas eletroquímicas em corrosão**. Edusp, Editora da Universidade de São Paulo. São Paulo, 2003.

[64] BOZZINI, B.; MELE, C.; SGURA, I. On the observation of inductive high-frequency impedane behaviour during the electrodeposition of Au-Sn alloys. *Journal of applied electrochemistry*, 34, p. 277-281, 2004.

[65] PHAM, K. C.; MCPHAIL, D. S.; MATTEVI, C.; WEE, A. T. S.; CHUA, D. H. Graphene-carbon nanotube hybrids as robust catalyst supports in proton exchange membrane fuel cells. *Journal of the electrochemical society*, 163, p. 255-263, 2016.

[66] LASIA, A. Electrochemical Impedance Spectroscopy and Its Applications. In: **Modern Aspects of Electrochemistry**, B. E. Conway, J. Bockris, and R.E. White, Edts, Kluwer Academic/Plenum Publishers (New York, USA), p. 143-248, 1999.

[67] ENSAFI, A. A.; JAMEI, H. R.; HEYDARI-BAFROOEI, E.; REZAEI, B. Electrochemical study of quinone redox cycling: a novel application of DNA-based biosensors for monitoring biochemical reactions. *Bioelectrochemistry*, 111, p. 15-22, 2016.

[68] VARCOE, J. R.; ATANASSOV, P.; DEKEL, D. R.; HERRING, A. M.; HICKNER, M. A.; KOHL, P. A.; KUCERNAK, A. R.; MUSTAIN, W. E.; NIJMEIJER, K.; SCOTT,

K.; XU, T.; ZHUANG, L. Anion-exchange membranes in electrochemical energy systems. **Energy & Environmental Science**, 7, p. 3135 – 3191, 2014.

[69] LIM, K. H.; OH, H. S.; JANG, S. E. ; KO, Y. J.; KIM, H. J.; KIM, H. Effect of operating conditions on carbon corrosion in polymer electrolyte membrane fuel cells. **Journal of Power Sources**, 193, p. 575-579, 2009.

[70] XU, Y.; QU, J.; SHEN, Y.; FENG, W. Different graphene layers to enhance or prevent corrosion of polycrystalline copper. **RSC Advances**, 8, p. 15181-15187, 2018.

CHAPTER 5 - RECENT TRENDS IN THE ELECTROANALYTICAL DETECTION OF FOOD FRAUD

*Text adapted from: FARIA, R. A. D.; HENEINE, L. G. D.; MATENCIO, T.; MESSADDEQ, Y. Recent trends in the electroanalytical detection of food fraud. **International Journal of Biosensors & Bioelectronics**, 5(3), p. 63–67, 2019.*

Ricardo Adriano Dorledo de Faria,^{1,2} Luiz Guilherme Dias Heneine,³ Tulio Matencio,⁴
Younès Messaddeq^{2,5}

¹Department of Chemical Engineering, Universidade Federal de Minas Gerais, Brazil

²Center for Optics, Photonics and Lasers (COPL), Université Laval, Canada

³Department of Applied Immunology, Fundação Ezequiel Dias, Brazil

⁴Department of Chemistry, Universidade Federal de Minas Gerais, Brazil

⁵UNESP, Brazil

5.1 ABSTRACT

Food fraud is a criminal act that has continuously increased in the recent years and represents an important issue to consumers' confidence, which encompass economic, social, health and religious aspects. Electrochemical sensors are a promising category of analytical techniques for food authenticity assessment due to their low cost, simplicity/easiness-to-perform, sensitivity and sensibility in comparison to other consolidated assays. Herein, a background on the transduction mechanisms of potentiometric, amperometric and impedimetric sensors is provided in addition to some current applications on the authentication of food products.

Keywords: Food fraud, authentication, electrochemical sensors, analytical techniques

5.2 INTRODUCTION

Significant focus towards the quality standard of the food industry reflects consumers increasing concern about the authenticity and quality of what they eat. The general term “food fraud” corresponds to the act of substituting, adding or adulterating a food product in order to obtain economic gain [1]. It differs from the simple definition of “contamination” because the former necessarily relates to an intentional activity [2]. The Grocery Manufacturers Association (GMA) complements that these criminal acts are carried out by “*unapproved enhancements, dilution with a lesser-value ingredient, concealment of damage or contamination, mislabeling of a product or ingredient, substitution of a lesser-value ingredient or failing to disclose required product information*” [3]. The economically motivated adulteration represents to the North American industry an average cost of 10 – 15 billion dollars per year and some studies estimate that approximately 10% of the shelf products in the market still contain some adulteration [3]. Furthermore, this activity involves the use of a lower valued ingredient at the place of a higher valued one, consisting as a potential disrupting agent of the economy that stimulates the unfair market competition at regional and global levels [4]. From the consumers’ point-of-view, although it is usually not directly associated to health risks, this may pose a threat to allergic population, in addition to go against some religious, social and life-style aspects [5].

In the light of the criminal nature of fraud, one must take in account the factors that leads a company to commit this act in order to preserve the consumer’s rights. According to the routine activity theory of Cohen and Felson [6], a crime happens when at a certain moment and place the following three aspects converge: (i) the presence of motivated agents to commit the crime, (ii) suitable targets and (iii) the absence of agents capable to avoid it. These authors emphasize that the absence of only one of these components is enough to prevent the crime occurrence. In this sense, measures of fraud control takes a crucial place in counteracting the fraud vulnerability by diminishing the possibilities of offenders to find opportunities in committing the crime [7].

Despite the food fraud phenomenon does not demerit exclusively the current age since there are some historical reports even from the Roman and Greek Empires, it

has received more attention in the recent years with the advent and development of more technological methods to detect the presence of fraudulent ingredients in food products [8]. After a bibliographic search in the Web of Science database using the keywords “food fraud” (figure 10), it becomes evident the importance of this issue especially in this decade. It surely gained force with the outcome of fraud scandals worldwide, such as the presence of melamine in Chinese milk in 2008 [9] and the incident involving horsemeat in Europe in 2013 [10].

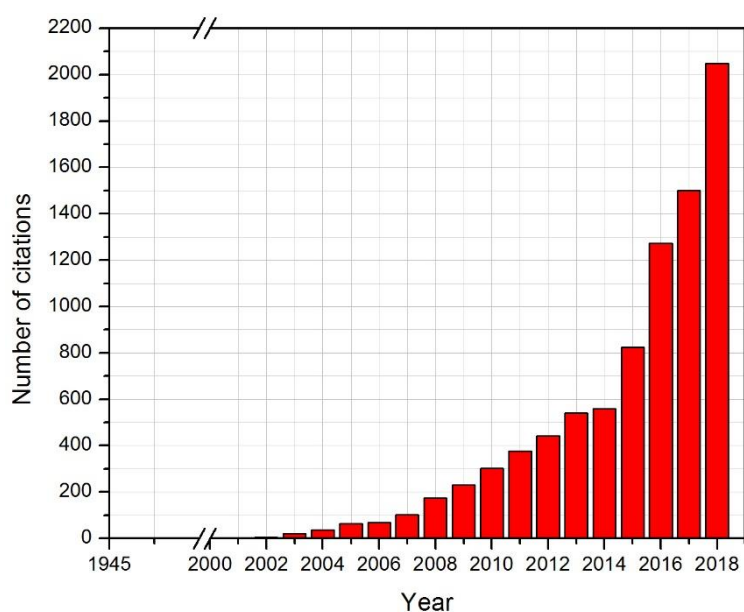


Figure 10 - Evolution of the number of citations of articles containing “food fraud” as a keyword according to the Web of Science database (from 1945 to 2018)

In response to the increasing concern on food authenticity, the scientific community has devoted great attention to develop accurate methods to detect the presence of fraudulent components in food products. The main studied techniques nowadays contemplates physical, chemical, biochemical and molecular transductions [11]. Sheika [11] mentions that the physical techniques consist on the microscopic/macroscopic analysis of the food structure, the chemical and biochemical methods comprise mainly chromatographies, spectroscopies, immunologic and electrophoretic techniques and the molecular transduction involves the use of DNA-based analysis. According to Danezis *et al.* [12], chromatographic

and molecular methods are present in almost half of the published articles related to food authentication. However, among all these possibilities, the electrochemical sensors stand out as a promising tool for the detection of food fraud. The mechanism of recognition of these sensors rely on the conversion of the input signal (analyte recognition) into an electrical output signal that is proportional to the concentration of the target molecule. Depending on the type of measured output signal (e.g. voltage, current, impedance), the electrochemical devices can be categorized mainly into potentiometric, amperometric and impedimetric sensors [13]. Some authors defend that the electrochemical devices can be more sensitive, cheap, amenable for *in-situ* and point-of-care applications (due to the possibility of miniaturization of the electrodes), besides they can require small volumes of sample [14-16].

5.3 POTENTIOMETRIC SENSORS

The working principle of potentiometric sensors consist on measuring the difference in the potential between the working and reference electrodes in an electrochemical cell at the open circuit. This potential can be calculated from the Nernst equation in which the cell potential E_{ef} refers to the value at zero current (electromotive force) [16]. In the Equation 9, E_0^* refers to the standard potential of the electrode (V), R is the universal gas constant ($8.314 \text{ J.K}^{-1}.\text{mol}^{-1}$), T is the temperature (K), F is the Faraday's constant ($96,500 \text{ C.mol}^{-1}$), Z_i corresponds to the valence of the ion, a_i is the activity of the species present in the sample [17].

$$E_{ef} = E_0^* + \frac{RT}{Z_i F} \ln a_i \quad (9)$$

A deeper interpretation of the Nernst equation leads to the inference about some features of the potentiometric sensors. As notable from the equation, there is a primary dependence between the potential and the logarithm of the ion activity. Since R and F are constants, the slope of the curve, which relates the sensitivity of the device, depends mainly on the temperature and on the valence of the ion. Thus, in

order to achieve proper reproducibility of the sensing response, it is necessary to keep fixed the temperature; otherwise, small changes on it could affect the sensitivity of the sensor (which can represent a challenge for *in-situ* applications) as seen in Figure 11. For example, considering a potentiometric sensor exposed to a variation of 10% of the activity of magnesium cations at 298 K, a variation of only 1.2 mV would be expected. Thus, only high variations of the analyte concentration are expected to provide a significant variation of the potential. Figure 11 also shows how the charge of the analyte of interest affects the output potential. Considering, three hypothetical contaminating ions in a food product with valences $Z_i = 1$, $Z_i = 2$ and $Z_i = 3$ (K^+ , Mg^{2+} and Fe^{3+} for instance), it is possible to observe that the ion with the higher value of Z_i is subjected to the lowest variations of the potential, which would provide the lower sensitivity of the sensor towards this analyte.

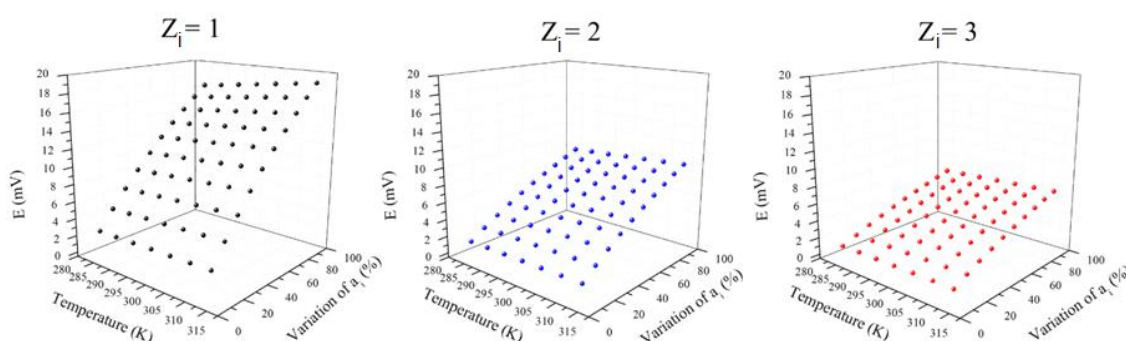


Figure 11 - Influence of the temperature, valence of the target ion and the variation of its activity on the expected potential and sensitivity of potentiometric sensors

Concerning the use of this technology in the food fraud inspection, Trivedi *et al* [18] developed a potentiometric sensor for identification of milk adulteration with urea by means of the sensitive detection of NH_4^+ cations by an ion sensitive membrane containing urease enzyme. A significant amount of articles devoted to the development of potentiometric sensors for food authentication present the technology of electronic tongues for the transduction sensing. The electronic tongues is an instrument composed by a sensor array, and the systems of data acquisition and pattern identification to perform measurements in liquid samples [19].

Lvova *et al.* [20] tested an electronic tongue to investigate wine authenticity, pointing out not only the simplicity of potentiometry as a transduction technique but also its low cost, quickness and the possibility of monitoring plenty of parameters at the same time. In the context of the high number of reports denouncing olive oils fraud, Dias *et al.* [21] described the results obtained with a potentiometric electronic tongue for the authentication of extra virgin olive oils, achieving high sensitivity and the capability to distinguish samples from different origins.

In comparison to the amperometric sensors, the potentiometric transduction possess as an advantage the characteristic to be non-destructives once the reactants from the bulk solution are not consumed during the analyte recognition, thus, it develops no concentration gradients at the interface with the electrode making it easier to be used [22].

5.4 AMPEROMETRIC SENSORS

The amperometry sensing is a technique in which the electrical current developed from reductive and oxidative reactions is measured and interpreted in response to the analyte recognition. A fixed potential is applied to the transducer electrode to favor the redox reactions of the electroactive species from the bulk solution to the interface with the electrolyte [23]. Until today, the most famous amperometric sensor has been the glucose sensor firstly described by Clark and Lyons in 1962 [24]. The mechanism of transduction was based on the oxidation of glucose mediated by the enzyme glucose oxidase into hydrogen peroxidase. Finally, the hydrogen peroxidase is oxidized to produce free electrons (according to the reaction v bellow) that will be measured as a current signal directly proportional to the glucose concentration.



This kind of device, as-called “first generation biosensor”, relates the concentration of the analyte or of the by-products from the enzymatic reactions to the electrical current developed on the electrode. In this case, the H₂O₂ production can be

inspected under a +0.7 V vs Ag/AgCl fixed potential or the O₂ concentration can also be monitored under a -0.7 V vs Ag/AgCl potential. To exploit the sensing phenomena at softer conditions, the second generation biosensors were developed using as main principle the use of electron carriers mediators that avoid the O₂ dependence and diminish the influence of other electroactive species on the sensor response. The main disadvantage of this category is the lower stability in comparison to the first generation group. Thus, the third generation enzymatic sensors have been developed to overwhelm the previous limitations and to improve the response time to obtain quicker responses, in a mechanism in which the electron transfer takes place directly between the enzyme and the electrode [25]. Despite most of the commercial glucose sensors relies on the enzymatic amperometric transduction, the use of enzymes possesses some important disadvantages such as the low stability and high cost and, for this reason, some researchers have studied alternatives to develop non-enzymatic sensors even based on other electrochemical techniques [26].

Among the analytes of interest in the food industry, the determination of azithromycin in animal source foods was studied by Jafari *et al.* [25] due to the risk that this antibiotic can impose to consumers' health when present in excess in food products. The authors reported the use of differential pulse voltammetry as an electrochemical transduction technique to detect azithromycin, obtaining a limit of detection (LOD) equal to 0.1 nM with high reproducibility ($n = 8$; standard deviation of 2.5%). The research published by Montiel *et al.* [26] using a disposable magnetic beads-based amperometric platform described the detection of the peanut allergenic proteins Ara h 1 and Ara h 2 at low LOD and with shorter assay time in comparison to the commercial kit based on the Enzyme-Linked Immunosorbent Assay (ELISA). Benedé *et al.* [27] worked on the detection of ovomucoid, an egg white allergen, by employing a strategy of magnetic bioconjugated binding at the surface of a screen-printed carbon electrode under the influence of a fixed -0.2 V (*versus* Ag pseudo reference electrode) potential. The calibration plot was linear in the concentration range from 0.3 to 25 ng.mL⁻¹ and this amperometric sensor was also more sensitive (LOD = 0.1 ng.mL⁻¹) than the commercial ELISA kit. Amperometric electronic noses also comprise a powerful category of sensors for monitoring food composition by means of the detection of volatile components. Gliszczyńska-Świąło and

Chmielewski [28] highlighted that, in comparison to gas chromatography that is commonly used for the same purpose, the electronic noses possess as main advantages their simplicity, usually not requiring sample preparation, the low cost of each sample analysis and the short response time. Thus, they comprise an important tool for authentication of products that are commonly target of fraud, such as vegetable oils, meat products, seafood, beverages, fruits and honeys [28].

5.5 IMPEDIMETRIC SENSORS

EIS is the technique that governs the transduction in impedimetric sensors. The EIS principle consist on applying a small sinusoidal potentiostatic perturbation on the electrochemical system under investigation in order to measure the impedance as a consequence of the resultant current (it is also possible to apply a current signal to obtain a resultant potential in the galvanostatic mode) [29]. Assessing the components of the global impedance (real and imaginary impedance, phase angle, magnitude of impedance) and/or modelling the EIS data to an electrical equivalent circuit in order to obtain the values of resistors, capacitors and inductors. For instance, it is possible to presume the analyte presence/concentration [29].

Recently, some impedimetric sensors have been reported in the literature for horsemeat adulteration screening and for glucose detection. The horsemeat immunosensor was capable to selectively detect the target analyte in buffered solution and in a solution prepared from commercial raw meat, presenting a LOD of 0.0004% (value that was lower than others reported in the literature by using spectrometry, chemiluminescence, fluorescence, voltammetry and amperometry) [30]. The glucose sensor, containing 3-aminophenylboronic acid as a probe, was also highly sensitive and presented a LOD equal to 8.53×10^{-9} M. Besides its high sensitivity and low response towards other sugars (fructose and sucrose), this sensor presented as another advantage the capability to provide the output signal in few seconds (4.0 ± 0.6 s) at optimal conditions [29]. In both publications, we highlighted the use of screen-printed carbon electrodes a cheap material to construct the sensors, which make it cheap due to the easiness of its mass production.

Furthermore, EIS represented an interesting transduction technique for online applications, besides the possibility to be carried out at a single frequency, which make it easy-to-perform [30,31].

Das *et al.* [32] focused on developing an on-chip impedimetric sensor for identification and quantification of soap as an adulterant in milk. The authors pointed out that the traditional techniques used to detect fraud in milk, such as Near-Infrared and FTIR spectroscopy, High Performance Liquid Chromatography and Liquid Chromatography, are very laborious, require long processing times and demand expensive equipment despite the accuracy of the results.

Other applications of EIS as a transduction method in sensors has also comprised the detection of allergens, microorganisms, monitoring of vegetable oils and fruits quality [33,34].

5.6 CONCLUSION

In the context of consumers' vulnerability and protection, the food fraud detection has gained particular attention especially in the current decade. Aspects related to economic losses, consumer confidence, health risks, lifestyle and religious traditions motivated the scientific community to develop analytical techniques towards the recognition and quantification of fraudulent ingredients in many food products. The most exploited techniques commercially available mainly arises from spectrometric and chromatographic transduction mechanisms. However, some limitations, such as the sophisticated required apparatus, the time-consuming methodology and high cost of the equipment, hinder the viability of employing them in routine tests. As an alternative to the mentioned techniques, the electroanalytical assays represent an interesting opportunity in the food authentication scenario. High sensitive potentiometric sensors have been described in the literature to detect fraud especially in milk and alcoholic beverages by using electronic tongues in a fast and simple way. Despite advantageous because it is a non-destructive method (there is no concentration gradient of the electroactive species), the necessity of keeping the temperature very well controlled limits the potentiometric transduction to be used in

in-situ analysis and hinders its reproducibility. Researches describing the use of amperometric sensors for inspection of fruits, honeys, dairy and meat products, for example, have shown low LOD towards analytes of interest with performances comparable to traditional techniques already available in the market. As a disadvantage, the common use of enzymes to mediate the amperometric response by producing intermediary electroactive species have led to the development of high cost and low stable sensors. Devices based on the EIS transduction technique have also been capable to detect low concentrated fraudulent ingredients in food products. Furthermore, since the impedimetric sensors lies on a non-destructive based technique (besides the possibility of using miniaturized electrodes), these devices are amenable for *in-situ* and online measurements, which makes them very useful for the food quality industry. In this context, the use of electrochemical transduction in the field of food authentication has been shown to be promising and advantageous in comparison to other analytical techniques. The choice for the most appropriate electroanalytical assay most depends, though, on the target analyte, the aimed application (whether it is necessary to perform online *in-situ* measurements or not), the physicochemical conditions of the medium in which the sensing will be performed (temperature and presence of interfering species for example), the expected limit of detection/sensitivity and the required stability.

5.7 REFERENCES

- [1] CHARLEBOIS, S.; SUMMAN, A. A risk communication model for food regulatory agencies in modern society. **Trends in Food Science & Technology**, 45(1), p. 153-165, 2015.
- [2] MANNING, L.; SOON, J. M. Food safety, food fraud, and food defense: a fast evolving literature. **Journal of Food Science**, 81(4), p. 823-834, 2016.
- [3] GROCERY MANUFACTURERS ASSOCIATION. **Consumer product fraud and deterrence**. Available in: <https://www.gmaonline.org/downloads/research-and-reports/consumerproductfraud.pdf> (accessed on 26 April 2019).
- [4] HONG, E.; LEE, S. Y.; JEONG, J. Y.; PARK, J. M.; KIM, B. H.; KWON, K.; CHUN, H. S. Modern analytical methods for the detection of food fraud and adulteration by

food category. **Journal of the Science of Food and Agriculture**, 97(12), p. 3877-3896, 2017.

[5] NIZAR, N. N. A.; ZAINAL, I. H.; BONNY, S. Q.; PULINGAM, T.; VYTHALINGAM, L. M.; ALI, M. E. DNA and nanobiosensor technology for the detection of adulteration and microbial contamination in religious food. **Preparation and Processing of Religious and Cultural Foods**, p. 409-431, 2018.

[6] COHEN, L. E.; FELSON, M. Social change and crime rate trends: a routine activity approach. **American Sociological Review**, 44(4), p. 588-608, 1979.

[7] RUTH, S. M.; HUISMAN, W.; LUNING, P. A. Food fraud vulnerability and its key factors. **Trends in Food Science & Technology**, 67, p. 70-75, 2017.

[8] CHARLEBOIS, S.; SCHWAB, A.; HENN, R.; HUCK, C. W. Food fraud: an exploratory study for measuring consumer perception towards mislabeled food products and influence on self-authentication intentions. **Trends in Food Science & Technology**, 50, p. 211-218, 2016.

[9] PEI, X.; TANDON, A.; ALLDRICK, A.; GIORGI, L.; HUANG, W.; YANG, R. The China melamine milk scandal and its implications for food safety regulation. **Food Policy**, 36, p. 412-420, 2011.

[10] FALKHEIMER, J.; HEIDE, M. Trust and Brand Recovery Campaigns in Crisis: Findus Nordic and the Horsemeat Scandal. **International Journal of Strategic Communication**, 9, p. 134-147, 2015.

[11] SHEIKHA, A. F. E. DNAFoil: novel technology for the rapid detection of food adulteration. **Trends in Food Science & Technology**, 86, p. 544-542, 2018.

[12] DANEZIS, G. P.; TSAGKARIS, A. S.; CAMIN, F.; BRUSIC, V.; GEORGIU, C. A. Food authentication: techniques, trends & emerging approaches. **Trends in Analytical Chemistry**, p. 85:123-132, 2016.

[13] HAMMOND, J. L.; FORMISANO, N.; ESTRELA, P.; CARRARA, S.; TKAC, J. Electrochemical biosensors and nanobiosensors. **Essays in Biochemistry**, 60, p. 69-90, 2016.

[14] MARTIN, A.; VILELA, D.; ESCARPA, A. Food analysis on microchip electrophoresis: an updated review. **Electrophoresis**, 33, p. 2212-2227, 2012.

[15] ZHU, C.; YANG, G.; LI, H.; DU, D.; LIN, Y. Electrochemical sensors and biosensors based on nanomaterials and nanostructures. **Analytical Chemistry**, 87(1), p. 230-249, 2015.

[16] NAVEEN, M. H.; GURUDATT, N. G.; SHIM, Y. B. Applications of conducting polymer composites to electrochemical sensors: a review. **Applied Materials Today**, 9, p. 419-433, 2017.

- [17] WANG, Y.; XU, H.; ZHANG, J.; LI, G. Electrochemical sensors for clinical analysis. **Sensors**, 8, p. 2043-2081, 2008.
- [18] TRIVEDI, U. B.; LAKSHMINARAYANA, D.; KOTHARI, I. L.; PATEL, N. G.; KAPSE, H. N.; MAKHIJA, K. K.; PATEL, P. B.; PANCHAL, C. J. Potentiometric biosensor for urea determination in milk. **Sensors and Actuators B: Chemical**, 140(1), p. 260-266, 2009.
- [19] JIANG, H.; ZHANG, M.; BHANDARI, B.; ADHIKARI, B. Application of electronic tongue for fresh foods quality evaluation: a review. **Food Reviews International**, p. 1-24, 2018.
- [20] LVOVA, L.; YAROSHENKO I.; KIRSANOV, D.; NATALE, C. D.; PAOLESSE, R.; LEGIN, A. Electronic tongue for brand uniformity control: a case study of apulian red wines recognition and defects evaluation. **Sensors**, 18(8), p. 2584, 2018.
- [21] DIAS, L. G.; FERNANDES, A.; VELOSO, A. C. A.; MACHADO, A. A. S. C.; PEREIRA, J. A.; PERES, A. M. Single-cultivar extra virgin olive oil classification using a potentiometric electronic tongue. **Food Chemistry**, 160, p. 321-329, 2014.
- [22] HOLFORD, T. R. J.; DAVIS, F.; HIGSON, S. P. J. Recent trends in antibody based sensors. **Biosensors and Bioelectronics**, 34(1), p. 12-24, 2012.
- [23] THÉVENOT, D. R.; TOTH, K.; DURST, R. A.; WILSON, G. S. Electrochemical biosensors: recommended definitions and classification. **Biosensors and Bioelectronics**, 16, p. 121-131, 2001.
- [24] CLARK, L. C. J.; LYONS, C. Electrode systems for continuous monitoring in cardiovascular surgery. **Annals of the New York Academy of Sciences**, 102, p. 29-45, 1962.
- [25] JAFARI, S.; DEGHANI, M.; NASIRIZADEH, N.; AZIMZADEH, M. An azithromycin electrochemical sensor based on an aniline MIP film electropolymerized on a gold nano urchins/graphene oxide modified glassy carbon electrode. **Journal of Electroanalytical Chemistry**, 829, p. 27-34, 2018.
- [26] MONTIEL, V. R. V.; TORRENTE-RODRÍGUEZ, R. M.; CAMPUZANO, S.; PELLICANÒ, A.; REVIEJO, Á. J.; COSIO, M. S.; PINGARRÓN, J. M. Simultaneous determination of the main peanut allergens in foods using disposable amperometric magnetic beads-based immunoassay platforms. **Chemosensors**, 4, p. 1-14, 2016.
- [27] BENEDÉ, S.; MONTIEL, R. V.; POVEDANO, E.; VILLALBA, M.; MATA, L.; GALÁN-MALO, P.; TORRENTE-RODRÍGUEZ, R. M.; VARGAS, E.; REVIEJO, A. J.; CAMPUZANO, S.; PINGARRÓN, J. M. Fast amperometric immunoplatfrom for ovomucoid traces determination in fresh and baked foods. **Sensors and Actuators B: Chemical**, 265, p. 421-428, 2018.

- [28] GLISZCZYŃSKA-ŚWIGŁO, A.; CHMIELEWSKI, J. Electronic nose as a tool for monitoring the authenticity of food. A review. **Food Analytical Methods**, 10, p. 1800-1816, 2017.
- [29] FARIA, R. A. D.; HENEINE, L. G. D.; MATENCIO, T.; MESSADDEQ, Y. Faradaic and non-faradaic electrochemical impedance spectroscopy as transduction techniques for sensing applications. **International Journal of Biosensors and Bioelectronics**, 5(1), p. 29-31, 2019.
- [30] FARIA, R. A. D.; IDEN, H.; BHARUCHA, E.; LINS, V. F. C.; MESSADDEQ, Y.; MATENCIO, T.; HENEINE, L. G. D. A new tool for the detection of horsemeat adulteration in raw meat. **Journal of Biosensors and Bioelectronics**, 9(4), p. 1-7, 2018.
- [31] FARIA, R. A. D.; IDEN, H.; HENEINE, L. G. D.; MATENCIO, T.; MESSADDEQ, Y. Non-enzymatic impedimetric sensor based on 3-aminophenylboronic acid functionalized screen-printed carbon electrode for highly sensitive glucose detection. **Sensors**, 19, p. 1686, 2019.
- [32] DAS, C.; CHAKRABORTY, S.; KARMAKAR, A.; CHATTOPADHYAY, S. On-chip detection and quantification of soap as an adulterant in milk employing Electrical Impedance Spectroscopy. **International Symposium on Devices, Circuits and Systems**, Howrah, p. 1-4, 2018.
- [33] NEETHIRAJAN, S.; WENG, X.; TAH, A.; CORDERO, J. O.; RAGAVAN, K. V. Nano-biosensor platforms for detecting food allergens – new trends. **Sensing and Bio-Sensing Research**, 18, p. 13-30, 2018.
- [34] GROSSI, M.; RICCÒ, B. Electrical Impedance Spectroscopy (EIS) for biological analysis and food characterization: a review. **Journal of Sensors and Sensors Systems**, 6, p. 303-325, 2017.

CHAPTER 6 - A NEW TOOL FOR THE DETECTION OF HORSEMEAT ADULTERATION IN RAW MEAT

*Text adapted from: FARIA, R. A. D.; IDEN, H.; BHARUCHA, E.; LINS, V. F. C.; MESSADDEQ, Y.; MATENCIO, T.; HENEINE, L. G. D. A new tool for the detection of horsemeat adulteration in raw meat. **Journal of Biosensors and Bioelectronics**, 9, p. 4, 2018.*

Ricardo Adriano Dorledo de Faria^{1,2}, Hassan Iden², Eric Bharucha², Vanessa de Freitas Cunha Lins¹, Younès Messaddeq^{2,3}, Tulio Matencio⁴, Luiz Guilherme Dias Heneine⁵

¹Department of Chemical Engineering, Universidade Federal de Minas Gerais (UFMG), Brazil

²Center for Optics, Photonics and Lasers (COPL), Université Laval, Canada

³Institute of Chemistry, UNESP, Araraquara, São Paulo, Brazil

⁴Department of Chemistry, Universidade Federal de Minas Gerais (UFMG), Brazil

⁵Department of Applied Immunology, Fundação Ezequiel Dias (FUNED), Brazil

6.1 ABSTRACT

This work deals with the development of an impedimetric immunosensor sensitive to horse immunoglobulin G (IgG). The biosensing platform involve the electrodeposition of polyaniline onto screen-printed carbon electrode as electrochemical transducer matrix. Cyclic Voltammetry and Scanning Electron Microscopy were used to monitor the formation of the recognition layer through the immobilization of anti-horse IgG antibodies on the conductive polymer. Electrochemical Impedance Spectroscopy (EIS) was performed to test the specific detection of horse serum in PBS buffer, indicating that the immunosensor was sensitive to the target analyte and without any response to heterologous sera (swine and bovine). The constructed sensors were first tested with Phosphate Buffered Saline (PBS) homogenates of commercial samples of raw ground horsemeat, pork and beef diluted at 10^{-5} , 10^{-4} and 10^{-3} % w/v in PBS. The total time for performing the test was approximately 72 minutes and a selective response of the device is obtained with a 0.004% limit of detection.

Keywords: Horsemeat adulteration; Immunosensor; Electrochemical Impedance Spectroscopy.

6.2 INTRODUCTION

Food fraud is an illegal intentional practice that involves mainly the addition of adulterant-substances, counterfeiting and the mislabeling of food products [1]. Meat products are a special target for adulteration, in which the manufacturers replace high-cost species for low-valued ones aiming economic gain, because of its traditional presence in human diet as a major protein source [2]. The magnitude of the impact caused by this criminal act reflects on high economic losses, consumers' confidence and health risks (since the fraudulent substance can be an allergen for a population group) [3-5].

In January 2013, the horsemeat scandal (also named "horsegate") in Europe drew great attention worldwide to the importance of meat adulteration screening. In this incident, the Food Safety Authority of Ireland denounced the presence of undeclared horsemeat in extensive amount of beef and pork products of European suppliers [6]. Horsemeat is used instead other meats due to its low-cost of production (e.g. the price per ton of horsemeat is estimated to be approximately USD 1,300, while the same amount of beef cost around USD 5,300). In most of cases, horses are slaughtered at the end of their lives or when they suffer some diseases, as a result the market do not recognize potential economic application or nutritional value on their meat [7]. As consequences, the global market suffered a huge economic recession, bovine products underwent a price increase of 45% between 2008 and 2012 and the sales of ready-made beef meals significantly decreased in the same year [1].

In this context, many techniques have been developed for authentication of meat products based on their physical, chemical, optical and biochemical properties, such as ELISA, chromatography, DNA-based assays, mass spectrometry and fluorescence spectroscopy [8-10]. Despite efficient and sensitive, these methods are

laborious, expensive, time-consuming, sophisticated, demand highly trained staff and are difficult to use in online applications [11-13].

In this regard, immunosensors based on the EIS are promising candidates for meat speciation. The impedimetric immunosensors are a subcategory of biosensors that combine the great specificity of the antibody-antigen bonds with the high sensitivity of a non-destructive electrochemical technique [14]. Furthermore, among the advantages of the technology of biosensors, the easiness-to-perform, not requiring highly specialized staff, possibility of miniaturization, possibility of performing real-time detection and the low cost are particularly very propitious features for application in food authenticity [15-17].

A typical impedimetric immunosensor consists of a conductive transducer matrix onto which a layer containing immobilized antibodies as elements of recognition will bind a target analyte, causing changes in the dielectric properties at the interface between electrode and electrolyte [18,19]. Herein, as a strategy for horsemeat adulteration screening, we immobilized goat anti-horse Immunoglobulin G (IgG) on the surface of screen-printed carbon electrodes (SPCEs) containing conductive polyaniline (PANI) to monitor the variations of impedance caused by its exposition to the target analyte.

6.3 MATERIALS AND METHODS

6.3.1 Apparatus and chemicals

Triplicate electrochemical tests were carried out using a Princeton Applied Research VersaSTAT 3 potentiostat/galvanostat (Ametek Scientific Instruments, Canada) interfaced with the VersaStudio software. The measurements were performed using SPCEs immersed in an electrolyte containing 0.01M PBS buffer (pH 7.4) and 0.1 M KCl at room temperature. The SPCEs were purchased from Pine Research Instrumentation and are consisted of a carbon working electrode (model RRPE1002C, 5 mm x 4 mm), carbon as a counter-electrode and an Ag/AgCl reference electrode.

Ultraviolet-visible spectroscopy (UV-VIS) was performed using a Cary series UV-VIS-NIR spectrophotometer (Agilent Technologies). The scanning electron microscopy (SEM) images were recorded using a Quanta 3D FEG microscope.

Phosphate saline buffer (PBS), glutaraldehyde (25%) and bovine serum were purchased from Sigma-Aldrich (USA). Potassium chloride was obtained from Fisher Scientific (Belgium). Aniline (purity $\geq 99\%$) was acquired from Alfa Aesar and sulfuric acid 98% was purchased from Anachemia (Canada). Lyophilized whole horse serum, whole pig serum and goat anti-horse polyclonal immunoglobulin G (IgG) were purchased from MP Biomedicals (Fisher Scientific, Canada). Casein of high purity grade was purchased from Amresco (USA). Ground horsemeat, pork and beef were purchased from the local market of Quebec City (Quebec, Canada). All solutions were prepared with ultrapure deionized water with an 18 M Ω .cm resistivity.

6.3.2 Functionalization of the SPCEs for recognition of horse IgG

Prior to functionalization, the SPCEs were treated in 0.05 M sulfuric acid by cycling potential from -2.5 to +2.5 V vs Ag/AgCl at 50 mV.s⁻¹. This method is an effective, simple and cheap procedure to remove organic contaminants from the carbon ink, improving its electroactivity and increasing its surface roughness [20].

Afterwards, PANI was electrodeposited on the pretreated SPCE to improve its electrical conductivity. The polymerization was carried out by CV, scanning 15 cycles from -0.4 to 1.0 V vs Ag/AgCl at 50 mV.s⁻¹ in an aqueous solution of 0.1 M aniline containing 0.1 M H₂SO₄ [21]. We studied various concentrations of aniline to obtain PANI as an electrochemical transducer matrix for application in an immunosensor and we found that 0.1 M is an ideal concentration because it improves the electroactivity of the electrode and consequently the sensitivity of the device.

Subsequently, 30 μ L of an aqueous solution of 1% v/v glutaraldehyde was deposited on the working electrode, which was kept in this solution for 1h. After, the SPCEs were washed with 0.01 M PBS (pH 7.4) to remove the nonbonding aldehydes. Then, a 100 μ g.mL⁻¹ solution of anti-horse antibodies was added to the surface for 1h, when the electrode was newly washed with PBS. Finally, they were

incubated in a 1 % w/v casein solution in 0.01 M PBS to block possible remaining reactive sites present on the surface, avoiding unspecific cross-reactions.

6.3.3 Characterization of the biosensor

CV was used to the electrochemical monitoring of the functionalization steps to obtain the biosensor, which was performed as a single cycle from -0.4 to 1.0 V vs Ag/AgCl at 50 mV.s⁻¹. The structural modifications on the SPCE surface due to functionalization were also inspected by SEM with an acceleration voltage of 5 kV. Energy dispersive X-ray spectroscopy (EDX) coupled with SEM equipment was recorded to inspect the effect of the acid pre-treatment in the SPCE.

6.3.4 Electrochemical sensing of horse IgG

6.3.4.1 Detection of horse IgG in buffer solution

Horse serum was diluted in 0.01 M PBS (pH 7.4) to obtain the homologous analyte solutions at the following concentrations: 1 pg.mL⁻¹, 10 pg.mL⁻¹, 100 pg.mL⁻¹, 1 ng.mL⁻¹, 100 ng.mL⁻¹ and 1 µg.mL⁻¹. The biosensor was exposed to 30 µL of the mentioned solutions during 20 minutes. After each incubation, the biosensor was gently washed with 0.01M PBS in order to remove unbound and physically adsorbed molecules from the electrode surface.

EIS was performed in 0.01 M PBS containing 0.1 M KCl as supporting electrolyte. A perturbation amplitude of 10 mV around the OCP was applied in a range of frequencies varying from 10 kHz to 100 mHz. The EIS data were fitted to an electrical equivalent circuit with the commercial software Zview (Scribner and Associates, version 2.9b).

To test the selectivity of the biosensor, the impedance response with other meat species was also investigated. For this purpose, the device was incubated in

heterologous swine and bovine sera at the same concentrations and experimental conditions.

6.3.4.2 Detection of horse IgG in commercial raw meats

In order to evaluate the capability of the biosensor to recognize the target analyte in real samples, the device was exposed to horsemeat, pork and beef. To accomplish this, the commercial ground meats were diluted in 0.01 M PBS (pH 7.4) to the final concentration of 1% w/v. Each buffered solution was then homogenized for 30 minutes by using a VWR vortex mixer. Then, the solutions were centrifuged at 10,000 x g for 15 minutes at room temperature. The supernatant was collected and filtered using a 0.45 µm filter.

To estimate the concentration of proteins [*P*] extracted from the horsemeat, pork and beef by using the previous protocol and based on Equation 10 [22], the absorbance of each sample was measured by UV-Vis spectroscopy at 280 nm (A_{280}) and 260 nm (A_{260}) with a path length fixed at 1 cm.

$$[P] = 1.55A_{280} - 0.76 A_{260} \quad (10)$$

The centrifuged and filtered samples were diluted 1,000; 10,000 and 100,000 times in 0.01 M PBS. To perform the detection tests, 30 µL of meat solution was dropped on the working electrode of the biosensors and the impedance measurement was performed after 20 minutes incubation period.

6.4 RESULTS AND DISCUSSION

6.4.1 Characterization of the immunosensor by CV

CV was employed to inspect the interfacial electrochemical characteristics of the SPCE during the functionalization. Figure 12 shows that the electrode suffered

significant changes due to each step of its modification. The as-received SPCE exhibited a very low value of current due to the low electroactivity of carbon. After treating the electrode via cycling in sulfuric acid at extreme potentials, the material is activated by the removal of organic compounds of its surface. The application of high anodic and cathodic potentials on the electrode provokes the oxygen and hydrogen evolve from the carbon surface improving its heterogeneous electron transfer kinetics [20,23], which causes an increase of its electrical charge.

After the electropolymerization of PANI, the electron transfers remarkably increased, due to its high electroactivity. The PANI conjugated backbone structure comprised of alternating single and double bonds along its chain, which facilitates the electron transfer thorough the extended π network and provides its semiconductor features [24]. Furthermore, the redox peaks observed in the voltammogram can be associated to the different oxidation states of PANI. Leucoemeraldine is the fully reduced state, pernigraniline is the fully oxidized state and emeraldine corresponds to the partially oxidized form, whose doped state (emeraldine salt) is the most interesting one for electrochemical applications because it is the only electrically conducting phase [25].

When PANI was exposed to the glutaraldehyde solution, the redox peaks height decreased due to the crosslinking reaction between the amino terminal groups from the polymer and the $-CHO$ group of the aldehyde [26]. Next, the exposition to antibodies and casein caused new decreases of the overall voltammetric signal, because of the insulator behavior of these organic compounds, which block the path of electron transport and hinder the faradaic reaction rates [27, 28].

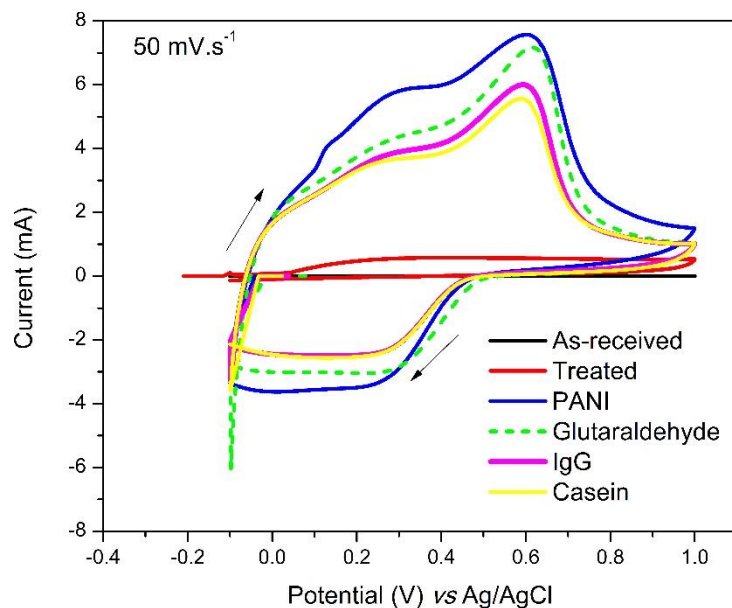


Figure 12 - Cyclic voltammogram of the stepwise functionalization of SPCE to develop the horsemeat biosensor obtained at a scan rate of $50 \text{ mV}\cdot\text{s}^{-1}$ in 0.1 M KCl (pH 7.4)

6.4.2 Characterization of the immunosensor by SEM-EDX

The morphology of the SPCE is a very important parameter for developing the biosensor, mainly because it is related to the available surface area for antibody binding, consequently affecting the performance of the device.

Figure 13a shows that the bare SPCE has pores with higher roughness and contains some isolated graphite flakes on the surface. After the acid treatment (Figure 13b), the electrode seemed to suffer a subtle removal of the small particles with consequent greater exposition of graphite.

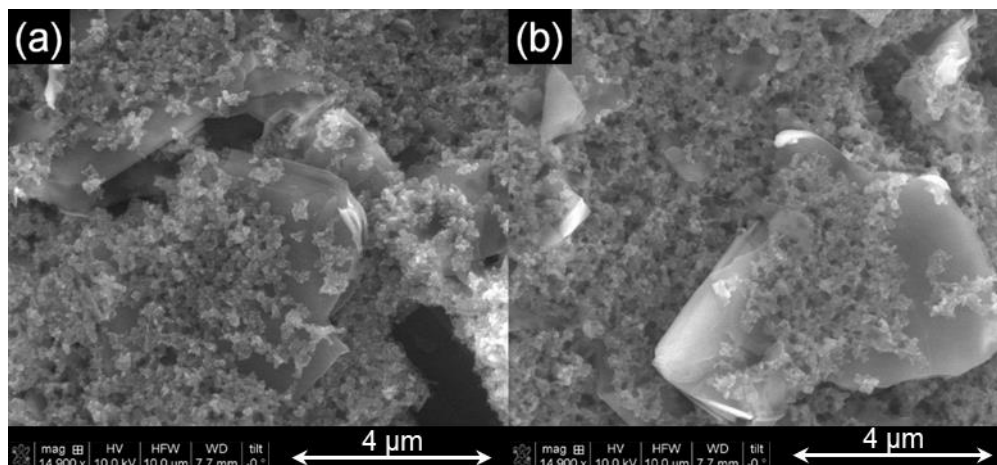


Figure 13 - SEM image of the SPCE before (a) and after (b) acid treatment using CV

The EDX spectrum shown in Figure 14 indicates that the SPCE is mainly composed of carbon, oxygen, chlorine and sodium. The presence of sodium and chlorine are probably related to the insertion of additives in the carbon ink [29]. Despite the manufacturers do not provide details about ink composition due to proprietary information, it is known that it contains not only graphite but also solvents and some polymeric binders [30]. After the acid treatment, the main observed alteration was the introduction of hydroxyl groups on the SPCE surface due to the application of extreme potentials, which can be verified by the significantly increase of the oxygen peak.

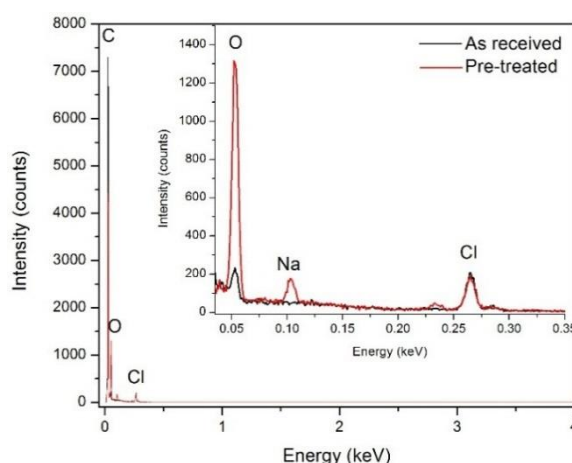


Figure 14 - EDX spectrum of the SPCE before and after the acid treatment using CV. The inset shows the spectrum in the lower energy region (up to 0.35 keV)

Figure 15a depicts the morphology of PANI electrodeposited onto the treated SPCE, which is in agreement with the results reported by other authors [31, 32]. The polymer was obtained as a spongy, porous and branched film with high surface area and interconnected fibers network. Although the glutaraldehyde attachment did not cause an obvious change in the electrode structure (Figure 15b), the immobilization of anti-horse IgG could be noted in Figure 15c. The attached antibodies were present as some small protein clusters on the PANI fibers, whose size could not be accurately measured since the length of an antibody is supposed to be around only 11 nm [33, 34]. Finally, it is shown in Figure 15d that the electrode containing casein became brighter and changed the texture of the material with respect to the previous step, confirming the efficiency of the blocking. EDX was not employed as a technique for studying the modifications caused in these functionalization steps because its depth resolution is not expected to provide enough information about the surface alterations caused by the biomolecules immobilization.

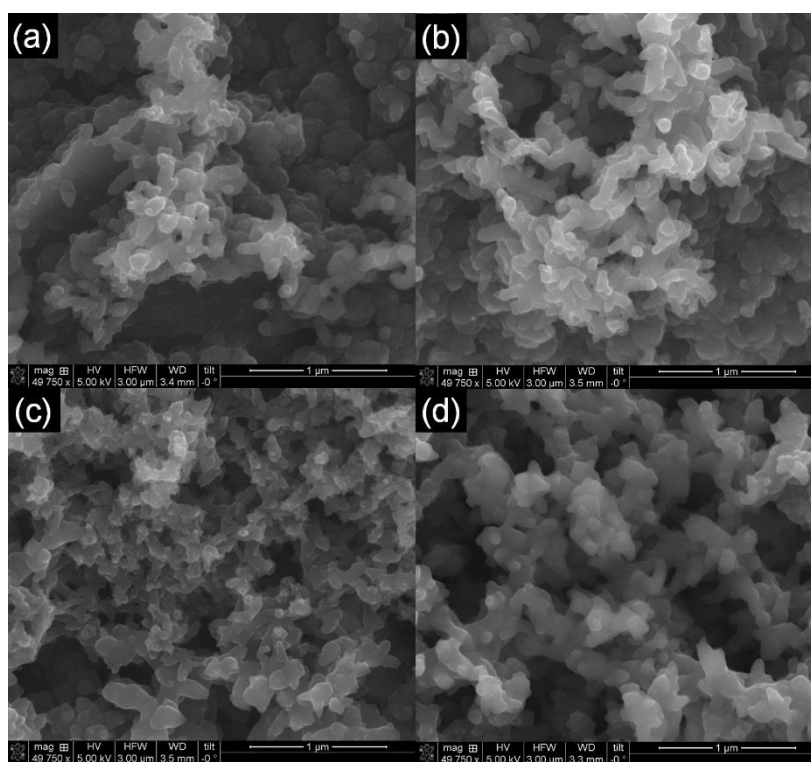


Figure 15 - SEM images of the treated SPCE modified by the deposition of PANI (a), glutaraldehyde (b), anti-horse IgG (c) and casein (d)

6.4.3 Immunosensor padronization: horse serum IgG detection

Aiming to assess the capability of the biosensor to detect the target analyte (horse IgG), it was assayed with horse serum at various concentrations. Figure 16 shows the impedance spectrum obtained before and after the exposure of the biosensor to the solutions containing horse serum diluted in PBS buffer at various concentrations. The Nyquist plot is a typical form to represent EIS data and it is represented as a correlation between the real (Z') and the imaginary (Z'') impedance. In this type of representation, the semicircle diameter relates to the electron transfer limited processes and the linear part at the low frequencies region corresponds to diffusion-limited processes [35]. The interpretation of impedance plots provides useful information about interface properties of an electrode and allows inferring about the presence of adsorbed substances at the surface [36].

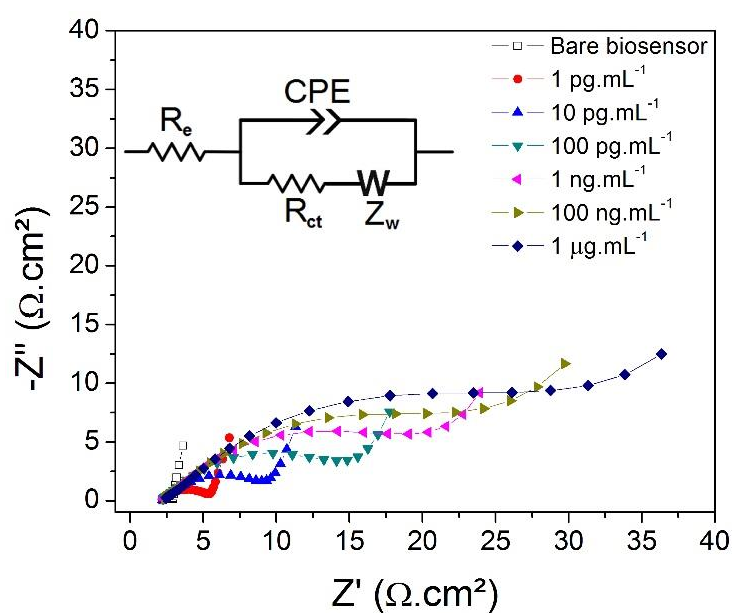


Figure 16 - Nyquist plot of the immunosensor before and after the exposure to horse serum at various concentrations in PBS buffer

Briefly, it is possible to observe that the semicircle diameter increased with increasing horse serum concentration. However, to quantify the impedimetric response of an electrochemical system, the EIS data is generally fitted with an equivalent circuit comprising electrical elements such as resistors, capacitors and/or

inductors. The inset in Figure 16 represents the equivalent circuit used to model the impedance data.

This model (Randles equivalent circuit) consists of an electrolyte resistance (R_e) in series with a constant phase element (CPE) associated in parallel with the pair R_{ct} and Warburg impedance (Z_w). The CPE is used instead a pure capacitor due to the inhomogeneity of the electrode surface, which can cause coupling of the solution resistance and the irregular distribution of the capacitance over the electrode [37]. The R_{ct} is related to the semicircle diameter of the Nyquist plot and represents the barrier to the electron transfer over the conductive PANI transducer. This element is commonly monitored as a useful parameter to evaluate the performance of Faradaic biosensors because it is significantly affected by the interaction of antigen-antibody at the electrode surface [38-40]. In this work, the condition of chi-squared $\chi^2 < 10^{-3}$ [41-43] was employed as a criterion for validating the proposed Randles circuit, which was satisfied when fitting all the experimental measurements.

6.4.4 Validation of impedance data by Kramer's-Kronig transform

In order to validate EIS data, Kramer's-Kronig (K-K) transform was employed to evaluate whether the designed biosensor was affected by extrinsic factors. This method is based on the Linear Systems Theory, which examines if a certain system is sufficiently linear, causal and stable to confirm the robustness of the impedance result [44]. The K-K method consists in calculating the values of Z' by means of the experimental Z'' and the theoretical Z'' values from the experimental Z' according to the respective Equations 11 and 12, in which ω is the angular frequency of the input voltage.

$$Z'(\omega) = \frac{2}{\pi} \cdot \int_0^{\infty} \frac{\omega' \cdot Z''(\omega')}{\omega^2 - \omega'^2} d\omega' \quad (11)$$

$$Z''(\omega) = \frac{-2}{\pi} \cdot \int_0^{\infty} \frac{\omega \cdot Z'(\omega')}{\omega^2 - \omega'^2} d\omega' \quad (12)$$

Figure 17 presents the Bode diagram of the experimental EIS data and the associated K-K transform plots with respect to the magnitude of impedance ($|Z|$) and

the phase angle ($-\phi$). The curves are practically superimposed, which indicates the goodness of fit of the K-K transform to the experimental data, confirming that the biosensors developed for testing the sensitivity against horse serum and the selectivity against swine and bovine sera were not affected by external factors but only by changes in the electrode-electrolyte interface.

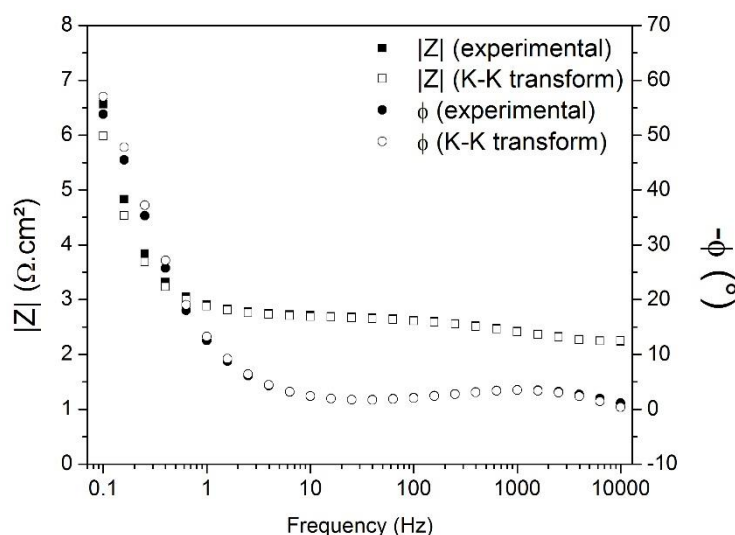


Figure 17 - Bode diagram of both experimental and K-K transform plots of the horsemeat biosensor

6.4.5 Analysis of the sensitivity and selectivity of the biosensor towards horse serum in buffer solution

The impedance data were interpreted with respect to the variation of R_{ct} when the biosensor was exposed to horse, swine and bovine sera diluted at various concentrations in PBS buffer. ΔR_{ct} was calculated as the difference between the R_{ct} obtained after and before the exposition of the biosensor to each serum solution.

As seen in the calibration plot (Figure 18), a progressive increase of R_{ct} was observed only when the biosensor was exposed to its homologous (horse) serum, thus demonstrating the formation of the immunocomplex between the antigen (horse IgG) and the antibodies immobilized as units of recognition on the electrode surface.

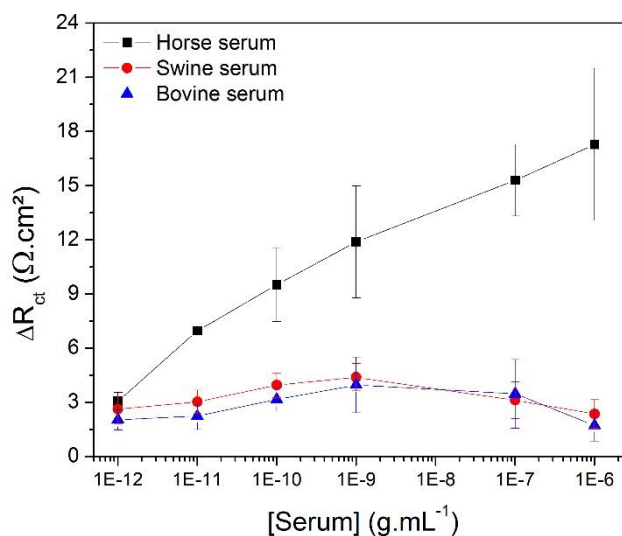


Figure 18 - Calibration curve of the immunosensor exposed to horse, swine and bovine serum at various concentrations in PBS buffer

The impedimetric immunosensor responded linearly towards the logarithm of the target analyte concentration, indicating that there is a strong relationship between the concentration of horse serum [S_{horse}] (g.mL⁻¹) and the ΔR_{ct} (Ω.cm²) according to Equation 13.

$$\Delta R_{ct} = 0.92266 \ln[S_{horse}] + 30.32904 \quad (13)$$

Contrarily, when the heterologous swine and bovine sera were kept in contact with the electrode, a random variation of R_{ct} was observed, which indicates there was no recognition of analyte in these solutions. A t-Student test with 95% confidence level revealed that there is no significant difference among the impedance increase of the immunosensor exposed to the horse serum at 10⁻¹² g.mL⁻¹ and to the swine ($p = 0.46$) and bovine ($p = 0.07$) sera at the same concentration. For this reason, the linearity of the impedimetric response was considered at the concentration range from 10⁻¹¹ g.mL⁻¹ to 10⁻⁶ g.mL⁻¹. Table 3 presents the coefficients of logarithmic regression (R^2) with respect to the impedance response of the immunosensor exposed to horse, swine and bovine sera at the mentioned concentrations.

Table 3 - R^2 value related to the logarithm fit of the correlation between ΔR_{ct} and concentration of horse, swine and bovine serum diluted in PBS buffer

	Horse serum	Swine serum	Bovine serum
R^2 (-)	0.995	0.0211	0.0126

6.4.6 Analysis of commercial meat samples

For further evaluation of the biosensor, the recognition capability against the target analyte in real commercial raw meats was evaluated. The biosensor was exposed to solutions at unknown concentrations of horsemeat, pork and beef purchased from local market. After estimating the concentration of proteins in the commercial meat solutions at 1%w/v by UV-VIS spectroscopy, the following values were found: 3.44×10^{-4} g.mL⁻¹ (horsemeat), 2.65×10^{-4} g.mL⁻¹ (pork) and 2.65×10^{-4} g.mL⁻¹ (beef). The samples were diluted one thousand, ten thousand and a hundred thousand times before the exposure to the biosensor. Figure 19 presents the resultant impedance response of the biosensor reacted to real samples at the three concentrations.

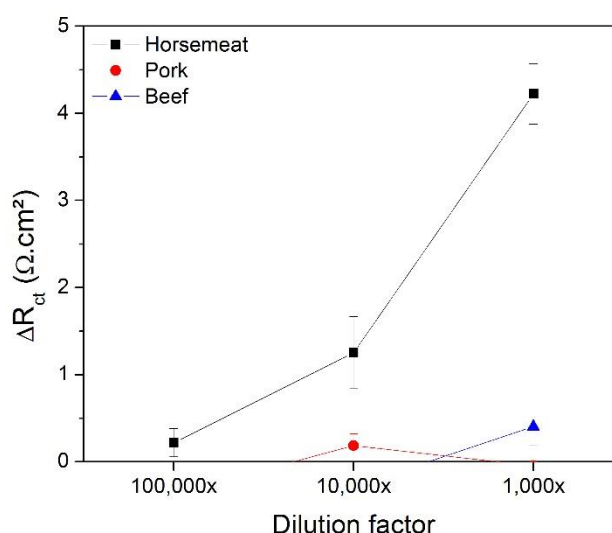


Figure 19 - Calibration curve of the immunosensor exposed to horsemeat, pork and beef solutions diluted 1,000; 10,000 and 100,000 times

The impedance data obtained by testing the biosensor against real sample of horsemeat were better adjusted to a linear regression plot following the Equation 14 ($R^2 = 0.9578$), in which $[M_{horse}]$ ($\text{g}\cdot\text{mL}^{-1}$) is the concentration of horsemeat.

$$\Delta R_{ct} = 4.0 \times 10^5 [M_{horse}] + 0.25984 \quad (14)$$

The presence of interferers in the real samples, such as the nutritional components (fat, vitamins, inorganic salts, etc) probably affected the biosensor performance by preventing the target analyte to bind the units of recognition present in the electrode surface. The impedimetric response in real sample was lower than the ones obtained for all sera in buffer solution. This fact indicates that the meat components hinders the capability of the antibodies binding molecules independently whether they are the target analyte or unspecific compounds.

Concerning the time to perform the EIS test, to record the impedance measurement it was necessary 1.87 ± 0.49 min, which corresponds only to 3.37% of the total time related to the other steps (preparation of the meat sample, incubation period of the biosensor and OCP monitoring). Thus, the total time of approximately 72 min for performing the entire test could be consistently reduced by optimizing the protocol to extract the meat samples and/or the period of incubation in the analyte solution.

6.4.7 Limit of detection (LOD) of the proposed immunosensor

The LOD can be defined as the lowest detectable concentration of an analyte in a sample. The resultant signal from the exposure to the analyte at the LOD (x_L) can be expressed as a function of the mean of the blank measurements (\bar{x}_{bl}) and its standard deviation (SD_{bl}) according to Equation 15 [45], where k is a factor equal to 3.3 related to the confidence level for estimating LOD [45].

$$x_L = \bar{x}_{bl} + kSD_{bl} \quad (15)$$

Based on the equations 13, 14 and 15, it was possible to estimate that the LOD of the immunosensor is 27.6 fg.mL^{-1} towards the horse serum diluted in buffer solution and $1.54 \text{ } \mu\text{g.mL}^{-1}$ of commercial horsemeat, which represents a percentage concentration of 0.004% w/v of proteins in horsemeat solution. This LOD is lower than those reported in the literature by detecting the presence of various species in meats using mass spectrometry (0.24%) [46], ELISA (0.6 - 0.01%) [47, 48] and DNA-based assays (0.1%) [49, 50].

In order to consider adventitious presence of other species contaminants, the Food Standards Agency [51] considered that the products containing less than 0.1% of a mislabeled meat contaminant can be considered equivalent to zero (fraud absence). From 1%, it should be considered the possibility of adulteration or negligence. Notwithstanding, the presence of beef or pork traces must be informed in the product label so as to protect religious faiths [52].

6.5 CONCLUSIONS

This work reported the development of an impedimetric immunosensor for specific detection of horsemeat as a technology for screening meat adulteration. For this purpose, polyaniline electrodeposited on the surface of a SPCE served as the conductive matrix. CV and SEM/EDX analysis confirmed the functionalization of the polymeric transducer substrate by the immobilization of anti-horse IgG antibodies on the electrode surface. EIS technique was validated by using K-K transform, which proved that the impedance data were consistent and stable. When exposed to horse serum diluted in PBS buffer, the developed immunosensors were very sensitive and selective exclusively towards the target analyte at various concentrations (with LOD equal to 27.6 fg.mL^{-1}), not presenting significant variation of R_{ct} to swine and bovine sera. The proposed device was also capable of recognizing the target analyte in real samples. The exposure to horsemeat at 10^{-5} , 10^{-4} and 10^{-3} %w/v caused successive linear increases in the R_{ct} due to the recognition of horse IgG in the samples. The immunosensor did not detect the presence of target analyte in commercial pork and bovine meat homogenates and presented a LOD of 0.004%w/v. From the

perspective of assay time, it was necessary approximately 70 minutes to perform the whole detection test, of which the obtaining of EIS data demanded only 3.37%. To fully assess the real application of the proposed impedimetric immunosensor, future tests should focus on evaluating the effect of not only raw but also cooked meat on its performance, the stability of the sensor over long periods of storage and the presence of the target analyte as a contaminant at various concentrations in real samples.

6.6 REFERENCES

- [1] MOYER, D.C.; DEVRIES, J. W.; SPINK, J. The economics of a food fraud incident – Case studies and examples including Melamine in Wheat Gluten. **Food Control**, 71, p. 358–364, 2017.
- [2] MEIRA, L.; COSTA, J.; VILLA, C.; RAMOS, F.; OLIVEIRA, M. B. P. P.; MAFRA, I. EvaGreen real-time PCR to determine horse meat adulteration in processed foods. **LWT - Food Science and Technology**, 75, p. 408–416, 2017
- [3] MAGIATI, M.; MYRIDAKI, V. M.; CHRISTOPOULOS, T. K.; KALOGIANNI, D. P. Lateral flow test for meat authentication with visual detection. **Food Chemistry**, 274, p. 803-807, 2018.
- [4] FUSEINI, A.; WOTTON, S. B.; KNOWLES, T. G.; HDLEY, P. J. Halal meat fraud and safety issues in the UK: a review in the context of the European Union. **Food Ethics**, 1(2), p. 127-142, 2017
- [5] TEIXEIRA, L. V.; TEIXEIRA, C. S.; OLIVEIRA, D. A. A. Identificação espécie-específica de carnes e produtos cárneos de origem bubalina e bovina pela técnica de PCR-RFLP. **Arquivo Brasileiro de Medicina Veterinária e Zootecnia**, 67(1), p. 309-314, 2015.
- [6] FALKHEIMER, J.; HEIDE, M. Trust and Brand Recovery Campaigns in Crisis: Findus Nordic and the Horsemeat Scandal. **International Journal of Strategic Communication**, 9(2), p. 134-147, 2015.
- [7] ARSALANE, A.; NOUREDDINE, E. B.; RHOFIR, K.; TABYAOUI, A.; KLILOU, A. Beef and horse meat discrimination and storage time classification using a portable device based on DSP and PCA method. **International Journal of Intelligent Enterprise**, 4(1-2), p. 58-75, 2017.

- [8] DANEZIS, G. P.; TSAGKARIS, A. S.; CAMIN, F.; BRUSIC, V.; GEORGIU, C. A. Food authentication: techniques, trends & emerging approaches. **Trends in Analytical Chemistry**, 85(A), p. 123-132, 2016.
- [9] OTTAVIAN, M.; FASOLATO, L.; FACCO, P.; BAROLO, M. Foodstuff authentication from spectral data: Toward a species-independent discrimination between fresh and frozen–thawed fish samples. **Journal of Food Engineering**, 119(4), p. 765-775, 2013.
- [10] KAMRUZZAMAN, M.; MAKINO, Y.; OSHITA, S. Rapid and non-destructive detection of chicken adulteration in minced beef using visible near-infrared hyperspectral imaging and machine learning. **Journal of Food Engineering**, 170, p. 8-15, 2016.
- [11] ROPODI, A. I.; PANAGO, E. Z.; NYCHAS, G. J. E. Multispectral imaging (MSI): A promising method for the detection of minced beef adulteration with horsemeat. **Food Control**, 73, p. 57–63, 2017.
- [12] PANAGO, E. Z.; PAPADOPOULOU, O.; CARSTENSEN, J. M.; NYCHAS, G. J. E. Potential of multispectral imaging technology for rapid and non-destructive determination of the microbiological quality of beef filets during aerobic storage. **International Journal of Food Microbiology**, 174, p. 1-11, 2014.
- [13] KAMRUZZAMAN, M.; MAKINO, Y.; OSHITA, S.; LIU, S. Assessment of Visible Near-Infrared Hyperspectral Imaging as a Tool for Detection of Horsemeat Adulteration in Minced Beef. **Food and Bioprocess Technology**, 8(5), p. 1054–1062, 2015.
- [14] WEN, W.; YAN, X.; ZHU, C.; DU, D.; LIN, Y. Recent advances in electrochemical immunosensors. **Analytical Chemistry**, 89(1), p. 138-156, 2017.
- [15] XU, R.; WEI, S.; ZHOU, G.; REN, J.; LIU, Z.; TANG, S.; WU, X. Multiplex TaqMan locked nucleic acid real-time PCR for the differential identification of various meat and meat products. **Meat Science**, 137, p. 41–46, 2018.
- [16] SINGH, P. K.; JAIRATH, G.; AHLAWAT, S. S.; PATHERA, A.; SINGH, P. Biosensor: an emerging safety tool for meat industry. **Journal of Food Science and Technology**, 53(4), p. 1759–1765, 2016.
- [17] Mehrotra, P. Biosensors and their applications - a review. **Journal of Oral Biology and Craniofacial Research**, 6, p. 153-159, 2016.
- [18] SHARMA, R.; DEACON, S. E.; NOWAK, D.; GEORGE, S. E.; SZYMONIK, M. P.; TANG, A. A. S.; TOMLINSON, D. C.; DAVIS, A. G.; MCPHERSON, M. J.; WÄLTI, C. Label-free electrochemical impedance biosensor to detect human interleukin-8 in serum with sub-pg/ml sensitivity. **Biosensors and Bioelectronics**, 80, p. 607–613, 2016.

[19] KOKKINOS, C.; ECONOMOU, A.; PRODRMIDIS, M. I. Electrochemical immunosensors: Critical survey of different architectures and transduction strategies. **Trends in Analytical Chemistry**, 79, p. 88-105, 2016.

[20] PINE RESEARCH. **Screen-printed electrode information. Carbon and ceramic electrode information.** Document DRP 10036, <https://www.pineresearch.com/shop/wp-content/uploads/sites/2/2016/10/DRP10036-Screen-Printed-ElectrodesOverview REV001.pdf> , accessed in Oct. 2018.

[21] YUKIRD, J.; WONGTANGPRASERT, T.; RANGKUPAN, R.; CHAILAPAKUL, O.; PISITKUN, T.; RODTHONGKUM, N. Label-free immunosensor based on graphene/polyaniline nanocomposite for neutrophil gelatinase-associated lipocalin detection. **Biosensors and Bioelectronics**, 87, p. 249-255, 2017.

[22] PROMEGA. **Calculating nucleic acid or protein concentration. Using the GloMax® Multi+ Microplate Instrument.** <https://www.promega.com/-/media/files/resources/application-notes/pathlength/calculating-nucleic-acid-or-protein-concentration-using-the-glomax-multi-microplate-instrument.pdf>, accessed in Oct. 2018.

[23] ZHANG, L.; XIAO, J.; WANG, H.; SHAO, M. Carbon-based electrocatalysts for hydrogen and oxygen evolution reactions. **ACS Catalysis**, 7(11), p. 7855-7865, 2017.

[24] QAZI, T. H.; RAI, R.; BOCCACCINI, A. R. Tissue engineering of electrically responsive tissues using polyaniline based polymers: a review. **Biomaterials**, 35(33), p. 9068-9086, 2014.

[25] LAI, J.; YI, Y.; ZHU, P.; SHEN, J.; WU, K.; ZHANG, L.; LIU, J. Polyaniline-based glucose biosensor - a review. **Journal of Electroanalytical Chemistry**, 782, p. 138-153, 2016.

[26] CHOWDHURY, A. D.; DE, A.; CHAUDHURI, C. R.; BANDYOPADHYAY, K.; SEN, P. Label free polyaniline based impedimetric biosensor for detection of *E. coli* O157:H7 bacteria. **Sensors and Actuators B**, 171-172, p. 916-923, 2012.

[27] FARIA, R. A. D.; LINS, V. F. C.; NAPPI, G. U.; MATENCIO, T.; HENEINE, L. G. D. Development of an impedimetric immunosensor for specific detection of snake venom. **BioNanoScience**, p. 1-9, 2018.

[28] AFKHAMI, A.; HASHEMI, P.; BAGHERI, H.; SALIMIAN, J.; AHMADI, A.; MADRAKIAN, T. Impedimetric immunosensor for the label-free and direct detection of botulinum neurotoxin serotype A using Au nanoparticles/graphene-chitosan composite. **Biosensors and Bioelectronics**, 93, p. 124-131, 2017.

[29] TSAI, J. Z.; CHEN, C. J.; SETTU, K.; LIN, Y. F.; CHEN, C. L.; LIU, J. T. Screen-printed carbon electrode-based electrochemical immunosensor for rapid detection of microalbuminuria. **Biosensors and Bioelectronics**, 77, p. 1175-1182, 2016.

- [30] BOLADO, F. P.; SANTOS, D. H.; ARDISANA, P. J. L.; PERNÍA, A. M.; GARCÍA, A. C. Electrochemical characterization of screen-printed and conventional carbon paste electrodes. **Electrochimica Acta**, 53, p. 3635-3642, 2008.
- [31] OBAID, A. Y.; EL-MOSSALAMY, E. H.; AL-THABAITI, S. A.; EL-HALLAG, I. S.; HERMAS, A. A.; ASIRI, A. M. Electrodeposition and Characterization of Polyaniline on Stainless Steel Surface via Cyclic, Convulsive Voltammetry and SEM in Aqueous Acidic Solutions. **International Journal of Electrochemical Science**, 9, p. 1003-1015, 2014.
- [32] MATHEBE, N. G. R.; MORRIN, A.; IWUOHA, E. I. Electrochemistry and scanning electron microscopy of polyaniline/peroxidase-based biosensor. **Talanta**, 64, p. 115-120, 2004.
- [33] RETH, M. Matching cellular dimensions with molecular sizes. **Nature Immunology**, 14(8), p. 765-767, 2013.
- [34] SABER, R.; SARKAR, S.; GILL, P.; NAZARI, B.; FARIDANI, F. High resolution imaging of IgG and IgM molecules by scanning tunneling microscopy in air condition. **Scientia Iranica**, 18(6), p. 1643-1646, 2011.
- [35] ARKAN, E.; SABER, R.; KARIMI, Z.; MOSTAFAIE, A.; SHAMSIPUR, M. Multiwall carbon nanotube-ionic liquid electrode modified with gold nanoparticles as a base for preparation of a novel impedimetric immunosensor for low level detection of human serum albumin in biological fluids. **Journal of Pharmaceutical and Biomedical Analysis**, 92, p. 74–81, 2014.
- [36] LIU, Y.; YIN, F.; LONG, Y.; ZHANG, Z.; YAO, S. Study of the immobilization of alcohol dehydrogenase on Au-colloid modified gold electrode by piezoelectric quartz crystal sensor, cyclic voltammetry, and electrochemical impedance techniques. **Journal of Colloid and Interface Science**, 258(1), p. 75-81, 2003.
- [37] LASIA, A. Electrochemical impedance spectroscopic and its applications. In **Conway BE**, Bockris JOM, White RE. Springer, New York, 2014.
- [38] RAMANATHAN, M.; PATIL, M.; EPUR, R.; YUN, Y.; SHANOV, V.; SCHULZ, M.; HEINEMAN, W. R.; DATTA, M. K.; KUMTA, P. N. Gold-coated carbon nanotube electrode arrays: Immunosensors for impedimetric detection of bone biomarkers. **Biosensors and Bioelectronics**, 77, p. 580–588, 2016.
- [39] GÜNDOĞDU, A.; AYDIN, E. B.; SEZGINTÜRK, M. K. A novel electrochemical immunosensor based on ITO modified by carboxyl-ended silane agent for ultrasensitive detection of MAGE-1 in human serum. **Analytical Biochemistry**, 537, p. 84–92, 2017.
- [40] SHARMA, A.; KUMAR, A.; KHAN, R. Electrochemical immunosensor based on poly (3,4-ethylenedioxythiophene) modified with gold nanoparticle to detect aflatoxin B1. **Materials Science and Engineering C**, 76, p. 802-809, 2017.

- [41] OSÓRIO, W. R.; GARCIA, L. R.; PEIXOTO, L. C.; GARCIA, A. A influência da macrosegregação e da variação dos espaçamentos dentríticos na resistência a corrosão da liga Al-4,5%Cu. **Revista Matéria**, 13(3), p. 542-552, 2008.
- [42] SARAC, A. S.; ATES, M.; KILIC, B. Electrochemical Impedance Spectroscopic Study of Polyaniline on Platinum, Glassy Carbon and Carbon Fiber Microelectrodes. **International Journal of Electrochemical Science**, 3, p. 777-786, 2008.
- [43] ATES, M.; SARAC, A. S. Electrochemical impedance spectroscopy of poly[carbazole-co-N-p-tolylsulfonyl pyrrole] on carbon fiber microelectrodes, equivalent circuits for modelling. **Progress in Organic Coatings**, 65, p. 281-287, 2009.
- [44] JINLONG, L.; HONGYUN, L.; TONGXIANG, L. Investigation of microstructure and corrosion behavior of burnished aluminum alloy by TEM, EWF, XPS and EIS techniques. **Materials Research Bulletin**, 83, p. 148-154, 2016.
- [45] IUPAC (1997) **Compendium of Chemical Terminology**. (2nd ed). Compiled by A. D. McNaught and A. Wilkinson. Blackwell Scientific Publications, Oxford.
- [46] SHRIVASTAVA, A.; GUPTA, V. B. Methods for the determination of limit of detection and limit of quantitation of the analytical methods. **Chronicles of Young Scientists**, 2(1), p. 21, 2011.
- [47] VON BARGEN, C.; BROCKMEYER, J.; HUMPF, H. U. Meat Authentication: A New HPLC-MS/MS Based Method for the Fast and Sensitive Detection of Horse and Pork in Highly Processed Food. **Journal of Agricultural and Food Chemistry**, 62(39), p. 9428-9435, 2014.
- [48] MANDLI, J.; FATIMI, I. E. L.; SEDDAOUI, N.; AMINE, A. Enzyme immunoassay (ELISA/immunosensor) for a sensitive detection of pork adulteration in meat. **Food Chemistry**, 255, p. 380-389, 2018.
- [49] MACEDO-SILVA, A.; BARBOSA, S. F. C.; ALKMIN, M. G. A.; VAZ, A. J.; SHIMOKOMAKI, M.; TENUTA-FILHO, A. Hamburger meat identification by dot-ELISA. **Meat Science**, 56, p. 189-192, 2000.
- [50] OLIVEIRA, A. C. S.; PEDROSO, S. C. S.; CARDILLI, D. J.; LEITE, J. P. L.; FERREIRA, G. V. L.; SILVA, A. S.; ROOS, T. B.; MORAES, C. M.; SOUSA, R. S.; MONTEIRO, R. S. D. Brazilian ground beef authentication by multiplex polymerase chain reaction. **Ciência Rural**, 48(2), p. 1-7, 2018.
- [51] CHUNG, H. H. Real-time polymerase chain reaction (RT-PCR) for the authentication of raw meats. **International Food Research Journal**, 25(2), p. 632-638, 2018.

[52] FOOD STANDARDS AGENCY. **European Commission’s “Technical solution” to the low-level presence of unauthorized GMOs**, 2010. Available in <https://www.reading.ac.uk/foodlaw/pdf/eu-10026-gm-contamination-proposals.pdf>. Accessed 4 oct. 2018.

[53] PREMANANDH, J. Horse meat scandal – A wake-up call for regulatory authorities. **Food Control**, 34(2), p. 568–569, 2013.

CHAPTER 7 – NON-ENZYMATIC IMPEDIMETRIC SENSOR BASED ON 3-AMINOPHENYLBORONIC ACID FUNCTIONALIZED SCREEN-PRINTED CARBON ELECTRODE FOR HIGHLY SENSITIVE GLUCOSE DETECTION

*Text adapted from: FARIA, R. A. D.; IDEN, H.; HENEINE, L. G. D.; MATENCIO, T.; MESSADDEQ, Y. Non-enzymatic impedimetric sensor based on 3-aminophenylboronic acid functionalized screen-printed carbon electrode for highly sensitive glucose detection. **Sensors**, 19, p. 1686, 2019.*

Ricardo Adriano Dorledo de Faria^{1,2}, Hassan Iden^{2,3}, Luiz Guilherme Dias Heneine⁴,
Tulio Matencio⁵, Younès Messaddeq^{2,6}

¹ Department of Chemical Engineering, Universidade Federal de Minas Gerais (UFMG), Belo Horizonte, Minas Gerais 30270-901, Brazil

² Center for Optics, Photonics and Lasers (COPL), Université Laval, Quebec City, QC G1V 0A6, Canada;

³ CDN Isotopes, Montreal, QC H9R 1H1, Canada

⁴ Department of Applied Immunology, Fundação Ezequiel Dias (FUNED), Belo Horizonte, Minas Gerais 30510-010, Brazil

⁵ Department of Chemistry, Universidade Federal de Minas Gerais (UFMG), Belo Horizonte, Minas Gerais 30270-901, Brazil

⁶ Institute of Chemistry, UNESP, Araraquara, São Paulo 14800-060, Brazil

7.1 ABSTRACT

A highly sensitive glucose sensor was prepared by a one-step method using 3-aminophenyl boronic acid as a unit of recognition and a screen-printed carbon electrode (SPCE) as an electrochemical transducer. Scanning Electron Microscopy confirmed the success of the functionalization of the SPCE due to the presence of clusters of boronic acid distributed on the carbon surface. In agreement with the Electrochemical Impedance Spectroscopy (EIS) tests performed before and after the functionalization, Cyclic Voltammetry (CV) results indicated that the electroactivity of the electrode decreased 37.9% owing to the presence of the poly phenylboronic acid on the electrode surface. EIS revealed that the sensor was capable to selectively detect glucose at a broad range of concentrations (limit of detection of 8.53×10^{-9} M),

not recognizing fructose and sucrose. The device presented a stable impedimetric response when immediately prepared, but suffered the influence of the storage time and some interfering species (dopamine, NaCl and animal serum). The response time at optimized conditions was estimated to be equal to 4.0 ± 0.6 s.

Keywords: sensor; glucose; Electrochemical Impedance Spectroscopy; boronic acid.

7.2 INTRODUCTION

The detection of glucose has drawn significant attention due to the importance of this saccharide as a major dietary source of energy and its consequent impact on humans' health. Glucose is the only carbohydrate present in the human serum and variations of its concentration can lead to hypoglycemia (in case of low concentration), diabetes and hypertension (in case of high concentration) [1]. According to the World Health Organization, diabetes (whose criterion of diagnosis is the glucose concentration ≥ 7.0 mmol/L in the plasma) has been responsible for high levels of mortality worldwide [2].

Nonetheless, the importance of detecting glucose is not restricted to clinical applications. The necessity of improving quality control in the food industry has prompted the development of reliable analytical methods for the continuous monitoring of sugars aiming to increase process efficiency and to prevent economic losses [3]. Many studies have been devoted to detect glucose for various applications, such as beverage quality control [4,5], biological fuel cells [6,7] and environmental monitoring [8,9].

Optical and electrochemical transductions are the most widely studied methods for this purpose. In common, both of them are generally based on the conversion of the signal from the reaction between an enzyme (glucose oxidase is most widely used) and the glucose molecule, yielding metabolites that can change the color or electrochemical features of a certain matrix [10]. The hexokinase method, for example, consists of a series of chemical reactions involving glucose to the production of nicotinamide-adenine-dinucleotide-reduced (NADH), whose

concentration is proportional to the absorbed light measured at 340 nm wavelength [10].

As an advantage over the optical devices, the electrochemical-based sensors are more sensitive. Among the electrochemical techniques, EIS has attracted special attention not only due to its high sensitivity, but mainly because it allows the use of label-free and non-enzymatic methods [11,12]. In this technique, a sinusoidal potentiostatic perturbation is applied to an electrode under study immersed in a conductive solution, generating a frequency-dependent AC current [13]. Thus, the frequency-dependent impedance is the complex ratio between the applied potential and the resultant current. The interpretation of impedance parameters (the inherent resistance, capacitance and/or inductance) can provide plenty of information on the interfacial phenomena that take place on the studied electrode, such as the recognition of an analyte of interest [14,15].

In the literature, there are scientific articles devoted to the detection of glucose by enzymatic electrochemical sensors. Clark and Lyons [16] first reported the development of a device capable to detect glucose by means of the oxidation of the sugar mediated by the enzyme glucose oxidase (GOx) in presence of oxygen and water producing hydrogen peroxide and gluconic acid. Since then many studies described methods to overwhelm the limitations of first-generation glucose sensors, for instance the need for high operational potentials, the low activity of GOx or the interference of other sugars in the response of glucose dehydrogenase (an enzyme with higher activity than GOx) [17,18]. Although the majority of the commercial glucose sensors is based on enzymatic methods (which provides great sensitivity and selectivity), the use of enzymes possess some important limitations. The main disadvantages of the use of enzymes for bioapplications include the difficulty of immobilization due to its low stability (pH and temperature dependent activity), the high cost, low mobility and low mass-transfer rate [19, 20].

Recently, several groups have directed great efforts to develop glucose sensors with/without enzymes by using optical or electrochemical techniques [21-23], however the enzymatic sensibility, sensitivity of the device, selectivity, sophisticated fabrication and high cost still remain as important challenges to be overcome.

In the present paper, we developed a 3-aminophenyl boronic acid-based sensor that detects glucose at low concentrations by using EIS as a transduction technique. This non-enzymatic sensor exhibited a low limit of detection and high selectivity towards glucose when exposed also to fructose and sucrose. The effect of interfering species commonly present in biological fluids was also examined, as well as the time of response of the sensor, its repeatability and reproducibility. Besides, the use of screen-printed carbon electrode (SPCE) as a transducer substrate for this impedimetric sensor represents a key point of the presented technology since this material is well known to be cheap (rapid and low-cost mass production), easily applied to point-of-care applications for being portable and the easiness of functionalization [24-26].

7.3 MATERIALS AND METHODS

7.3.1 Materials and chemicals

3-aminophenylboronic acid, sodium nitrate was purchased from J.T. Baker, sulfuric acid 98% was purchased from Anachemia (Canada), potassium chloride and sodium chloride were purchased from Fisher Scientific (Belgium), D-(+)-glucose, D-(-)-fructose, sucrose, dopamine, potassium ferricyanide and potassium ferrocyanide were obtained from Sigma Aldrich. All chemicals were of analytical grade and the solutions were prepared using ultrapure deionized water (18 M Ω .cm resistivity). Bovine serum was provided by Fundação Ezequiel Dias (Belo Horizonte/MG, Brazil).

Screen-printed carbon electrodes (RRPE1002C), consisting of carbon as working (dimensions of 5 mm x 4 mm) and counter electrodes and Ag/AgCl as reference electrode, were purchased from Pine Research.

7.3.2. Instrumentation and apparatus

Potentiostat VersaSTAT 3 from AMETEK Scientific Instruments (Canada) interfaced with VersaStudio software. EIS was performed using an electrochemical cell containing 0.1 M KCl as supporting electrolyte and both $K_3[Fe(CN)_6]$ and $K_4[Fe(CN)_6]$ at 0.005 M as redox probe couple.

Scanning Electron Microscopy (SEM) was performed using a Quanta 3D FEG microscope.

7.3.3. Functionalization and characterization of the SPCE

Prior to the functionalization, the SPCE was submitted to a potential cycling from -2.5 to +2.5 V vs Ag/AgCl in 0.05 M H_2SO_4 aqueous solution at $0.05 V \cdot s^{-1}$ in order to remove its organic contaminants and to improve the surface electroactivity [28]. In the previous chapter, we demonstrated that this pre-treatment is crucial to enhance the charge-transfer kinetics of the electrode by introducing hydroxyl groups on the surface and by exposing the graphite flakes edges from the carbon ink to the electrolyte [29].

To the treated electrode, 20 μL of 0.4 M 3-aminophenylboronic acid and 20 μL of 0.4 M $NaNO_2$ both diluted in 0.1 M H_2SO_4 were added to the working electrode. The reaction was left for 10 minutes after which, the electrode was washed exhaustively in a large volume of ultrapure water. The scheme presented in Figure 20 describes the steps to prepare the proposed glucose sensor.

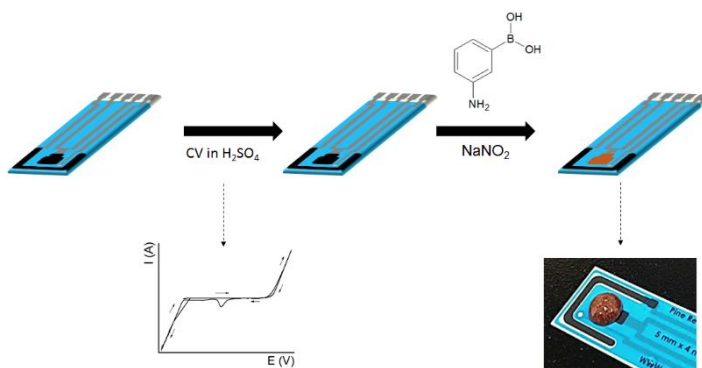


Figure 20 - Functionalization steps to obtain the glucose sensor

EIS was performed to investigate the changes in the electrochemical behavior of the SPCE due to the functionalization. The test was carried out at an AC amplitude of 0.01 V around the open circuit potential (OCP), which was previously stabilized for 300 s, with a frequency range varying from 10,000 to 0.1 Hz. Five points per frequency decade were recorded.

7.3.4. Selective detection of glucose by EIS

The impedance of the functionalized sensor was determined by EIS with the same parameters previously presented to obtain a basal value. Afterwards, 60 μL of aqueous glucose solutions at 10^{-8} , 10^{-7} , 10^{-6} , 10^{-5} , 10^{-4} , 10^{-3} , 10^{-2} , and 10^{-1} M were separately added to the working electrode, which was incubated for 300 s and carefully rinsed with a large volume of ultrapure water in order to remove the unbound and weakly adsorbed molecules from its surface. Finally, the electrode was immersed in the electrolyte and EIS was performed. This procedure was repeated in triplicate for all glucose concentrations tested.

To assess the selectivity of the glucose sensor, its working electrode was exposed separately to aqueous solutions of both fructose and sucrose at the same glucose concentrations and EIS parameters.

The results were analyzed by modelling the EIS data to an appropriate electrical equivalent circuit in Zview software version 2.9b (Scribner and Associates).

The effect of common interfering species on the performance of the sensor was investigated by EIS after exposing the device to 0.1 M NaCl, 0.02 M dopamine and bovine serum in the absence and presence of glucose at 10^{-8} M.

7.3.5. Evaluation of the sensor's stability

The chemical stability of the proposed glucose sensor was tested in terms of its repeatability according to the methodology described by Kannan and Rout [30], in which a hundred consecutive EIS measurements are carried out. Additionally, the

impedimetric response of the device was examined after 7, 14 and 21 days from its preparation.

7.4 RESULTS AND DISCUSSION

7.4.1. Characterization of the functionalized SPCE

SEM images of the SPCE before and after the functionalization were recorded to verify the presence of the deposited boronic acid. Figure 21 shows that the bare electrode contained irregularly flaked graphite particles randomly distributed along the inhomogeneous surface of the carbon ink as also observed in the literature [31, 32]. Following the incubation with the boronic acid, the transducer electrode was covered with clusters of circular shaped particles dispersed mainly around the graphite flakes.

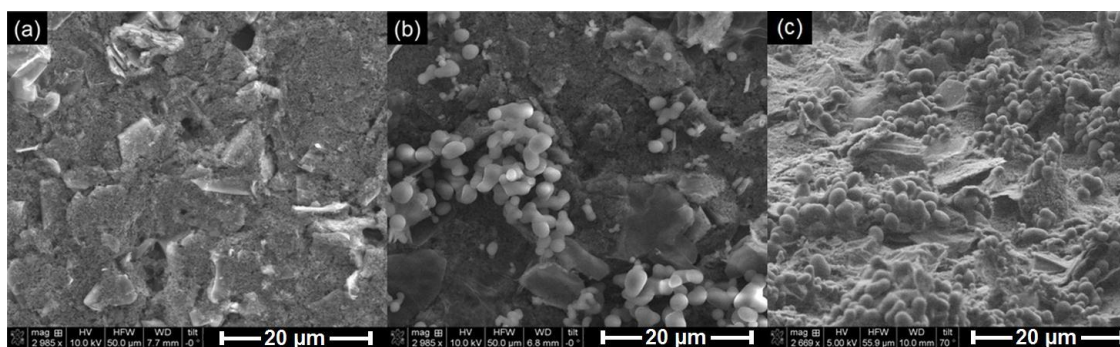


Figure 21 - SEM images of the SPCE before (a) and after (b) functionalization with 3-aminophenylboronic acid and (c) inclined view of the functionalized electrode

The functionalized electrode was also characterized by EIS. The Nyquist plot displayed in Figure 22 was interpreted by fitting the data to the electrical equivalent circuit presented in the figure. In the proposed circuit, R_e is the electrolyte resistance and two time constants were considered to represent multiple charge transfer kinetics of the SPCE with a resistance R , the R_{ct} , the constant phase elements “CPE1” and “CPE2” and the Warburg impedance W . The Warburg impedance is due to the diffusion of the ions $\text{Fe}(\text{CN})_6^{3-/4-}$ from the bulk electrolyte to the electrode and it

appears as a 45° straight line at low frequencies [33]. The CPE element represents a non-ideal capacitor and replaces the capacitance due to its roughness and heterogeneous surface [34]. The impedance associated to this parameter is described by Equation 16, where Q is a constant that describes the magnitude of CPE, ω is the angular frequency ($\omega = 2\pi f$), j is an imaginary number ($j = \sqrt{-1}$) and n is an exponent related to the heterogeneity of the surface ($0 < n < 1$) [35]. Due to the complexity of the SPCE structure, consisting of the graphitic flakes and the carbon ink with different relaxation times, two pairs of time constants resistor/CPE were employed to fit the EIS data. The pair $R/CPE1$ arises from the graphitic phase which is more electroactive and possess, thus, a higher charge transfer kinetics, while the pair $R_{ct}/CPE2$ corresponds to the more insulator carbon ink, whose mechanisms of charge transfer can be seen at lower frequencies followed by the diffusion of the electroactive species.

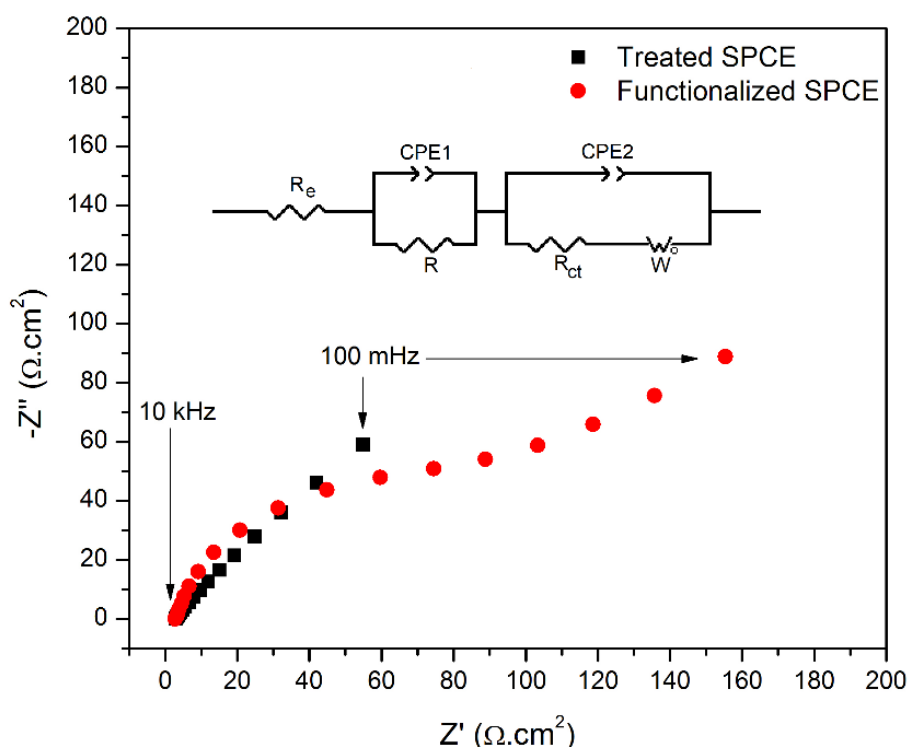


Figure 22 - Impedimetric monitoring of the SPCE before and after functionalization with 3-aminophenylboronic acid

$$CPE = \frac{1}{Q(j\omega)^n} \quad (16)$$

Considering the criterion of $\chi^2 < 10^{-3}$ as an indicative of the fitting quality [36], it was possible to ensure that the proposed equivalent circuit was suitable to model the experimental data.

The functionalization led to an increase of 96.156 $\Omega \cdot \text{cm}^2$ (1570.15%) in the R_{ct} of the SPCE due to the capability of the boronic acid to change the dielectric characteristics of the electrode, acting as a barrier to the electron transfer kinetics of the redox probe at the interface with the electrolyte [37].

The effect of the boronic acid to the electroactivity of the transducer matrix was evaluated by estimating the electroactive area of the SPCE before and after the functionalization by the Randles-Sevcik equation (Equation 17). In the equation, i_p is the peak current [A], n is the number of electrons involved in the redox reaction, A is the electroactive area [cm^2], C and D correspond respectively to the concentration [$\text{mol} \cdot \text{cm}^{-3}$] and the diffusion coefficient [$\text{cm}^2 \cdot \text{s}^{-1}$] of the redox species and v is the scan rate [$\text{V} \cdot \text{s}^{-1}$].

$$i_p = 2.69 \times 10^5 \times n^{3/2} \times A \times C_r \times D^{1/2} \times v^{1/2} \quad (17)$$

As seen in Figure 23, there was a linear trend between the square root of the scan rate and both anodic and cathodic current peaks as a consequence of a reversible reaction mechanism limited by diffusion [38]. The electroactive area of the electrode, which possess a geometric area of 0.2 cm^2 , was estimated as $0.4694 \pm 0.0191 \text{ cm}^2$ before the functionalization. After the SPCE modification, there was a reduction of 37.9% of its electroactive area ($A = 0.2915 \pm 0.0083 \text{ cm}^2$). This result corroborates the increase of R_{ct} from the Nyquist plot of Figure 22, demonstrating that the boronic acid was immobilized on the carbon surface as an insulating layer capable to hind the interfacial charge transfer.

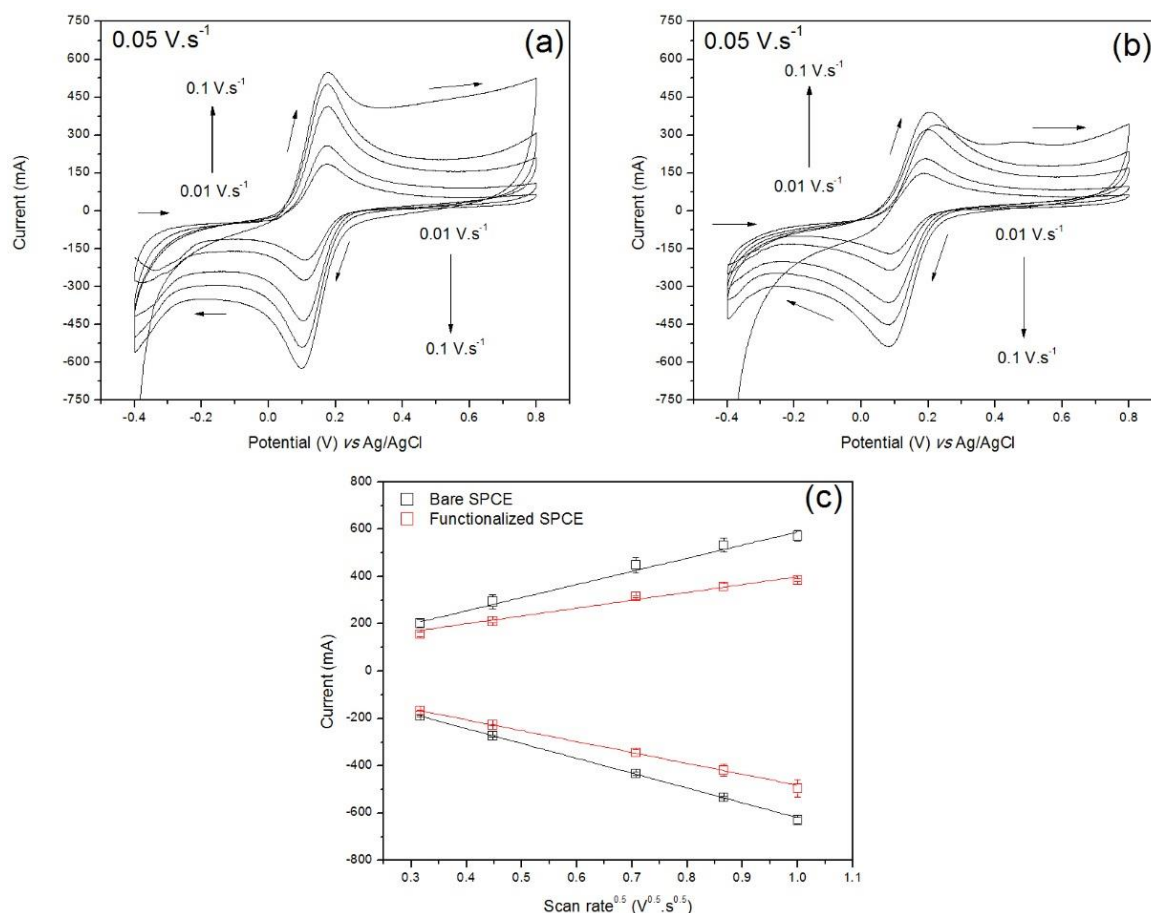


Figure 23 - Cyclic voltammograms related to the bare (a) and functionalized (b) SPCE under different scan rates (0.1, 0.075, 0.05, 0.02 and 0.01 mV.s⁻¹) in 0.1 M KCl + 5 mM Fe(CN)₆^{3-/4-} and (c) the relationship between the anodic/cathodic current peaks of the redox species at the electrodes and the square root of corresponding scan rates

7.4.2 Detection of glucose in aqueous solution by EIS

The functionalized SPCE was investigated toward the detection of glucose at various concentrations. As seen in Figure 24, the semicircle diameter increases with increasing the target analyte concentration, which is an indicative of the recognition capability of the sensor. This result was expected because, as shown in Figure 25, the boronic acid immobilized on the electrode surface interacts with the diols from glucose molecules forming a saccharide nonconductive layer that blocks the charge transfer between the ions [Fe(CN)₆]^{3-/4-} on the interface with the electrolyte [37-39].

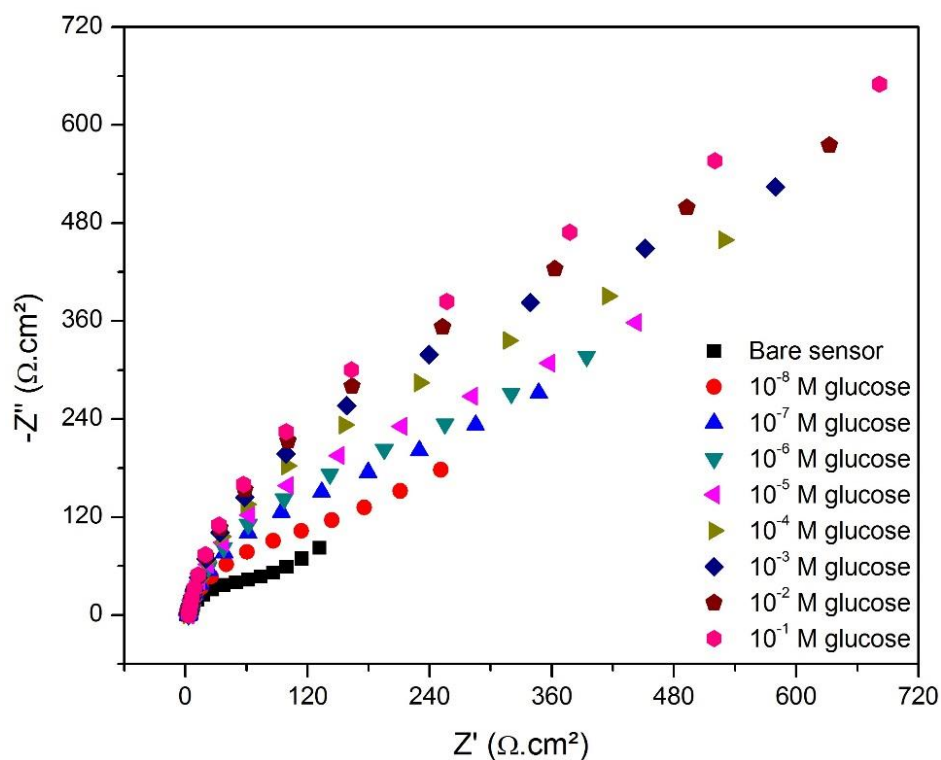


Figure 24 - Nyquist plot of the glucose sensor exposed to the target analyte at various concentrations

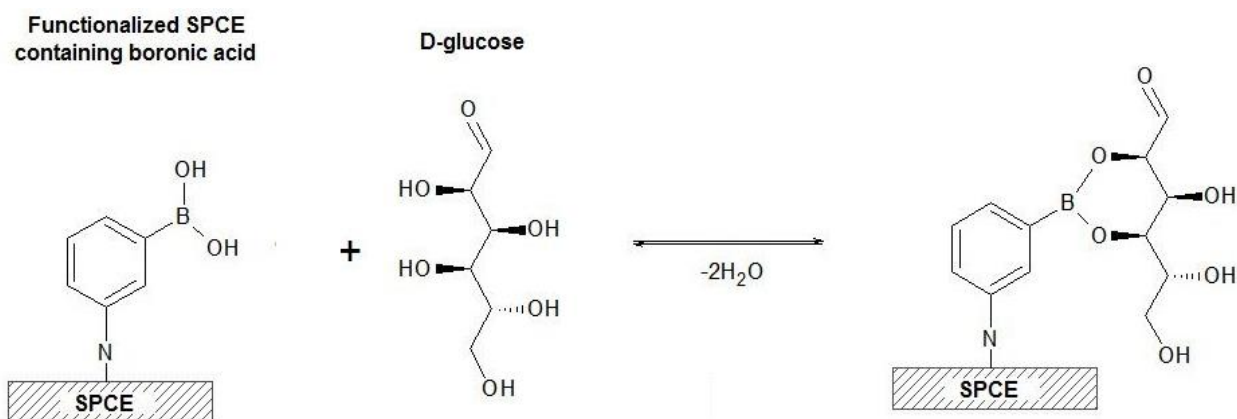


Figure 25 - Scheme of the binding process between the boronic acid immobilized on the SPCE surface and the D-glucose molecule

The equivalent circuit previously described was employed to fit the experimental data related to the glucose detection. The variation of the R_{ct} from the modeling (ΔR_{ct}) was used to plot the calibration curve shown in Figure 26. The ΔR_{ct} value represents the difference of R_{ct} from the sensor after and before its exposure to the

different concentrated sugar solutions. It is evident the increase of ΔR_{ct} upon exposition of the sensor to glucose at higher concentrations. A good linear correlation expressed by a logarithmic equation (Equation 18, $R^2 = 0.99872$) was obtained between the glucose concentration (from 10^{-8} to 10^{-1} M) and the ΔR_{ct} . In this equation, $y = \Delta R_{ct}$ ($\Omega \cdot \text{cm}^2$), $x = [\text{glucose}]$ (M), $a = 751.54 \Omega \cdot \text{cm}^2$, $b = -27.40 \Omega \cdot \text{cm}^2 \cdot \text{M}^{-1}$ and $c = -6.50 \times 10^{-9}$ M. On the contrary, the exposure to fructose and sucrose did not increase the resistance of the sensor, but the R_{ct} randomly varied in the same concentration range. Since the mechanism of recognition of the proposed sensor was based on the bond between the diol groups from glucose and the boronic acid, some non-specificity could be observed in the impedimetric response of the sensor toward fructose and sucrose, because both possess the same target group. However, some authors have described different conditions that favor the selectivity of the interaction of just one of these saccharides by varying the pH, thermodynamic aspects, the nature of the electrolyte, etc [40]. Wang *et al.* [37] for example, developed a gold-based impedimetric sensor using bis-boronic acid for the specific recognition of glucose (compared also to fructose, galactose and mannose).

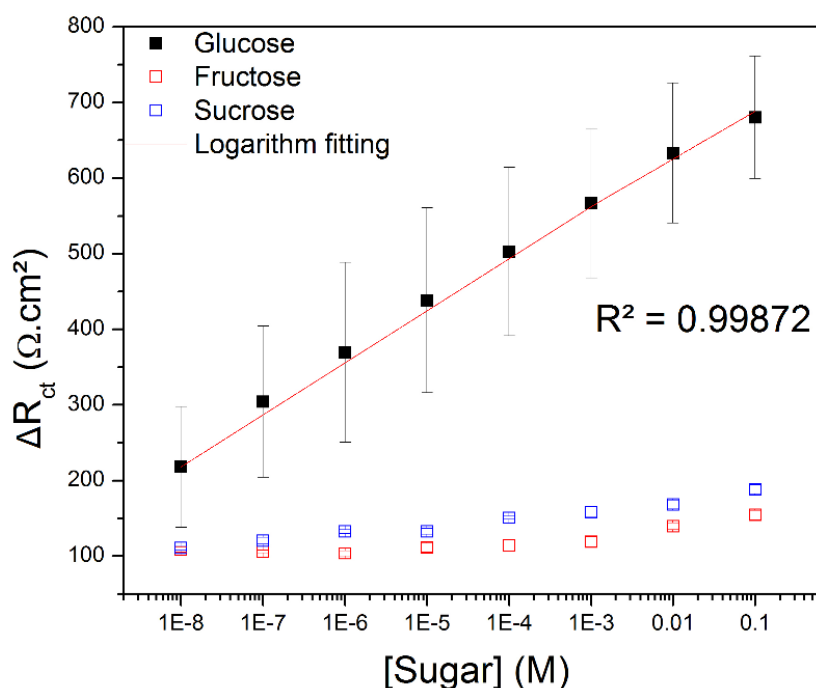


Figure 26 - Variation of the charge transfer resistance (ΔR_{ct}) of the glucose sensor exposed to glucose, fructose and sucrose at various concentrations

$$y = a - b \times \ln(x + c) \quad (18)$$

The sensitivity (S) of the sensor was estimated as the derivative of the logarithmic function between the output signal (ΔR_{ct}) and the glucose concentration as expressed in Equation 19. As expected for a nonlinear plot (semi-logarithm), the sensitivity is a function of the analyte concentration. The lower was the glucose concentration, the higher was the sensitivity of the device and its value is equal to $27.40/(x+6.50 \times 10^{-9})$ in $\Omega \cdot \text{cm}^2 \cdot \text{M}^{-1}$.

$$S = \frac{\partial y}{\partial x} = \frac{-b}{x + c} \quad (19)$$

The limit of detection (LOD) of the proposed sensor was estimated according to the $3SD/m$ criterion, in which SD is the standard deviation regarding the bare sensor and m is the slope of the linear plot of the calibration curve [41]. Based on this method, the LOD was equal to 8.53×10^{-9} M. As seen in Table 4, the proposed sensor was more sensitive than some others described in the literature by means of enzymatic and non-enzymatic devices based on optical and electrochemical techniques.

Table 4 - Comparison of the performance of various enzymatic and non-enzymatic glucose sensors with the sensor based on SPCE containing 3-aminophenylboronic acid.

Use of enzyme	Transducer substrate/unit of recognition	LOD [μM]	Technique of detection	Reference
No	SPCE containing 3-aminophenylboronic acid	0.0085	EIS	Present work
Yes	WS ₂ nanosheets	2.9	Spectrophotometry	[42]
Yes	Chitosan-coated Fe ₃ O ₄ NPs	0.43	Chemiluminescence	[43]
Yes	MoS ₂ -based field-effect transistor	0.3	Measurement of the source-drain current	[44]
Yes	chitosan/kappa-carrageenan polyelectrolyte complex	5	Square wave voltammetry	[45]
Yes	WS ₂ quantum dots	0.3	Fluorescence measurement	[1]
No	Ni NPs polyvinylpyrrolidone (PVP) stabilized graphene nanosheets (GNs) with chitosan (CS)	0.03	Chronoamperometry	[46]
No	NiO NPs electrodeposited on reduced graphene oxide–copper oxide nanocomposite bulk modified carbon ceramic electrode	2.63	CV	[47]
No	Ag NPs on multiwall carbon nanotubes	0.0003	Amperometry	[48]

NPs = nanoparticles

The low LOD of the proposed sensor indicates that this technology is a promising candidate for clinical applications. According to the literature, the level of glucose in the body of health patients varies from 4.4 to 6.6 mM [49], which is approximately 10^6 times higher than the LOD of the proposed sensor. Furthermore, despite other transduction methods can achieve higher sensitivity, such as the amperometric device cited by Baghayeri *et al.* [48], which obtained LOD = 0.0003 μM , our proposed impedimetric sensor possesses as incontestable advantages the easiness of preparation by means of a single-step functionalization and the low cost of the SPCE.

7.4.3 Repeatability and reproducibility analysis

The stability of the same sensor was assessed by examining the repeatability of its basal impedance over 100 consecutive measurements. The objective of this test was also to evaluate the robustness of the acquired data, ensuring that the oscillations on the R_{ct} values arising from the contact of the electrode with the electrolyte are not significant if compared to the variation caused by the analyte recognition. Figure 27 shows that the difference between the R_{ct} value from the first and the hundredth measurements was equal to 1.3%. Considering all the data, the R_{ct} varied by up to 8.7%, indicating that the developed sensor presents a significant repeatability.

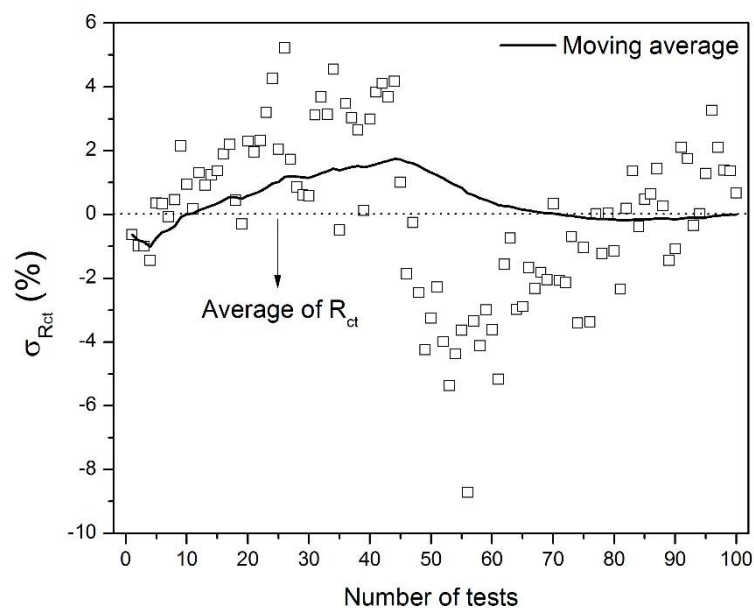


Figure 27 - Relative residual errors referring to the impedance of the glucose sensor during 100 consecutive measurements

To evaluate the possibility of using this technology in practical applications, the stability of the sensor was examined by storing the device at room temperature in a dried and closed recipient during 21 days. EIS was performed every seven days after storage and the R_{ct} values were simulated by modelling the equivalent circuit. Next, the sensor was exposed to 10^{-8} M glucose in order to evaluate its sensitivity. The results presented in Figure 28 reveal that the impedance of the bare sensor increased during the period of storage with a maximum value in the seventh day perhaps due to a sensor-to-sensor variation and not specifically to the time of incubation. The higher was the basal R_{ct} of the sensor the lower was its capability to bind the target analyte. The highest sensitivity was achieved with the fresh sensor, when the bare device presented an intrinsic R_{ct} equal to $93.5 \Omega \cdot \text{cm}^2$ and, after the exposure to glucose at 10^{-8} M, experienced an increase of 133.2%. This fact suggests that the storage influenced the performance of the sensor probably as a consequence of the redox reactions that spontaneously takes place on the carbon electrode, favoring the development of oxides on its surface. Thus, the formed insulator layer can act as a barrier to the charge transfer phenomenon and make the sensor unable to recognize the glucose molecules. In this sense, other storage

conditions should be tested in order to maintain reproducible the performance of the device.

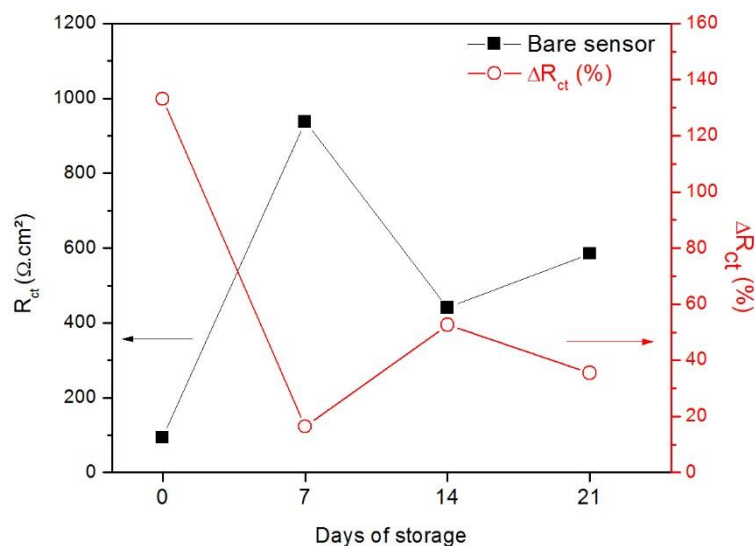


Figure 28 - Variation of the R_{ct} of the sensor in function of the period of storage

7.4.4. Response time

The response time (τ) can be defined as the time required by a sensor upon its exposure to a target analyte to yield a stable output signal [50]. Therefore, as the τ value is lower, more appropriate is the device to be used for clinical diagnosis. In this work, to optimize the acquisition of the EIS data related to the detection of glucose, the values of the magnitude of impedance ($|Z|$) and the imaginary (Z'') and real (Z') impedances were analyzed at five specific frequencies: 10^{-1} , 10^0 , 10^1 , 10^2 and 10^3 Hz. This analysis allows determining the best set up to perform EIS at a single frequency.

Figure 29 contains the results obtained by correlating the τ value in each frequency and the coefficient of linear regression (R^2) of each impedance component due to the exposure of the sensor to glucose at various concentrations. Among the impedance components, Z'' and $|Z|$ presented the highest R^2 values indicating strong relationship between the concentration of glucose and these parameters in all the frequency range.

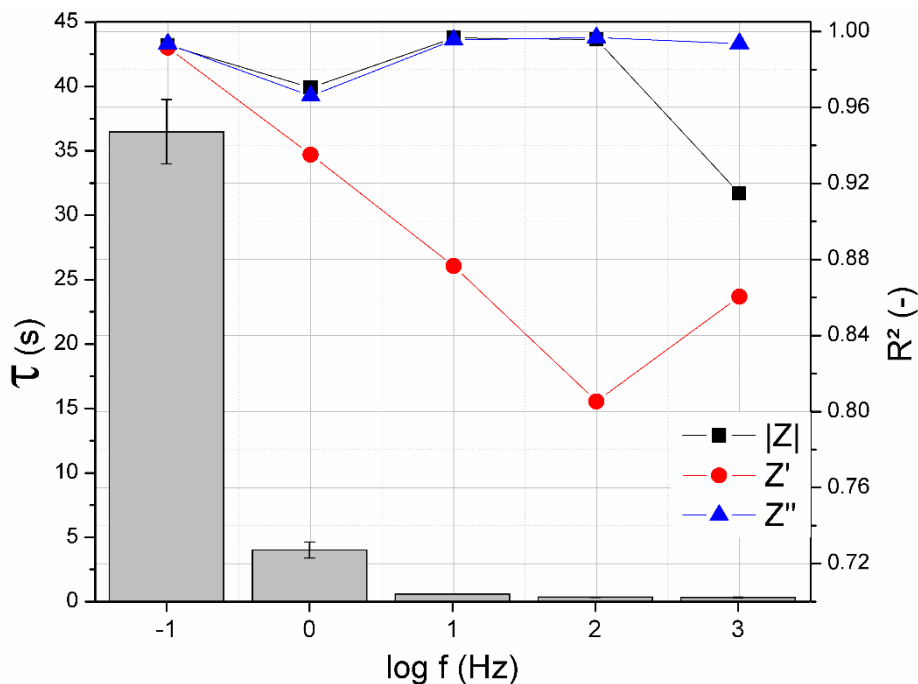


Figure 29 - Relationship between the time to record $|Z|$, Z' and Z'' at 1000, 100, 10, 1 and 0.1 Hz and the respective correlation coefficient of these impedance parameters and the glucose concentration

Obviously, the higher is the frequency, the lower is the time required to acquire the impedance data. It is well known that several phenomena interfere in the impedance spectrum at different frequency ranges as illustrated in the scheme of Figure 30. At high frequencies the impedance is strongly related to characteristics of the electrolyte, which is not representative of the analyte recognition. At very low frequencies analysis can lead to the effect of diffusional mechanisms. For this reason, to avoid both non-representative effects of the detection of glucose, the analysis of EIS at 10^0 Hz could provide the best response of the sensor considering the great R^2 values from both $|Z|$ and Z'' as well as the corresponding low τ , which was equal to 4.0 ± 0.6 s.

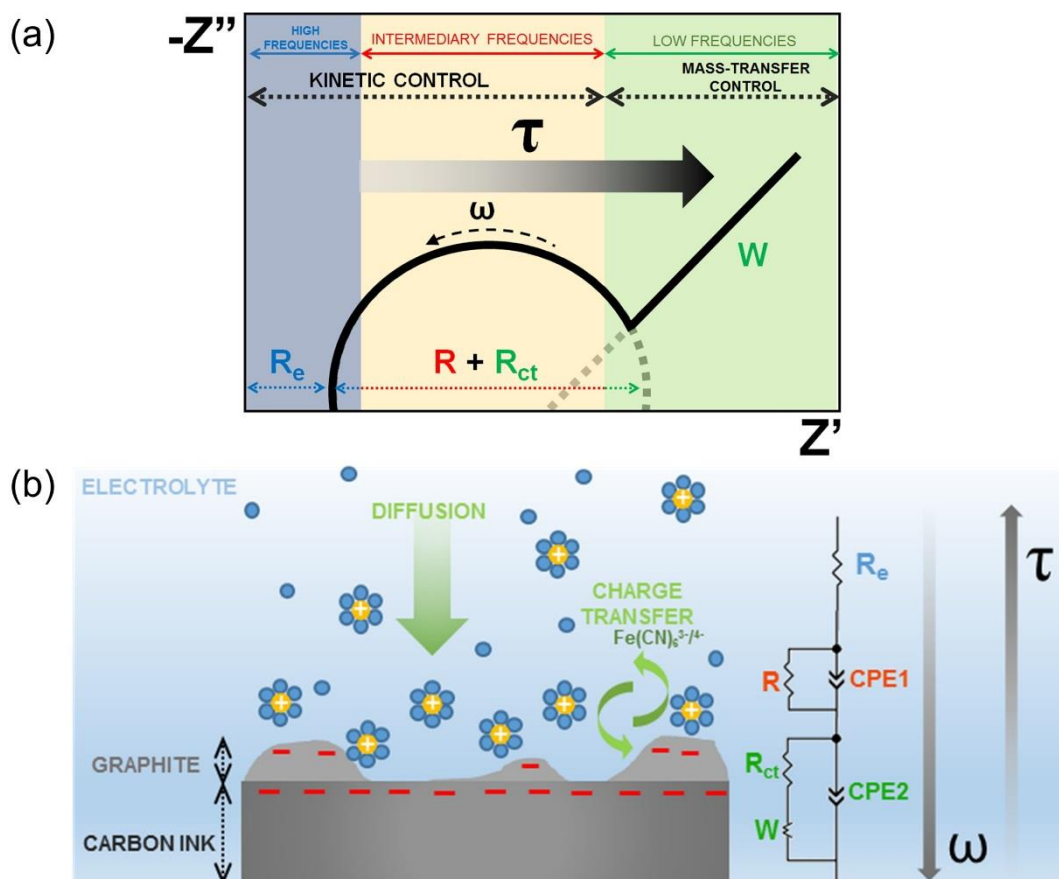


Figure 30 - Scheme of the relationship among the time response and the impedance parameters as a function of the frequency in the Nyquist plot (a) as a consequence of the interfacial phenomena occurring between the SPCE and the electrolyte (b). In the illustration, the yellow spheres with the signal “+” correspond to the cations solvated by the molecules from the bulk solution (blue spheres) and the signal “-” on the different regions of the SPCE corresponds to the electrons electrostatically attracted toward the interfaces

7.4.5 Investigation of the effect of dopamine, NaCl and serum on the performance of the glucose sensor

The capability of the sensor to detect glucose in solutions containing common interfering species for diabetes diagnosis was examined. Dopamine and NaCl are well known interferers studied in glucose detection [51,52] due to the possibility of charge transfer with electrochemical transducers. In this study, the effect of animal

serum on the impedance of the sensor was also assessed in order to simulate the real environment (human blood) in which this device could be employed.

Figure 31 shows the R_{ct} value of the bare sensor in absence/presence of each contaminant in a solution containing or not containing 10^{-8} M glucose. Despite the exposure of the sensor to the interfering species caused some variations on the impedance, a marked increase of R_{ct} occurred when the sensor was kept in contact with the solutions containing both glucose and interfering species. The presence of 10^{-8} M glucose in the solutions containing animal serum, dopamine and NaCl generated an increase of R_{ct} equal to 193.0%, 87.7% and 86.4% respectively. Once these results refer exclusively to the presence of glucose, the R_{ct} variations were calculated as the difference between the analytical signal of the sensor in presence of the solution of contaminant with glucose and the solution containing only the contaminant.

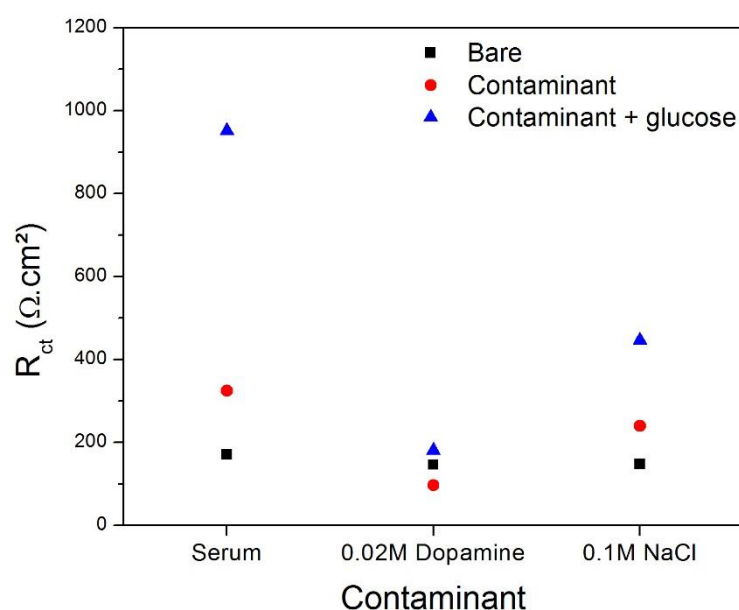


Figure 31 - Variation of the R_{ct} of the glucose sensor in function of the interference of bovine serum, 0.02 M dopamine and 0.1 M NaCl in the absence and presence of glucose at 10^{-8} M

According to Yuan *et al.* [52], NaCl can cause the inactivation of some metal electrodes in the detection of glucose due to its poisoning effect on electrocatalysis. Rinaldi and Carballo [51] observed that human blood could interfere on the

impedance of a glucose sensor but not significantly affected its sensitivity (slope of the calibration curve), obtaining a LOD equal to 0.37 mM. The exposure to dopamine was expected to decrease the impedance of the sensor since this molecule can interact to the conductive electrode in a reaction involving the exchange of two electrons and protons [53]. Thus, considering the performance of the impedimetric sensor to detect 10^{-8} M glucose in a medium containing the common interfering species NaCl, dopamine and the constituents of blood (herein simulated with animal serum), it is possible to infer that this device is a promising tool for monitoring the glucose levels in blood for diabetes diagnosis.

7.5 CONCLUSIONS

The fabrication of a non-enzymatic glucose sensor was reported based on the single-step attachment of 3-aminophenyl boronic acid on the surface of a SPCE. The changes in the electroactivity of the SPCE confirmed the success of the functionalization step and SEM images revealed that the boronic acid molecules were incorporated as dispersed clusters on the surface of the electrode. EIS measurements were carried out for detecting glucose at various concentrations and the sensor exhibited a broad linear range of detection with excellent selectivity to the target analyte, presenting a low signal to fructose and sucrose and a LOD equal to 8.53×10^{-9} M. The low LOD observed represents an important breakthrough in non-enzymatic glucose sensing since the use of enzymes possesses important limitations despite their high sensitivity. Further tests indicated that the sensor provided stable signal and the detection could be performed at the single frequency of 1 Hz in order to minimize the response time. The storage time of the sensor was responsible for diminishing the capability of recognition at the studied experimental conditions. Finally, despite suffering some influence of dopamine, NaCl and animal serum as interfering species, the as-developed sensor is a promising tool for detection of glucose foremost due to its simple preparation, high sensitivity and low cost of the SPCE.

7.6 REFERENCES

- [1] DUAN, X.; LIU, Q.; WANG, G.; SU, X. WS₂ quantum dots as a sensitive fluorescence probe for the detection of glucose. **Journal of Luminescence**, 207, p. 491-496, 2018.
- [2] WORLD HEALTH ORGANIZATION. **Global Report on Diabetes**. WHO Library Cataloguing-in-Publication Data, ISBN 978 92 4 156525 7 (2016) France (accessed 10 October 2018).
- [3] SILVA, L.M.C.; SANTOS, V.P.S.; SALGADO, A.M.; PEREIRA, K.S. Biosensors for contaminants monitoring in food and environment for human and environmental health. In: **State of the Art in Biosensors – General aspects**. IntechOpen: Rijeka, Croatia, 2013.
- [4] ZHAI, H.; FENG, T.; DONG, L.; WANG, L.; WANG, X.; LIU, H.; LIU, Y.; CHEN, L.; XIE, M. Development of dual-emission ratiometric probe-based on fluorescent silica nanoparticle and CdTe quantum dots for determination of glucose in beverages and human body fluids. **Food Chemistry**, 204, p. 444-452, 2016.
- [5] AMOR-GUTIÉRREZ, O.; RAMA, E.C.; COSTA-GARCÍA, A.; FERNÁNDEZ-ABEDUL, M.T. Paper-based maskless enzymatic sensor for glucose determination combining ink and wire electrodes. **Biosensors and Bioelectronics**, 93, p. 40-45, 2017.
- [6] YEHEZKELI, O.; TEL-VERED, R.; RAICHLIN, S.; WILLNER, I. Nano-engineered Flavin-Dependent Glucose Dehydrogenase/Gold Nanoparticle-Modified Electrodes for Glucose Sensing and Biofuel Cell Applications. **ACS Nano**, 5, p. 2385-2391, 2011.
- [7] HELLER, A.; FELDMAN, B. Electrochemical glucose sensors and their applications in diabetes management. **Chemical Reviews**, 108, p. 2482-2505, 2008.
- [8] GHANBARI, K.; BABAEI, Z. Fabrication and characterization of non-enzymatic glucose sensor based on ternary NiO/CuO/polyaniline nanocomposite. **Analytical Biochemistry**, 498, p. 37-46, 2016.
- [9] ZHONG, S-L.; ZHUANG, J.; YANG, D-P.; TANG, D. Eggshell membrane-templated synthesis of 3D hierarchical porous Au networks for electrochemical nonenzymatic glucose sensor. **Biosensors and Bioelectronics**, 96, p. 26-32, 2017.
- [10] GONZALES, W.V.; MOBASHSHER, A.T.; ABBOSH, A. The progress of glucose monitoring – a review of invasive to minimally and non-invasive techniques, devices and sensors. **Sensors**, 19, p. 800, 2019.

- [11] LEE, H.; HONG, Y.J.; BAIK, S.; HYEON, T.; KIM, D-H. Enzyme-based glucose sensor: from invasive to wearable device. **Advanced Healthcare Materials**, 7, p. 1701150, 2018.
- [12] LISDAT, F.; SCHÄFER, D. The use of electrochemical impedance spectroscopy for biosensing. **Analytical and Bioanalytical Chemistry**, 391, p. 1555-1567, 2008.
- [13] FARIA, R. A. D.; HENEINE, L. G. D.; MATENCIO, T.; MESSADDEQ, Y. Faradaic and non-faradaic electrochemical impedance spectroscopy as transduction techniques for sensing applications. **International Journal of Biosensors and Bioelectronics**, 5(1), p. 29-31, 2019.
- [14] RANDVIIR, E.P.; BANKS, C.E. Electrochemical impedance spectroscopy: an overview of bioanalytical applications. **Analytical Methods**, 5, p. 1098, 2013.
- [15] RANDVIIR E.P.; METTERS, J.P.; STANTON, J.; BANKS, C.E. Electrochemical impedance spectroscopy versus cyclic voltammetry for the electroanalytical sensing of capsaicin utilising screen printed carbon nanotube electrodes. **Analyst**, 138, p. 2970-2981, 2013.
- [16] CLARK, L.C.; LYONS, C. Electrode systems for continuous monitoring in cardiovascular surgery. **Annals of the New York Academy of Sciences**, 102, p. 29-45, 1962.
- [17] METKAR, S.K.; GIRIGOSWAMI, K. Diagnostic biosensors in medicine – a review. **Biocatalysis and Agricultural Biotechnology**, 17, p. 271-283, 2019.
- [18] HWANG, D.-W.; LEE, S.; SEO, M.; CHUNG, T.D. Recent advances in electrochemical non-enzymatic glucose sensors – a review. **Analytica Chimica Acta**, 1033, p. 1-34, 2018.
- [18] PERUMAL, V.; HASHIM, U. (2014) Advances in biosensors: principle, architecture and applications. **Journal of Applied Biomedicine**, 12, p. 1-15, 2014.
- [19] BILAL, M.; ASGHER, M.; CHENG, H.; YAN, Y.; Iqbal, H.M.N. Multi-point enzyme immobilization, surface chemistry, and novel platforms: a paradigm shift in biocatalyst design. **Critical Reviews in Biotechnology**, 39, p. 1-18, 2018.
- [20] SHEHAB, M.; EBRAHIM, S.; SOLIMAN, M. Graphene quantum dots prepared from glucose as optical sensor for glucose. **Journal of Luminescence**, 184, p. 110-116, 2017.
- [21] HATADA, M.; LOEW, N.; INOSE-TAKAHASHI, Y.; OKUDA-SHIMAZAKI, J.; TSUGAWA, W.; MULCHANDANI, A.; SODE, K. Development of a glucose sensor employing quick and easy modification method with mediator for altering electron acceptor preference. **Bioelectrochemistry**, 121, p. 185-190, 2018.

- [22] KIM, D.-M.; MOON, J.-M.; LEE, W.-C.; YOON, J.-H.; CHOI, C.S.; SHIM, Y.-B. A potentiometric non-enzymatic glucose sensor using a molecularly imprinted layer bonded on a conducting polymer. **Biosensors and Bioelectronics**, 91, p. 276-283, 2017.
- [23] FARIA, R.A.D.; MESSADDEQ, Y.; HENEINE, L.G.D.; MATENCIO, T. Application of screen-printed carbon electrodes as an electrochemical transducer in biosensors. **International Journal of Biosensors and Bioelectronics**, 5(1), p. 1-2, 2019.
- [24] GALDINO, F.E.; FOSTER, C.W.; BONACIN, J.A.; BANKS, C.E. Exploring the electrical wiring of screen-printed configurations utilised in electroanalysis. **Analytical Methods**, 7, p. 1208-1214, 2015.
- [25] HUGHES, R.M.; PEMBERTON, P.; HART, N.J.P. Fabrication of miniaturized screen-printed glucose biosensors, using a water-based ink, and the evaluation of their electrochemical behaviour. **Electroanalysis**, 30, p. 1616-1620, 2018.
- [26] BILAL, M.; IQBAL, H.M.N; GUO, S.; HU, H.; WANG, W.; ZHANG, X. State-of-the-art protein engineering approaches using biological macromolecules: a review from immobilization to implementation view point. **International Journal of Biological Macromolecules**, 108, p. 893-901, 2018.
- [27] PINE RESEARCH. **Screen-printed electrode information. Carbon and ceramic electrode information.** Document DRP 10036, <https://www.pineresearch.com/shop/products/electrodes/screen-printed-electrodes/carbon-spes/> (accessed 14 October 2018).
- [28] FARIA, R. A. D.; IDEN, H.; BHARUCHA, E.; LINS, V. F. C.; MESSADDEQ, Y.; MATENCIO, T.; HENEINE, L. G. D. A new tool for the detection of horsemeat adulteration in raw meat. **Journal of Biosensors and Bioelectronics**, 9, p. 1-7, 2018.
- [29] KANNAN, P.K.; ROUT, C.S. High performance non-enzymatic glucose sensor based on one-step electrodeposited nickel sulfide. **Chemistry – A European Journal**, 21, p. 9355-9359, 2015.
- [30] CINTI, S.; ARDUINI, F.; CARBONE, M.; SANSONE, L.; CACCIOTTI, I.; MOSCONE, D.; PALLESCHI, G. Screen-printed electrodes modified with carbon nanomaterials: a comparison among carbon black, carbon nanotubes and graphene. **Electroanalysis**, 27, p. 1-10, 2015.
- [31] MALVANO, F.; ALBANESE, D.; CRESCITELLI, A.; PILLOTON, R.; ESPOSITO, E. Impedimetric label-free immunosensor on disposable modified screen-printed electrodes for ochratoxin A. **Biosensors**, 6, p. 1-13, 2016.
- [32] HORSLEY, J.R.; YU, J.; WEGENER, K.L.; HOPPMANN, C.; RÜCK-BRAUN, K.; ABELL, A.D. Photoswitchable peptide-based 'on-off' biosensor for electrochemical

detection and control of protein-protein interactions. **Biosensors and Bioelectronics**, 118, p. 188-194, 2018.

[33] TERBOUCHE, A.; LAMECHE, S.; AIT-RAMDANE-TERBOUCHE, C.; GUERNICHE, D.; LERARI, K.; BACHARI, K.; HAUCHARD, D. A new electrochemical sensor based on carbon paste electrode/Ru(III) complex for determination of nitrite: Electrochemical impedance and cyclic voltammetry measurements. **Measurement: Journal of the International Measurement Confederation**, 92, p. 524–533, 2016.

[34] YAGATI, A.K.; CHOI, Y.; PARK, J.; CHOI, J-W.; JUN, H-S.; CHO, S. Silver nanoflower–reduced graphene oxide composite based micro-disk electrode for insulin detection in serum. **Biosensors and Bioelectronics**, 80, p. 307-314, 2016.

[35] ATES, M.; SARAC, A.S. Electrochemical impedance spectroscopy of poly[carbazole-co-N-p-tolylsulfonyl pyrrole] on carbon fiber microelectrodes, equivalent circuits for modelling. **Progress in Organic Coatings**, 65, p. 281-287, 2009.

[36] WANG, H-C.; ZHOU, H.; CHEN, B.; MENDES, P.M.; FOSSEY, J.S.; JAMES, T.D.; LONG, Y-T. A bis-boronic acid modified electrode for the sensitive and selective determination of glucose concentrations. **Analyst**, 138, p. 7146-7151, 2013.

[37] SUEA-NGAM, A.; RATTANARAT, P.; WONGRAVEE, K.; CHAILAPAKUL, O.; SRISA-ART, M. Droplet-based glucosamine sensor using gold nanoparticles and polyaniline-modified electrode. **Talanta**, 158, p. 134-141, 2016.

[38] FANG, H.; KAUR, G.; WANG, B. Progress in boronic acid-based fluorescent glucose sensors. **Journal of Fluorescence**, 14, p. 481-489, 2004.

[39] TORUN, Ö.; DUDAK, F.C.; BAŞ, D.; TAMER, U.; BOYACI, I.H. Thermodynamic analysis of the interaction between 3-aminophenylboronic acid and monosaccharides for development of biosensor. **Sensors and Actuators B: Chemical**, 140, p. 597-602, 2009.

[40] FARIA, R.A.D.; LINS, V.F.C.; NAPPI, G.U.; MATENCIO, T.; HENEINE, L.G.D. Development of an impedimetric immunosensor for specific detection of snake venom. **BioNanoScience**, 8, p. 988-996, 2018.

[41] LIN, T.; ZHONG, L.; SONG, Z.; GUO, L.; WU, H.; GUO, Q.; CHEN, Y.; FU, F.; CHEN, G. Visual detection of blood glucose on peroxidase-like activity of WS₂ nanosheets. **Biosensors and Bioelectronics**, 62, p. 302-307, 2014.

[42] CHAICHI, M.J.; EHSANI, M. A novel glucose sensor based on immobilization of glucose oxidase on the chitosan-coated Fe₃O₄ nanoparticles and the luminol–H₂O₂ – gold nanoparticle chemiluminescence detection system. **Sensors and Actuators B: Chemical**, 223, p. 713–722, 2016.

- [43] SHAN, J.; LI, J.; CHU, X.; XU, M.; JIN, F. ; WANG, X.; MA, L.; FANG, X.; WEI, Z.; WANG, W. High sensitivity glucose detection at extremely low concentrations using a MoS₂-based field-effect transistor. **Royal Society of Chemistry**, 8, p. 7942-7948, 2018.
- [44] RASSAS, I.; BRAIEK, M.; BONHOMME, A.; BESSUELLE, F.; RAFIN, G.; MAJDOUB, H.; JAFFREZIC-RENAULT, N. Voltammetric glucose biosensor based on glucose oxidase encapsulation in a chitosan-kappa-carrageenan polyelectrolyte complex. **Materials Science and Engineering C**, 95, p. 152-159, 2018.
- [45] LIU, Z.; GUO, Y.; DONG, C. A high performance nonenzymatic electrochemical glucose sensor based on polyvinylpyrrolidone–graphene nanosheets–nickel nanoparticles–chitosan nanocomposite. **Talanta**, 137, p. 87-93, 2015.
- [46] RAZMI, H.; SHIRDEL, H.; MOHAMMAD-REZAEI, R. NiO nanoparticles electrodeposited on reduced GO-CuO nanocomposite bulk modified CCE as a sensitive glucose sensors. **Nano-Micro Letters**, 12, p. 217-222, 2017.
- [47] BAGHAYERI, M.; AMIRI, A.; FARHADI, S. Development of non-enzymatic glucose sensor based on efficient loading Ag nanoparticles on functionalized carbon nanotubes. **Sensors and Actuators B: Chemical**, 225, p. 354–362, 2016.
- [48] SARANJI, S.N.; NOZAKI, S.; SAHU, S.N. ZnO nanorod-based non-enzymatic optical glucose sensor. **Journal of Biomedical Nanotechnology**, 11, p. 988-996, 2015.
- [49] KUMAR R.; AL-DOSSARY, O.; KUMAR, G.; UMAR, A. Zinc oxide nanostructures for NO₂ gas-sensor applications: a review. **Nano-Micro Letters**, 7, p. 97-120, 2015.
- [50] RINALDI, A.L.; CARBALLO, R. Impedimetric non-enzymatic glucose sensor based on nickel hydroxide thin film onto gold electrode. **Sensors and Actuators B: Chemical**, 228, p. 43-52, 2016.
- [51] YUAN, B.; XU, C.; DENG, D.; XING, Y.; LIU, L; PANG, H.; ZHANG, D. Graphene oxide/nickel oxide modified glassy carbon electrode for supercapacitor and nonenzymatic glucose sensor. **Electrochimica Acta**, 88, p. 708-712, 2013.
- [52] MARTÍN-YERGA, D.; RAMA, E.C.; GARCÍA, A.C. Electrochemical study and determination of electroactive species with screen-printed electrodes. **Journal of Chemical Education**, 93(7), p. 1270-1276, 2016.

CHAPTER 8 - A NOVEL IMPEDIMETRIC SENSOR FOR TRACE LEVEL DETECTION OF DIMETHYL SULFIDE (DMS)

*Text adapted from: IDEN, H.; FARIA, R. A. D.; HENEINE, L. G. D.; MATENIO, T.; MESSADDEQ, Y. A novel impedimetric sensor for trace level detection of dimethyl sulfide (DMS). Accepted for publication in **Journal of Materials Science: Materials in Electronics**, 2020. DOI:10.1007/s10854-020-03588-0.*

Hassan Iden^{1,2}, Ricardo Adriano Dorledo de Faria^{1,3}, Luiz Guilherme Dias Heneine⁴,
Tulio Matencio⁵, Younès Messaddeq^{1,6}

¹ Center for Optics, Photonics and Lasers (COPL), Université Laval, Quebec, Canada.

² CDN isotopes, Montreal, Canada

³ Department of Chemical Engineering, Universidade Federal de Minas Gerais (UFMG), Minas Gerais, Brazil.

⁴ Laboratory of Applied Immunology, Fundação Ezequiel Dias (FUNED), Minas Gerais, Brazil.

⁵ Department of Chemistry, Universidade Federal de Minas Gerais (UFMG), Minas Gerais, Brazil.

⁶ Institute of Chemistry, UNESP, São Paulo, Brazil.

8.1 ABSTRACT

An easy and effective method for the preparation of a new impedimetric sensor used for the detection of dimethyl sulfide (DMS) gas at a nanomolar level is presented. The sensor was prepared in two steps from a commercially available screen-printed carbon electrode (SPCE): a simple activation of the SPCE using cyclic voltammetry followed by electroless plating of the working electrode surface with gold clusters. Scanning electron microscopy (SEM) and energy-dispersive X-ray spectroscopy (EDX) techniques confirmed the successful functionalization of the SPCE, revealing the presence of gold particles dispersed on the carbon matrix. Electrochemical Impedance Spectroscopy (EIS) was used to study the sensitivity of the sensor towards DMS dissolved gas in aqueous solution and simulated ocean water. Analyses were performed in less than 3 minutes, and the sensor showed linearity in a concentration range from 1.0×10^{-10} M to 1.0×10^{-8} M with a limit of detection of 1.50×10^{-9} M and a limit of quantification of 2.27×10^{-9} M. To simulate the marine environment in which DMS is naturally present in nature, the impedance

of the sensor was monitored by online EIS. Moreover, results indicated that, despite not linearly, the sensor is a promising tool to detect the analyte even at 1.0×10^{-11} M, presenting an increase of resistance of 13.5% in relation to its bare condition.

Keywords: dimethyl sulfide; screen-printed carbon electrode; impedance; sensor

8.2 INTRODUCTION

Volatile organic sulfur compounds (VOSCs) have assigned to have an essential environmental function in global cycle warming, in acid rain creation, as well as in clouds formation [1-5]. Dimethyl sulfide (DMS) is a biogenic gas that belongs to VOSCs family and considered as the most common component in VOSCs [6,7]. DMS gas exists in water and earth. The majority of atmospheric DMS gas is believed to be produced in the marine environment by the degradation of dimethyl sulfopropionate (DMSP) via an enzyme called DMSP lyase [8,9]. DMSP is a metabolite produced by marine phytoplankton, algae, and some marine plants when they feel stressed in any environmental change [10,11]. While DMSP plays the role of osmoprotective agent for these species, its degradation by DMSP lyase liberates DMS gas, acrylic acid and others components to the ocean water, which is then around 10% of DMS gas emitted from the oceans surfaces to the atmosphere [12-15]. Moreover, ocean water is not the only source of DMS, but a significant amount of DMS is also generated from the soil and fresh water bacteria [7,15,16].

Due to the large amount of DMS gas produced in the oceans and its role in climate regulation, and in the food industry, numerous measurement techniques have been used to detect DMS at nM concentration. The standard technique used to analyse DMS at nM level is gas chromatography coupled with a mass or flame photometric detector [17-21]. However, the gas must be trapped cryogenically before analysis and then it is sent into a flame. The resulting combustion product generates chemiluminescence measured by the detector [18,22-24]. Despite their advantages to measure DMS accurately, these techniques are time-consuming, machines are heavy, impractical for continuous field measurement and expensive. In addition, their

detection limit is usually below the quantity present in seawater, and most of the time, a concentration step is required prior to analysis.

Modified screen-printed carbon electrodes SPCEs have received great attention recently as a miniaturised and cheap device used in electrochemistry, and in the fabrication of biosensors. In addition, SPCEs present plenty of advantages over conventional sensors such as the small volume of sample used in the analysis, low cost, as well as printing in different shape on flexible materials [25-28]. EIS has become accessible and useful tools for scientists, they have used to detect corrosion [29-33], to discover failure in battery [34-36], and to analyse pollutants in water [37, 38], in soil [38,39], and in food [40]. Our group is already interested in EIS technique and we have used this technique for the detection of meats adulteration [41], glucose and snake venom [42,43].

To the best of our knowledge, a simple and cheap technique that measures impedance variations and used cheap screen-printed carbon electrodes to measure DMS at nM concentration in the ocean water has not been developed. Our strategy is simple and based on modified screen-printed carbon electrodes coated with a thin layer of gold. The gold electrodes are fabricated from commercial screen-printed carbon electrodes by activation of their surface with sulfuric acid using CV, and then followed by deposition of gold using electroless deposition method. This method is cheap and reproducible. DMS was detected at very low concentration, below the quantity present in ocean water, and with a small effect of other interferences.

8.3 MATERIALS AND METHODS

8.3.1 Apparatus and chemicals

Cyclic voltammetry (CV) and Electrochemical Impedance Spectroscopy (EIS) were performed in a RRPE1002C screen-printed carbon electrode (SPCE) from Pine Research Instrumentation Inc. consisting of carbon ink as both working and counter electrode and Ag/AgCl as the reference electrode. The SPCE possesses a polyethylene terephthalate substrate with 15 mm x 61 mm x 0.36 mm dimensions

and a 4 mm x 5 mm working electrode. To functionalize the SPCE, gold(III) chloride trihydrate (>99.9%), hydroxylamine (50 wt. % in H₂O) and sulfuric acid 98% v/v were purchased from Sigma-Aldrich and used as-received, with no further purification.

All electrochemical experiments were carried out using a potentiostat VersaSTAT 3 (Princeton Applied Research) from AMETEK Scientific Instruments (Canada) equipped with an interface VersaStudio software. EIS measurements were performed in an electrochemical cell containing 0.1 M potassium chloride (KCl) as supporting electrolyte and 5 mM potassium ferrocyanide-ferricyanide (K₃[Fe(CN)₆]/K₄[Fe(CN)₆]) as redox probes. KCl (≥ 99.0 %) was purchased from Fisher Chemical and both K₃[Fe(CN)₆] (≥99.0%) and K₄[Fe(CN)₆] (98.5–102.0%) from Sigma-Aldrich. Energy-dispersive X-ray spectroscopy (EDX) was performed to characterize the gold clusters deposited on the carbon working electrode. Scanning Electron Microscopy (SEM) was performed using a Quanta 3D FEG microscope equipped with an EDX spectrometer. DMS (≥ 99% purity, Sigma Aldrich) was serially diluted in ultrapure water with 18.2 MΩ.cm resistivity to obtain solutions at various concentrations. These solutions were prepared immediately before the use to avoid DMS volatilization.

8.3.2 Functionalization of the SPCE with gold particles

Before gold electroless deposition, the working electrode was activated by applying potentials ranging from -2.5 to +2.5 V vs Ag/AgCl in a 50 mM aqueous sulfuric acid solution at a scan rate of 100 mV.s⁻¹. This procedure aimed to clean and to enhance sensing performances of the SPCE [41], as well as to create nucleation sites for gold electroless deposition. The working electrode surface was analysed and characterised by SEM, EDX analysis and CV. The electrochemical characterization was carried out by scanning the potential from -0.4 to +0.8 V vs Ag/AgCl at 50 mV.s⁻¹ in an electrolytic solution containing 0.1 M KCl and 5 mM of both K₃[Fe(CN)₆] and K₄[Fe(CN)₆].

Figure 32a depicts the functionalization steps to obtain the DMS sensor. After the electro-activation step, the SPCE was washed with deionised water prior to gold

deposition. Then, 20 μL of an aqueous solution of HAuCl_4 at 0.2 g.mL^{-1} was put onto the cleaned area of the working electrode, followed by the addition of 20 μL of 1.0 g.mL^{-1} hydroxylamine solution as a reducing agent to reduce gold (III) ions to metallic gold atoms deposited on the graphite flakes, forming gold clusters on the electrode. The mixture was left to react for 5 minutes at room temperature when gas is evolving and a color change took place in the solution (from yellow to colorless) and the working electrode turned yellow-golden, as shown in Figure 32b. Finally, the yellow-golden working electrode was exhaustively washed with deionised water to remove remaining salts and un-bounded molecules.

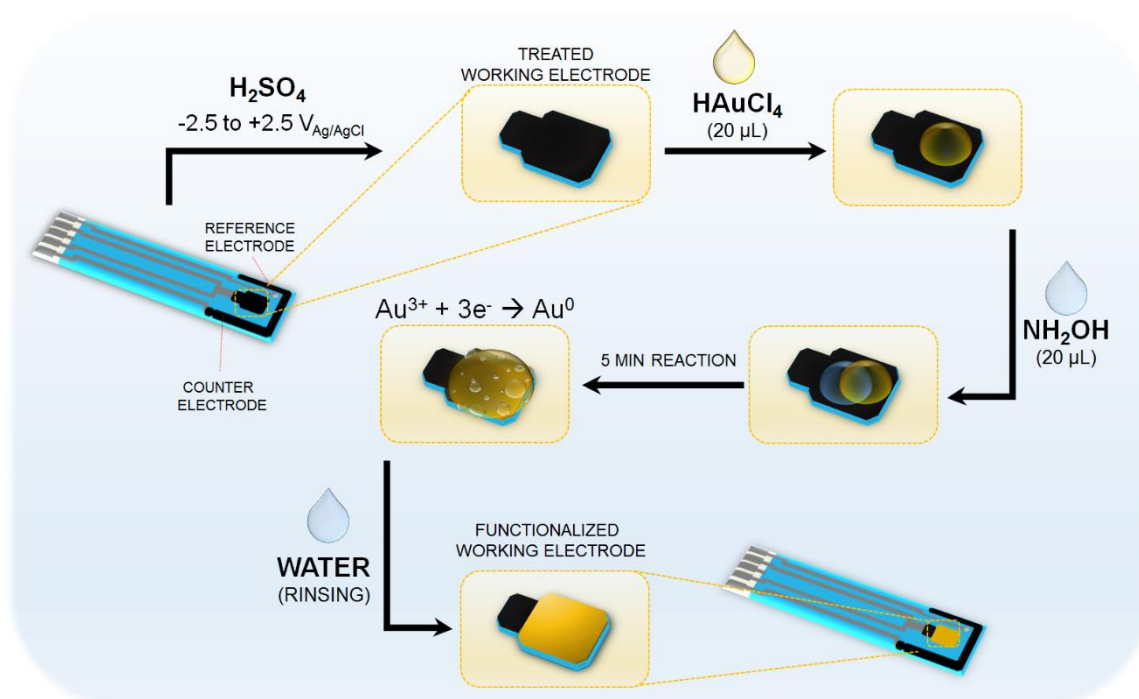


Figure 32 - Scheme of the procedure for the functionalization of SPCE with gold particles (a) and photograph of the finished sensor in the electrochemical cell (b)

8.3.3 EIS as a transduction technique for DMS sensing

For detecting DMS at various concentrations, the functionalized SPCE was exposed to aqueous solutions of the analyte from 5.0×10^{-11} to $1.0 \times 10^{-8} \text{ M}$. The electrochemical changes due to the contact of the working electrode with DMS were inspected by EIS through a frequency-domain ranging from 10,000 to 0.1 Hz under

the influence of an AC sinusoidal potential perturbation with 10 mV amplitude. In order to ensure that the tests were performed at the condition of electrochemical equilibrium, the impedance measurements were carried out only after 300 s of immersion in the electrolyte, when its open circuit potential (OCP), monitored meanwhile, varied less than 10 mV. The resultant EIS data was modelled to an equivalent circuit by using the software Zview 2.9b (Scribner and Associates) to deduce the values of the impedance elements.

Aiming to simulate the real condition in which DMS is naturally present in the environment, an artificial solution of ocean water was prepared according to the standard methodology described in ASTM D1141-98 (2003) [44], whose composition is presented in Table 5. This methodology consisted in initially preparing 7 liters of each of the stock solutions I ($555.6 \text{ g.L}^{-1} \text{ MgCl}_2 \cdot 6\text{H}_2\text{O}$, $57.9 \text{ g.L}^{-1} \text{ CaCl}_2$ and $2.1 \text{ g.L}^{-1} \text{ SrCl}_2 \cdot 6\text{H}_2\text{O}$) and II ($69.5 \text{ g.L}^{-1} \text{ KCl}$, $20.1 \text{ g.L}^{-1} \text{ NaHCO}_3$, $10.0 \text{ g.L}^{-1} \text{ KBr}$, $2.7 \text{ g.L}^{-1} \text{ H}_3\text{BO}_3$ and $0.3 \text{ g.L}^{-1} \text{ NaF}$). To a final volume of 10.0 L of artificial ocean water, 245.34 g of NaCl and 40.94 g of Na_2SO_4 were added to approximately 8.0 L of water. Then, a volume of 200 mL of stock solution I and 100 mL of stock solution II, respectively, were slowly added to the previous salts solution under vigorous stirring. The volume of the final solution was adjusted to 10.0 L and the pH to 8.2 with 0.1 N NaOH.

Table 5 - Chemical composition of the artificial solution of ocean water [44]

Component	Concentration (g.L^{-1})
$\text{MgCl}_2 \cdot 6\text{H}_2\text{O}$	11.112
CaCl_2	1.158
$\text{SrCl}_2 \cdot 6\text{H}_2\text{O}$	0.042
KCl	0.695
NaHCO_3	0.201
KBr	0.100
H_3BO_3	0.027
NaF	0.003
NaCl	24.534
Na_2SO_4	4.549

The variation of the elements from the equivalent circuit was inspected to verify the effect of the exposition of the functionalized electrode to DMS in the artificial ocean water. Real-time monitoring of the impedance was performed immersing the sensor in the artificial ocean water, to which DMS was added in order to achieve the desired concentrations (from 1.0×10^{-11} M to 1.0×10^{-8} M). The EIS data was collected after 3 min of reactions.

8.3.4 Electrochemical regeneration of the sensor

After exposing the sensor to DMS at each tested concentration and performing the EIS measurement, the device was submitted to an electrochemical regeneration step in order to make it reusable. This method consisted in a CV procedure in a potential range between -0.4 and +0.8 V vs Ag/AgCl at $100 \text{ mV}\cdot\text{s}^{-1}$. The potential was cycled until the voltammograms became stable (10 times) in an electrolyte containing 0.1 M H_2SO_4 in order to remove the DMS molecules attached to the electrode and any eventual corrosion product formed on the surface in case of the oxidation of gold in the electrolytes.

8.4 RESULTS AND DISCUSSION

8.4.1 Morphological and chemical characterization of the Au-modified electrode

The surface morphology of the SPCE before and after the deposition of the gold layer was examined by SEM/EDX techniques. Figure 33a indicates that the SPCE possesses a rough and heterogeneous structure composed by graphite flakes distributed along a carbon ink matrix. In our previous work [41], we demonstrated that the electrochemical treatment of the electrode via CV in sulfuric acid solution enhances its electro-activity by exposing the graphite flakes and increasing the oxygen groups (i.e. carboxylates and hydroxyls) content. After the functionalization, as seen in Figure 33b, small gold nanoparticles and aggregates were formed on the

graphite with size ranging from 637.61 ± 308.72 nm ($n = 18$) regarding the clusters to 43.57 ± 12.00 nm ($n = 65$) with respect to the smaller particles. The size determination was carried out by analyzing the SEM images with ImageJ version 1.52a with the macro "Analyze Particles".

The EDX spectrum in Figure 33c indicated that gold is the principal element with a main peak at 2.2 keV due to the presence of the clusters. Minor elements assigned to chlorine, carbon and oxygen arise from the composition of the SPCE ink matrix.

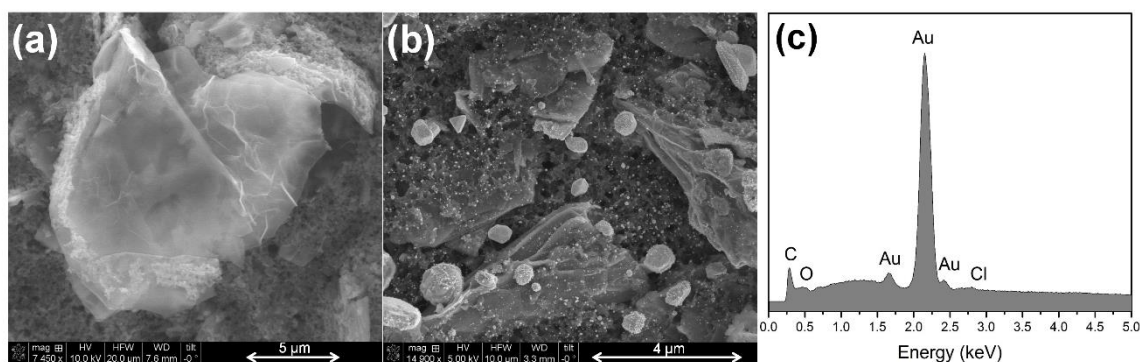


Figure 33 - SEM images of the SPCE before (a) and (b) after the deposition of gold and (c) the correspondent EDX spectrum of the clusters of gold on the graphitic flakes

8.4.2 Electrochemical detection of DMS

8.4.2.1 Sensitivity and linearity

The EIS technique has been widely exploited in sensing sciences because of its advantages over traditional techniques for the same application. Impedance measurement is a non-destructive assay since it is usually performed at the electrochemical equilibrium, and its simple performance, as well as its suitability for label-free and online applications, makes it less expensive than other methods. The changes in the impedance of a sensor can be examined to infer the recognition of an analyte of interest taking into account two main parameters: the capacitance and/or leakage resistance (in non-faradaic EIS) and the R_{ct} in case of faradaic EIS. In a non-

faradaic sensor, when a molecule from the sample binds the electrode surface, it can change the charge distribution at the interface electrode/electrolyte causing a variation of the double-layer capacitance and altering the conductivity of the transducer's surface. If the electrolyte contains electro-active species, though, the main effect of the analyte recognition is the alteration of the charge transfer rate between the electrode and the solution, which can be increased whether the analyte possess an insulator behavior or decreased in case of conductive molecules [45]. Typically, faradaic EIS provides lower limit of detection (LOD) and is more sensitive in a broader range of analyte concentrations [46].

After exposing the functionalized SPCE to aqueous solutions of DMS at various concentrations, EIS spectra were collected and plotted in the form of Nyquist diagrams. Figure 34 depicts a typical Nyquist plot consisting of a semicircle portion at high frequencies resulting from the charge transfer kinetics and a linear region at low frequencies corresponding to the diffusional barrier of the ions $\text{Fe}(\text{CN})_6^{3-/4-}$ from the bulk electrolyte towards the solid electrode. The increase of the semicircle diameter after each incubation of the sensor in higher concentrated DMS solutions is indicative of the successful binding of the analyte, which happens due to the affinity between the gold from the electrode and the sulfur atom from DMS. As shown in Figure 35, the molecular structure of DMS consisting of two $-\text{CH}_3$ insulator groups as well as its steric effect on the surface, hinders the interfacial electron transfer between the gold transducer and the redox probe, increasing the global impedance of the sensor. To further investigate the performance of the sensor, the EIS experimental data were fitted to the Randles equivalent circuit shown as an inset in Figure 34. This circuit consists of the ohmic resistance of the electrolyte (R_e), the R_{ct} related to the faradaic processes as previously mentioned, the Warburg impedance attributed to the diffusional limitation of the redox probe and a Constant Phase Element (CPE). The CPE replaces the ideal capacitance, mainly taking into account the heterogeneous and rough surface of the electrode. The CPE impedance (Z_{CPE}) is calculated as a function of the frequency-independent numerical values Q and n , the imaginary number j and the angular frequency ω ($\omega = 2\pi f$) as follows: $Z_{CPE} = 1/[Q(j\omega)^{-n}]$ [47]. The quality of fitting was ensured by low values of chi-squared (χ^2 approximately equal to 10^{-4}) as a criterion of validity [41].

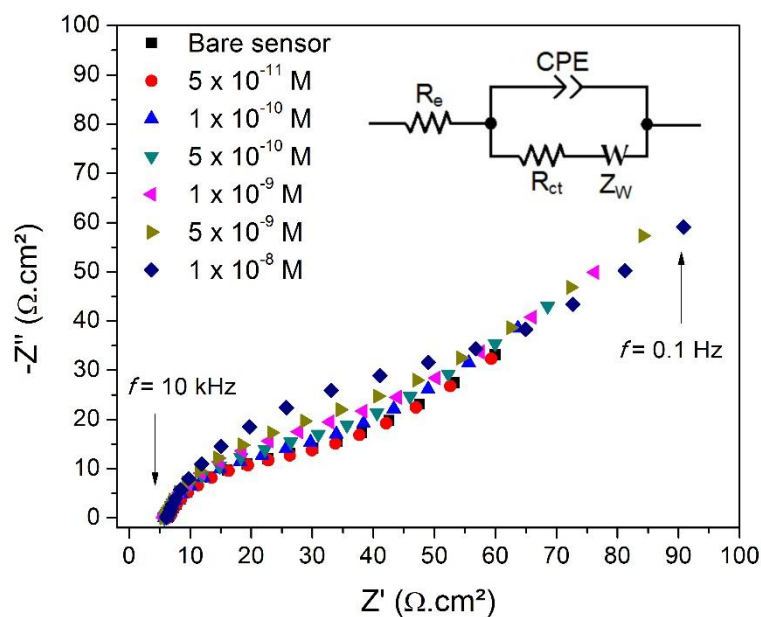


Figure 34 - Nyquist plots of the sensor after incubation for 3 min in aqueous solutions of DMS at various concentrations. The inset is the Randles equivalent circuit used to fit the EIS data

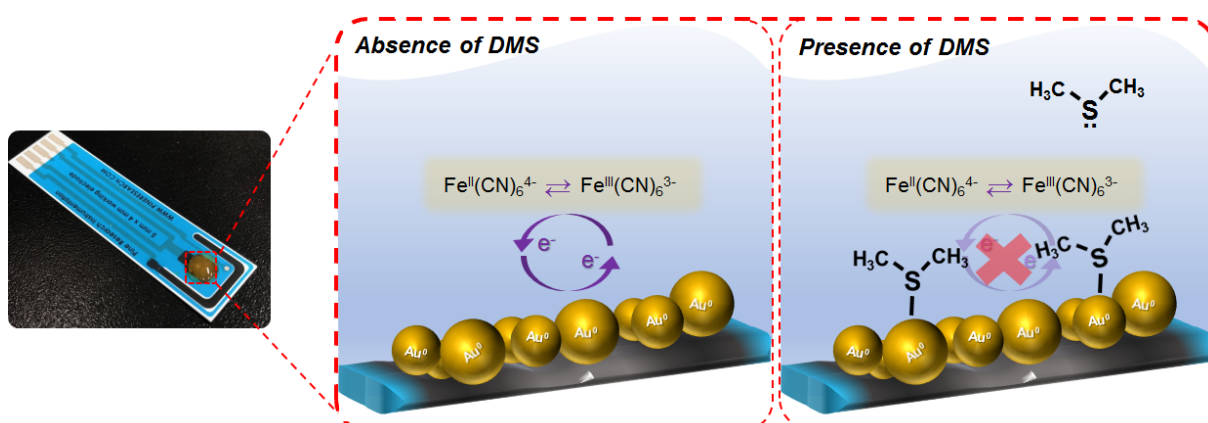


Figure 35 - Exposition of the gold transducer particles on the SPCE surface before and after the incubation in DMS solutions hindering the electron transfer processes between the Fe^{III} and Fe^{II} ions

Figure 36 shows the strong relation (root mean square value $R^2 = 0.9819$) between the variation of R_{ct} (ΔR_{ct}) of the sensor and the concentration of DMS as an indicative of the efficiency of the device in recognizing the target molecule. The ΔR_{ct} represents the difference between the R_{ct} value of the sensor after and before its incubation in each DMS concentrated solution.

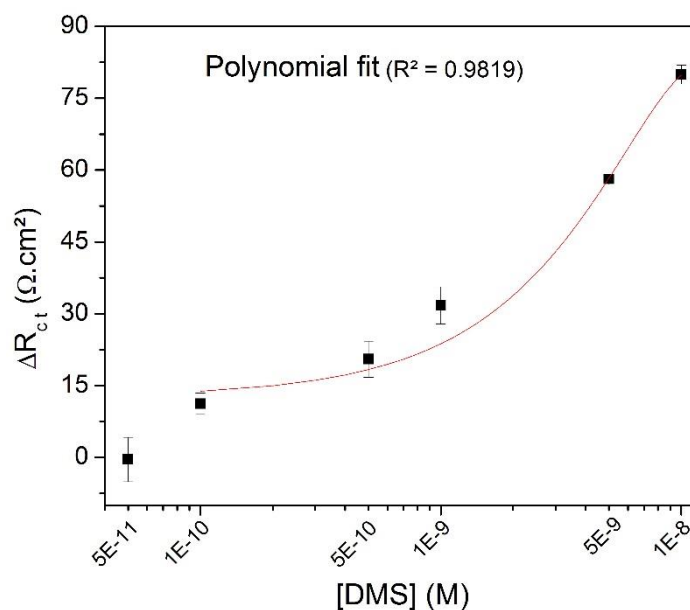


Figure 356 - Polynomial dependence between the ΔR_{ct} and the concentration of the aqueous DMS solution

A second-order polynomial relation was found to describe the dependence between the sensor output signal (in $\Omega \cdot \text{cm}^2$) and the concentration of the analyte (in M) in the range from 1.0×10^{-10} M and 1.0×10^{-8} M according to Equation 20.

$$\Delta R_{ct} = -4.82 \times 10^{17} [DMS]^2 + 1.15 \times 10^{10} [DMS] + 12.68$$

(20)

The sensor's sensitivity (S with the unit of $\Omega \cdot \text{cm}^2 \cdot \text{M}^{-1}$) was estimated as the derivative of the function that expresses the correlation between the output signal and the analyte concentration (Equation 20). As a derivative from a non-linear plot, the sensitivity is a function of the DMS concentration (Equation 21). Accordingly, the higher was the DMS concentration, the more sensible was the device in recognizing the molecule.

$$S = -9.64 \times 10^{17} [DMS] + 1.15 \times 10^{10} \quad (21)$$

8.4.2.2 Limit of detection (LOD) and limit of quantification (LOQ)

The LOD and the LOQ are key parameters in the development of analytical methods once they can indicate whether the sensor/technique is employable for a certain application. According to the International Union of Pure and Applied Chemistry (IUPAC) [48], the LOD is the smallest concentration of an analyte that a technique can detect assuming a stated statistical confidence level, distinguishing the output signal arisen from the detection phenomenon to the signal it would provide in the absence of the target molecule. Despite many authors [49-52] indiscriminately use the popular signal-to-noise method ($3SD/m$) to estimate the LOD, it is essential to take in account some statistical cares (such as to respect the minimum of 10 measurements of the blank sample as well as to consider performing the tests in different days/runs) to ensure the validity of this technique [53]. Hence, this method is usually employed in systems whose analytical response towards the target molecule concentration is linear (i.e. following a model of the type $y = a_1x + a_0$) [54]. According to Ribeiro and Ferreira [55], the signal-to-noise procedure is based on qualitative parameters and an alternative method to calculate the LOD is the procedure based on the analytical curve, which takes in account the standard error from the equation of the linear or non-linear regression at a certain confidence level. In the equation, s_y is the standard deviation, t is the confidence level-dependent value from the t-Student distribution, a_1 is the slope of the polynomial plot, N is the number of samples in the calibration plot, \bar{y} is the average of the measured output signals, y_c refers to the intercept of the superior limit of the confidence interval and is given by Equation 22, x_i is the analyzed concentration of the analyte and \bar{x} is the average of the tested analyte concentrations presented in the analytical curve. In Equation 23, “ a_0 ” refers to the intercept of the polynomial equation.

$$LOD = 2 \left(\frac{s_y t}{a_1} \right) \sqrt{\left(\frac{1}{N} \right) + 1 + \frac{(y_c - \bar{y})^2}{a_1^2 \sum_{i=1}^n (x_i - \bar{x})^2}} \quad (22)$$

$$y_c = a_0 + s_y t \sqrt{\left(\frac{1}{N}\right) + 1 + \frac{\bar{x}^2}{\sum_{i=1}^n (x_i - \bar{x})^2}} \quad (23)$$

Based on the method as mentioned above, the impedimetric sensor presented a LOD equal to 1.50×10^{-9} M. This value is suitable for the target application since the concentration of DMS in real marine environments is reported to be typically at nanomolar level [56-58]. According to Li *et al.* [59], DMS possesses an odor threshold value varying from 0.6 and 40 ppb and it must be detected at concentrations of ppm and ppb levels for applications involving environmental protection, industrial control, in the agriculture domain and for biomedical diagnosis. Besides, the estimated LOD is comparable or lower than those reported in the literature as shown in Table 6. In light of this context, the herein proposed impedimetric sensor possesses as advantages not just the low LOD suitable for the aimed application but also the simplicity of the transducer functionalization and experimental setup.

Table 6 - LOD of DMS sensors reported in the literature employing various transduction modes

Transducer	LOD [M]	Transduction signal	Reference
Gold particles on SPCE	1.50×10^{-9}	Impedance	This work
Hollow waveguide	1.54×10^{-7}	Tunable laser absorption	[60]
Optical biosniffer	5.20×10^{-4}	Optical quenching	[61]
ZnO	3.22×10^{-5}	Conductance	[62]
Titania nanotubular arrays	4.83×10^{-8}	Electrical current	[63]
Co ₃ O ₄ nanosheet-built hollow spheres	4.02×10^{-6}	Electrical resistance	[64]
Hydrogen-bond acidic polymer	6.28×10^{-10}	Surface acoustic wave	[65]

The LOQ (equal to 2.27×10^{-9} M) was estimated by using the same method [55] according to Equations 24, 25 and 26, in which x_c is the value of x where a_0 intercepts the regression plot and y_h refers to the signal associated to the x_c projection up to the limit of superior control. The proximity of the LOQ to the LOD value corroborates the possibility of using the proposed sensor for the aimed application since both are at the nanomolar level.

$$LOQ = \left(\frac{y - a_0}{a_1} \right) + \left(\frac{s_y t}{a_1} \right) \sqrt{\left(\frac{1}{N} \right) + 1 + \frac{(y_h - \bar{y})^2}{a_1^2 \sum_{i=1}^n (x_i - \bar{x})^2}} \quad (24)$$

$$x_c = \left(\frac{s_y t}{a_1} \right) \sqrt{\left(\frac{1}{N} \right) + 1 + \frac{\bar{x}^2}{\sum_{i=1}^n (x_i - \bar{x})^2}} \quad (25)$$

$$y_h = a_0 + 2s_y t \sqrt{\left(\frac{1}{N} \right) + 1 + \frac{(x_c - \bar{x})^2}{\sum_{i=1}^n (x_i - \bar{x})^2}} \quad (26)$$

8.4.3 Reusability of the sensor

The designed electrochemical sensor was easily regenerated after its exposure to DMS by running ten cycles of CV from -0.4 V to +1.0 V vs Ag/AgCl in 0.05 M H₂O₄ at 100 mV.s⁻¹. Afterwards, the cleaned electrode was characterized by CV from -0.4 V to +0.8 V vs Ag/AgCl (at 50 mV.s⁻¹) and by EIS, both in the electrolyte containing 0.1 M KCl and 5 mM of K₃[Fe(CN)₆] and K₄[Fe(CN)₆] as a redox couple. Figure 37 shows that the bare gold-based sensor presents two well-defined peaks assigned to the reversible Faradaic processes involving the redox couple. After binding DMS, there was a decrease of the electron transfer kinetics leading to a significant decrease of the current density, which was almost completely recovered after the regeneration step by CV. The Nyquist plot in Figure 37b corroborates the successful regeneration of the sensor showing that the curves related to the bare and regenerated sensor are

practically overlapped independent of the analyzed frequency, whereas the presence of DMS caused an increase of the diameter of the capacitive arc.

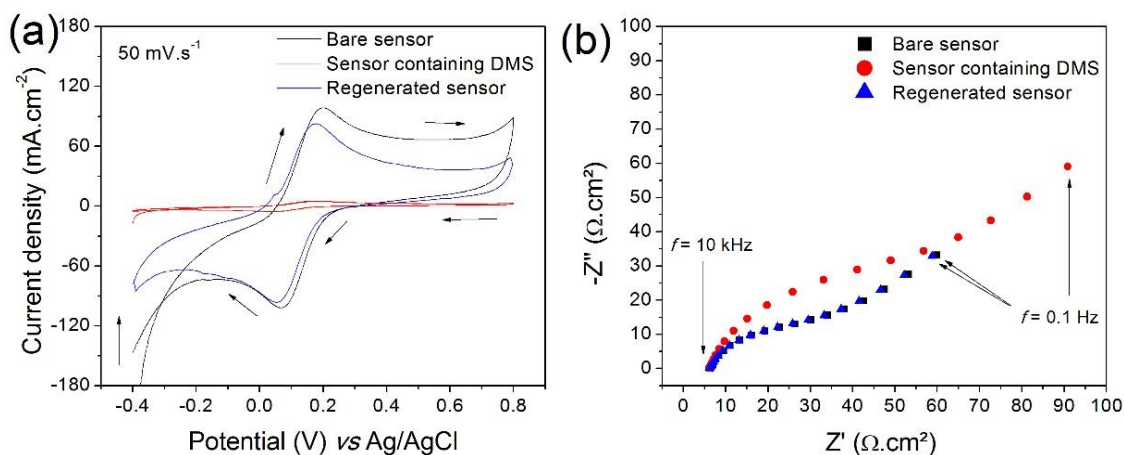


Figure 367 - Cyclic voltammogram (a) and Nyquist plot (b) of the bare, regenerated and contaminated sensor with an aqueous solution of DMS at 10^{-8} M

Another parameter to be taken into account to evaluate the cleanliness of the sensor surface is the peak-to-peak separation (ΔE_p), which is the difference between the anodic peak potential (E_{pa}) and the cathodic peak potential (E_{pc}). Ideally, a redox reaction involving the transfer of a single electron, such as the reaction of the $[\text{Fe}(\text{CN})_6]^{3-/4-}$ redox probe used in this work, should be equal to 58 mV. Thus, the increase of this value may indicate the presence of imperfections and/or contaminations on the electrode surface [64]. As seen in Table 7, the lower electron transfer kinetics arose from the sensor exposed to DMS and both anodic and cathodic peaks remained practically at the same position before and after the regeneration. The difference of only 0.86% in the ΔE_p between the bare and regenerated electrode newly confirmed the efficiency of the cleaning procedure in restabilising the electrochemical response of the sensor for further uses. The ΔE_p values in all the samples were larger than the expected 58 mV from an ideal Nernstian behavior of the redox reaction of the $[\text{Fe}(\text{CN})_6]^{3-/4-}$ ions, which was possibly due to the heterogeneous carbon matrix from the SPCE that contributes to decrease the kinetics of the electron transfer independently of the presence of DMS.

Table 7 - Values of E_{pa} , E_{pc} and ΔE_p related to the sensor before and after the exposure to DMS as well as after the regeneration step by CV in 0.05 M H_2SO_4

Sample	E_{pa} (mV vs Ag/AgCl)	E_{pc} (mV vs Ag/AgCl)	ΔE_p (mV)
Bare sensor	0.195	0.079	0.116
Sensor containing DMS	0.177	0.029	0.148
Regenerated sensor	0.170	0.053	0.117

8.4.4 DMS sensing in artificial ocean water

Once DMS is mainly present in marine ecosystems, it is of great importance to evaluate the capability of the proposed sensor to detect the molecule in its natural condition. Therefore, the influence of a simulated ocean water solution on the response of the device was examined in order to validate the sensor's real application.

Real-time EIS was performed as a tool to evaluate the variation of the impedance parameters during the incubation of the functionalized SPCE in the simulated ocean water before and after the addition of DMS at various concentrations (from 1.0×10^{-11} M to 1.0×10^{-8} M). Figure 38a shows that independently of the DMS concentration in the electrochemical cell, the molecule did not significantly alter the OCP. This fact indicates that the presence of the salts in the solution at their respective concentrations was not capable of provoking the occurrence of enough redox reactions at the electrode surface, which could affect the electrochemical equilibrium of the sensor and, consequently, its impedance. Instead, a stable plot profile was observed within a potential variation less than 5 mV. Accordingly, after collecting and modelling the EIS data, it was possible to observe that the solution resistance (Figure 38b) remained stable over the elapsed time. This solution response indicates not only the stability of R_e ($1.298 \pm 0.007 \Omega \cdot \text{cm}^2$) but also the good conductivity of the simulated ocean water to be used as a real electrolyte. Moreover, it is possible to infer that DMS did not remain diluted in the solution during the sensing test but it was attached to the electrode (otherwise, it would increase the R_e at higher concentrations because of its insulating behavior). Contrary, as seen in Figure 38c,

the presence of DMS increased the polarization resistance (R_p) of the electrode, confirming that the proposed sensor is a promising tool for the recognition of DMS even in the real environment in only 3 minutes. Herein, R_p was used instead R_{ct} because of the absence of a redox probe in the solution. The non-use of redox species in the electrolyte makes the sensor to operate as a non-faradaic device [45], which justifies the higher values of R_p in comparison to the previously observed R_{ct} in the faradaic EIS. To contemplate this alteration and to consider there was no diffusional barrier (which excludes the Warburg impedance), the equivalent circuit shown in the inset of Figure 38c was used as an adaptation of the Randles model.

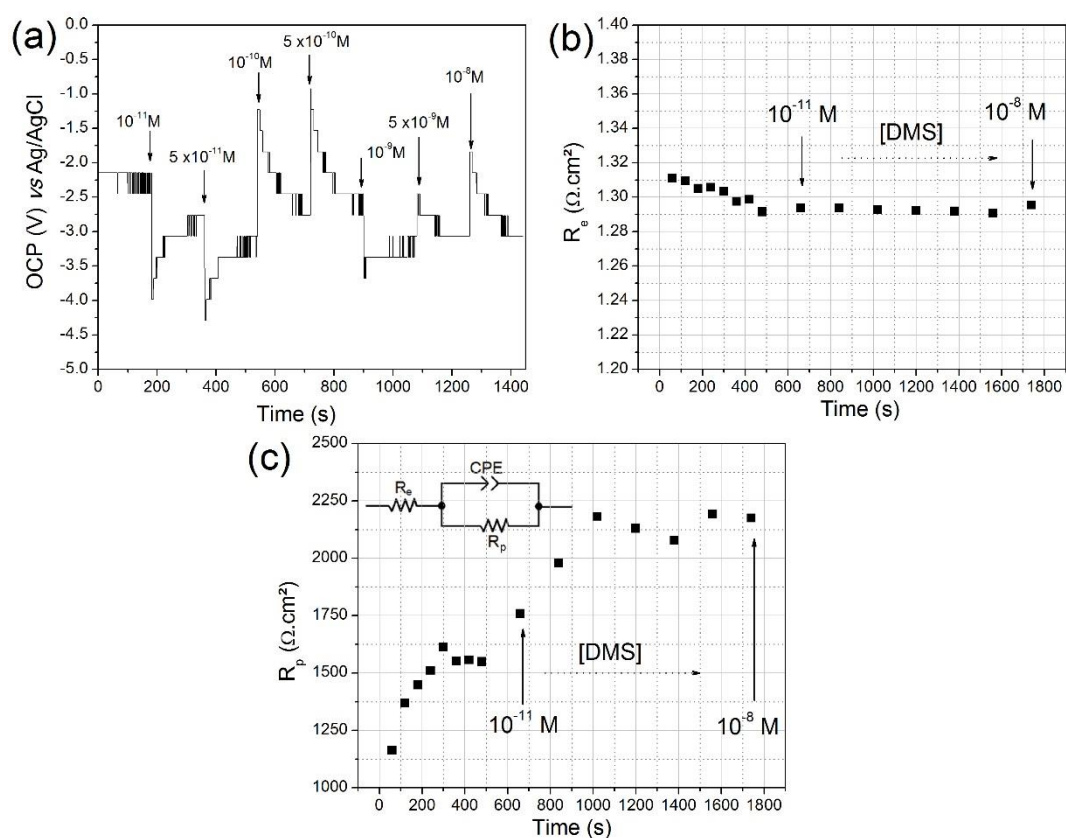


Figure 378 - Evolution of the OCP (a), R_e (b) and R_p (c) of the sensor due to the exposure to DMS from 1.0×10^{-11} M to 1.0×10^{-8} M in simulated ocean water

Despite the R_p output signal was not linear towards the concentration of DMS in the simulated ocean water, an evident increase of the resistance took place in the sensor as a response to the detection of the molecule, presenting a positive variation (at 1.0×10^{-11} M) of 13.5% in relation to the bare previous condition. The non-linearity

possibly arises from the fact that DMS is a volatile compound and, thus, the molecules could not be located close to the interface with the transducer surface during the whole measurement, diminishing the amount of detectable analyte in the solution. Therefore, the performance of the non-faradaic impedimetric DMS sensor can be further enhanced by ameliorating the gas confinement in the electrochemical cell as well as by the detection of the analyte in the vapour phase.

8.5 CONCLUSIONS

An impedimetric sensor for the detection of DMS was reported. The sensor was prepared by deposition of gold particles on a working electrode of a commercial screen-printed electrode. The proposed sensor is advantageous over traditional devices reported in the literature, mainly owing to the simplicity of fabrication, low cost, sensitivity and short time required for measurement (3 minutes). This sensor showed linear detection range for DMS from 1.0×10^{-10} to 1.0×10^{-8} M in aqueous solution with a LOD of 1.50×10^{-9} M and LOQ equal to 2.27×10^{-9} M. CV and EIS results showed that the sensor was reusable after simple acidic treatment with sulfuric acid, which leads the regenerated sensor to present an electrochemical response very similar to the bare condition. The online monitoring of the impedance of the sensor in simulated ocean water indicated that the gold transducer is stable in this medium and it could be used as a non-faradaic device to detect DMS. The real-time EIS measurement indicated that the sensor is a promising tool to detect DMS in ocean water, condition that simulates its real working environment, despite it did not present a linear response towards the analyte concentration.

8.6 REFERENCES

[1] MALIN, G; ERST, G.O. Algal production of dimethyl sulfide and its atmospheric role1. **Journal of Phycology**, 33(6): p. 889-896, 1997.

- [2] ANDREAE, M. O.; ANDREAE, T. W.; MEYERKS, D.; THIEL, C. Marine sulfur cycling and the atmospheric aerosol over the springtime North Atlantic. **Chemosphere**, 52(8): p. 1321-1343, 2003.
- [3] GIORDANO, M.; NORICI, A.; HELL, R. Sulfur and phytoplankton: acquisition, metabolism and impact on the environment. **New Phytologist**, 166(2): p. 371-382, 2005.
- [4] HOWARD, E. C.; HENRIKSEN, J. R.; BUCHAN, A.; REISCH, C. R.; BÜRGMANN, H.; WELSH, R.; YE, W.; GONZÁLEZ, J. M.; MACE, K.; JOYE, S. B.; KIENE, R. P.; WHITMAN, W. B.; MORAN, M. A. Bacterial Taxa That Limit Sulfur Flux from the Ocean. **Science**, 314(5799): p. 649-652, 2006.
- [5] CHARLSON, R. J.; LOVELOCK, J. E.; MEINRAT, O. A.; WARREN, S. G. Oceanic phytoplankton, atmospheric sulphur, cloud albedo and climate. **Nature**, 326(6114): p. 655-661, 1987.
- [6] LOVELOCK, J. E.; MAGGS, R. J.; RASMUSSEN, R. A. Atmospheric Dimethyl Sulphide and the Natural Sulphur Cycle. **Nature**, 237(5356): p. 452-453, 1972.
- [7] BENTLEY, R.; CHASTEEN, T. G. Environmental VOSCs—formation and degradation of dimethyl sulfide, methanethiol and related materials. **Chemosphere**, 55(3): p. 291-317, 2004.
- [8] ANDREAE, M. O. Ocean-atmosphere interactions in the global biogeochemical sulfur cycle. **Marine Chemistry**, 30: p. 1-29, 1990.
- [9] JOHNSTON, A. W. B.; GREEN, R. T.; TODD, J. D. Enzymatic breakage of dimethylsulfoniopropionate—a signature molecule for life at sea. **Current Opinion in Chemical Biology**, 31: p. 58-65, 2016.
- [10] ALBRECHT, B. A. Aerosols, Cloud Microphysics, and Fractional Cloudiness. **Science**, 245(4923): p. 1227-1230, 1989.
- [11] STEFELS, J. Physiological aspects of the production and conversion of DMSP in marine algae and higher plants. **Journal of Sea Research**, 43(3): p. 183-197, 2000.
- [12] SUNDA, W.; KIEBER, D. J.; KIENE, R. P.; HUNTSMAN, S. An antioxidant function for DMSP and DMS in marine algae. **Nature**, 418(6895): p. 317-320, 2002.
- [13] GAGE, D. A.; RHODES, D.; NOLTE, K. D.; HICKS, W. A.; LEUSTEK, T.; COOPER, A. J.; HANSON, A. D. A new route for synthesis of dimethylsulphoniopropionate in marine algae. **Nature**, 387(6636): p. 891-894, 1997.
- [14] ALCOLOMBRI, U.; BEN-DOR, S.; FELDMESSER, E.; LEVIN, Y.; TAWFIK, D. S.; VARDI, A. Identification of the algal dimethyl sulfide-releasing enzyme: A missing link in the marine sulfur cycle. **Science**, 348(6242): p. 1466-1469, 2015.

- [15] CARRIÓN, O.; PRATSCHER, J.; CURSON, A. R. J.; WILLIAMS, B. T.; ROSTANT, W. G.; MURRELL, J. C.; TODD, J. D. Methanethiol-dependent dimethylsulfide production in soil environments. **The ISME Journal**, 11(10): p. 2379-2390, 2017.
- [16] LIN, Y. S.; HEUER, V. B.; FERDELMAN, T. G.; HINRICHS, K. –U. Microbial conversion of inorganic carbon to dimethyl sulfide in anoxic lake sediment (Plußsee, Germany). **Biogeosciences**, 7(8): p. 2433-2444, 2010.
- [17] HABERHAUER-TROYER, C.; ROSENBERG, E.; GRASSERBAUER, M. Evaluation of solid-phase microextraction for sampling of volatile organic sulfur compounds in air for subsequent gas chromatographic analysis with atomic emission detection. **Journal of Chromatography A**, 848(1): p. 305-315, 1999.
- [18] KHAN, M. A. H.; WHELAN, M. E.; RHEW, R. C. Analysis of low concentration reduced sulfur compounds (RSCs) in air: Storage issues and measurement by gas chromatography with sulfur chemiluminescence detection. **Talanta**, 88: p. 581-586, 2012.
- [19] MESTRES, M.; BUSTO, O.; GUASCH, J. Headspace solid-phase microextraction analysis of volatile sulphides and disulphides in wine aroma. **Journal of Chromatography A**, 808(1): p. 211-218, 1998.
- [20] IYADOMI, S.; EZOE, K.; OHIRA, S.; TODA, K. Monitoring variations of dimethyl sulfide and dimethylsulfoniopropionate in seawater and the atmosphere based on sequential vapor generation and ion molecule reaction mass spectrometry. **Environmental Science: Processes & Impacts**, 18(4): p. 464-472, 2016.
- [21] SAID-AHMAD, W.; AMRANI, A. A sensitive method for the sulfur isotope analysis of dimethyl sulfide and dimethylsulfoniopropionate in seawater. **Rapid Communications in Mass Spectrometry**, 27(24): p. 2789-2796, 2013.
- [22] WANG, B.; SIVRET, E. C.; PARCSI, G.; STUETZ, R. M. Determination of VOSCs in sewer headspace air using TD–GC–SCD. **Talanta**, 137: p. 71-79, 2015.
- [23] NAGAHATA, T.; KAJIWARA, H.; OHIRA, S.; TODA, K. Simple Field Device for Measurement of Dimethyl Sulfide and Dimethylsulfoniopropionate in Natural Waters, Based on Vapor Generation and Chemiluminescence Detection. **Analytical Chemistry**, 85(9): p. 4461-4467, 2013.
- [24] ZHANG, M.; CHEN, L. Continuous underway measurements of dimethyl sulfide in seawater by purge and trap gas chromatography coupled with pulsed flame photometric detection. **Marine Chemistry**, 174: p. 67-72, 2015.
- [25] RAMOS, R. M.; BRANDÃO, P. F.; GONÇALVES, L. M.; VYSKOČIL, V.; RODRIGUES, J. A. Electrochemical sensing of total sulphites in beer using non-modified screen-printed carbon electrodes. **Journal of the Institute of Brewing**, 123(1): p. 45-48, 2017.

- [26] LEE, J.; HUSSAIN, G.; BANKS, C. E.; SILVESTER, D. S. Screen-Printed Graphite Electrodes as Low-Cost Devices for Oxygen Gas Detection in Room-Temperature Ionic Liquids. **Sensors**, 17(12): p. 2734, 2017.
- [27] YAMANAKA, K.; VESTERGAARD, M. D. C.; TAMIYA, E. Printable Electrochemical Biosensors: A Focus on Screen-Printed Electrodes and Their Application. **Sensors**, 16(10): p. 1761, 2016.
- [28] VASILESCU, A.; NUNES, G.; HAYAT, A.; LATIF, U.; MARTY, J. L. Electrochemical Affinity Biosensors Based on Disposable Screen-Printed Electrodes for Detection of Food Allergens. **Sensors**, 16(11): p. 1863, 2016.
- [29] AYAGOU, M. D. D.; TRAN, T. T. M.; TRIBOLLET, B.; KITTEL, J.; SUTTER, E.; FERRANDO, N.; MENDIBIDE, C.; DURET-THUAL, C. Electrochemical impedance spectroscopy of iron corrosion in H₂S solutions. **Electrochimica Acta**, 282: p. 775-783, 2018.
- [30] ZHANG, G. A.; ZHENG, Y.; GUO, X. P.; JIANG, F.; SHI, D. Y.; CHEN, Z. Y. Electrochemical corrosion behavior of carbon steel under dynamic high pressure H₂S/CO₂ environment. **Corrosion Science**, 65: p. 37-47, 2012.
- [31] ZHANG, G. A.; LIU, D.; LI, Y. Z.; GUO, X. P. Corrosion behaviour of N80 carbon steel in formation water under dynamic supercritical CO₂ condition. **Corrosion Science**, 120: p. 107-120, 2017.
- [32] PRAJITNO, D. H.; UMAR, E.; SYARIF, D. G. Application Electrochemical Impedance Spectroscopy Methods to Evaluation Corrosion Behavior of Stainless steels 304 in Nanofluids Media. **Journal of Physics: Conference Series**, 799: p. 012007, 2017.
- [33] NISHIKATA, A.; ICHIHARA, Y.; TSURU, T. An application of electrochemical impedance spectroscopy to atmospheric corrosion study. **Corrosion Science**, 37, p. 897-911, 1995.
- [34] MAJCHRZYCKI, W.; JANKOWSKA, E.; BARANIAK, M.; HANDZLIK, P.; SAMBORSKI, R. Electrochemical Impedance Spectroscopy and Determination of the Internal Resistance as a Way to Estimate Lead-Acid Batteries Condition. **Batteries**, 4(4): p. 70, 2018.
- [35] MURBACH, M. D.; SCHWARTZ, D. T. Analysis of Li-Ion Battery Electrochemical Impedance Spectroscopy Data: An Easy-to-Implement Approach for Physics-Based Parameter Estimation Using an Open-Source Tool. **Journal of The Electrochemical Society**, 165(2): p. A297-A304, 2018.
- [36] JIANG, J.; LIN, Z.; JU, Q.; MA, Z.; ZHENG, C.; WANG, Z.; Electrochemical Impedance Spectra for Lithium-ion Battery Ageing Considering the Rate of Discharge Ability. **Energy Procedia**, 105: p. 844-849, 2017.

- [37] GRUDEN, R.; BUCHHOLZ, A.; KANOUN, O. Electrochemical analysis of water and suds by impedance spectroscopy and cyclic voltammetry. **Journal of Sensors and Sensor Systems**, 3, p. 133-140, 2014.
- [38] CARON, W. -O.; LAMHAMEDI, M. S.; VIENS, J.; MESSADDEQ, Y. Practical Application of Electrochemical Nitrate Sensor under Laboratory and Forest Nursery Conditions. **Sensors**, 16(8): p. 1190, 2016.
- [39] GHAFFARI, S. A.; CARON, W. O.; LOUBIER, M.; RIOUX, M.; VIENS, J.; GOSSELIN, B.; MESSADDEQ, Y. A Wireless Multi-Sensor Dielectric Impedance Spectroscopy Platform. **Sensors**, 15(9): p. 23572-23588, 2015.
- [40] BOUMYA, W.; LAGHRIB, F.; LAHRICH, S.; FARAHI, A.; ACHAK, M.; BAKASSE, M.; EL MHAMMEDI, M. A.. Electrochemical impedance spectroscopy measurements for determination of derivatized aldehydes in several matrices. **Heliyon**, 3(10): p. e00392, 2017.
- [41] FARIA, R. A. D.; IDEN, H.; BHARUCHA, E.; LINS, V. F. C.; MESSADDEQ, Y.; MATENCIO, T.; HENEINE, L. G. D. A new tool for the detection of horsemeat adulteration in raw meat. **Journal of Biosensors and Bioelectronics**, 9, p. 1-7, 2018.
- [42] FARIA, R. A. D.; LINS, V. F. C.; NAPPI, G. U.; MATENCIO, T.; HENEINE, L. G. D. Development of an impedimetric immunosensor for specific detection of snake venom. **BioNanoScience**, 8, p. 988-996, 2018.
- [43] FARIA, R. A. D.; IDEN, H.; HENEINE, L. G. D.; MATENCIO, T.; MESSADDEQ, Y. Non-enzymatic impedimetric sensor based on 3-aminophenylboronic acid functionalized screen-printed carbon electrode for highly sensitive glucose detection. **Sensors**, 19, p. 1686, 2019.
- [44] ASTM D1141-98. **Standard Practice for the Preparation of Substitute Ocean Water**, 2013.
- [45] FARIA, R. A. D.; HENEINE, L. G. D.; MATENCIO, T.; MESSADDEQ, Y. Faradaic and non-faradaic electrochemical impedance spectroscopy as transduction techniques for sensing applications. **International Journal of Biosensors and Bioelectronics**, 5(1), p. 29-31, 2019.
- [46] NGUY, T. P.; PHI, T. V.; TRAM, D. T. N.; EERSELS, K.; WAGNER, P.; LIEN, T. T. N. Development of an impedimetric sensor for the label-free detection of the amino acid sarcosine with molecularly imprinted polymer receptors. **Sensors and Actuators B**, 246:461-470, 2017.
- [47] YAGATI, A. K.; PYUN, J. -C.; MIN, J.; CHO, S. Label-free and direct detection of C-reactive protein using reduced graphene oxide-nanoparticle hybrid impedimetric sensor. **Bioelectrochemistry**, 107, p. 37-44, 2016.

[48] IUPAC. **Compendium of Chemical Terminology**, 2nd ed.; the “Gold Book”; Blackwell Scientific Publications: Oxford, UK, ISBN 0-9678550-9-8, 1997.

[49] DIOUANI, M. F.; OUERGHI, O.; REFAI, A.; BELGACEM, K.; TLILI, C.; LAOUINI, D.; ESSAFI, M. Detection of ESAT-6 by a label free miniature immuno-electrochemical biosensor as a diagnostic tool for tuberculosis. **Materials Science and Engineering: C**, 74, p. 465–470, 2017.

[50] SÁENZ, H. S. C.; HERNÁNDEZ-SARAVIA, L. P.; SELVA, J. S. G.; SUKERI, A.; ESPINOZA-MONTERO, P. J.; BERTOTTI, M. Electrochemical dopamine sensor using a nanoporous gold microelectrode: a proof-of-concept study for the detection of dopamine release by scanning electrochemical microscopy. **Microchimica Acta**, 185(8), 2018.

[51] TRAN, V. -K.; KO, E.; GENG, Y.; KIM, M. K.; JIN, G. H.; SON, S. E.; HUR, W.; SEONG, G. H. Micro-patterning of single-walled carbon nanotubes and its surface modification with gold nanoparticles for electrochemical paper-based non-enzymatic glucose sensor. **Journal of Electroanalytical Chemistry**, 826, p. 29-37, 2018.

[52] NAJARZADEKAN, H.; SERESHTI, H. Transparent Polycaprolactam Electrospun Nanofibers Doped with 1,10-phenanthroline Optical Sensor for Colorimetric Determination of Iron (II) and Vitamin C. **Fibers and Polymers**, 19(10), p. 2149–2156, 2018.

[53] TALEUZZAMAN, M. Limit of Blank (LOD), Limit of Detection (LOD) and Limit of Quantification (LOQ). **Organic and Medical Chemistry**, 7(5), 2018.

[54] SHRIVASTAVA, A.; GUPTA, V.B. Methods for the determination of limit of detection and limit of quantitation of the analytical methods. **Chronicles of young scientists**, 2(1), 2011.

[55] RIBEIRO, F. A. L.; FERREIRA, M. M. C. Planilha de validação: uma nova ferramenta para estimar figuras de mérito na validação de métodos analíticos univariados. **Química Nova**, 31(1), p. 164-171, 2008.

[56] VISWANADHAM R.; BHARATHI, M. D.; SARMA, V. V. S. S. Variation in concentrations and fluxes of dimethylsulphide (DMS) from the indian estuaries. **Estuaries and Coasts**, 39(3), p. 695-706, 2016.

[57] WU, X.; TAN, T.; LIU, C.; LI, T.; LIU, X.; YANG, G. Distributions and Relationships of CO₂, O₂, and Dimethylsulfide in the Changjiang (Yangtze) Estuary and Its Adjacent Waters in Summer. **Journal of Ocean University of China**, 17(2), p. 320–334, 2018.

[58] SHEN, P. -P.; TANG, Y. -N.; LIU, H. -J.; LI, G.; WANG, Y.; QI, Y. -Z. Dimethylsulfide and dimethylsulfoniopropionate production along coastal waters of the northern South China Sea. **Continental Shelf Research**, 117, p. 118–125, 2016.

- [59] LI, J.; LUO, G.; DU, Z.; MA, Y. Hollow waveguide enhanced dimethyl sulfide sensor based on a 3.3 μm interband cascade laser. **Sensors and Actuators B: Chemical**, 255, p. 3550-3557, 2018.
- [60] WANG, S.; DU, Z.; YUAN, L.; MA, Y.; WANG, X.; HAN, R.; MENG, S. Measurement of Atmospheric Dimethyl Sulfide with a Distributed Feedback Interband Cascade Laser. **Sensors** 18, p. 3216, 2018
- [61] SAITO, H.; HASHIMOTO, Y.; MINAMIDE, T.; KON, T.; TOMA, K.; ARAKAWA, T.; MITSUBAYASHI, K. Fiber optic biosniffer (biochemical gas sensor) for gaseous dimethyl sulfide. **Sensors and Materials**, 28(12), p. 1295-1301, 2016.
- [62] SUCHORSKA-WOŹNIAK, P.; NAWROT, W.; RAC, O.; FIEDOT, M.; TETERYCZ, H. Improving the sensitivity of the ZnO gas sensor to dimethyl sulfide. **IOP Conference Series: Materials Science and Engineering** 104, 2015.
- [63] KUMAR, P.; MOHANTY, S. K.; GURUSWAMY, S.; SMITH, Y. R.; MISRA, M. Detection of food decay products using functionalized one-dimensional titania nanotubular arrays. **IEEE Sensors Letters** 1, p. 1-4, 2017.
- [64] LI, Y.; ZHOU, F.; GAO, L.; DUAN, G. Co_3O_4 nanosheet-built hollow spheres containing ultrafine neck-connected grains templated by PS@Co-LDH and their ppb-level gas-sensing performance **Sensors and Actuators B: Chemical** 261, p. 553-565, 2018.
- [65] Y. LONG, Y. WANG, Y. CHENG, X. YANG, K. YU, J. LI, X. DU, X. TANG, Y. JIANG. Detection of volatile organosulfur compounds by hydrogen-bond acidic polymer: A combined experimental and theoretical study. **Materials Letters** 237, p. 282-285, 2019.
- [66] FISCHER, L. M.; TENJE, M.; HEISKANEN, A. R.; MASUDA, N.; CASTILLO, J.; BENTIEN, A.; BOISEN, A. Gold cleaning methods for electrochemical detection applications. **Microelectronic Engineering**, 86(4-6), p. 1282–1285, 2009.

CHAPTER 9 – GENERAL CONCLUSIONS AND FUTURE PERSPECTIVES

9.1 THESIS FINDINGS AND SUGGESTIONS FOR FUTURE WORKS

Besides the theoretical aspects of sensing sciences with special emphasis on the EIS technique as transduction technique, several possible applications of SPCE-based devices were raised in this thesis. The main advantages of SPCEs are their small dimensions, relative low cost due to the ease industrial fabrication and the easiness of functionalization to obtain diverse (bio)sensors. Furthermore, results presented in the Chapter 2 revealed that SPCEs are suitable for use in impedimetric sensors because of their electrochemical properties. Despite of the low electron transfer kinetics at the interface with the electrolytes, the electro activity of the SPCEs (arising from graphite flakes dispersed in the ink carbon matrix) could be enhanced by an electrochemical pretreatment in an aqueous solution of H_2SO_4 . Exposed to electrolytes that simulate the faradaic and non-faradaic transduction modes of EIS, the SPCEs exhibited different corrosion mechanisms, but were electrochemically stable under both conditions.

Because it groups so important features, SPCEs have found a crucial role in the field of (bio)sensors. Amongst the main applications, the food analysis, medical diagnosis and environmental monitoring merit particular attention due to the increasing number of publications especially in the last two decades, a reflex of the unquestionable relevance of these issues. Within this context, three representative applications were elucidated in this thesis: the detection of food fraud (Chapter 6) by means of the recognition of horse serum as well as the detections of glucose (Chapter 7) and DMS (Chapter 8).

With different transduction modes (faradaic and non-faradaic) and functionalization mechanisms, all fabricated (bio)sensors described in this thesis consisted of a SPCE as a transducer substrate and detected the target analytes by means of the EIS technique. In common, the produced impedimetric (bio)sensors exhibited high sensitivity with low LODs, good selectivity towards their analytes, linear responses and low response times, corroborating each device's suitability for application in its respective field of interest.

The faradaic immunosensor produced to recognize horsemeat adulteration was capable to detect the presence of horse antibodies in a buffered solution at a concentration range from 1 pg.mL^{-1} to $1 \text{ }\mu\text{g.mL}^{-1}$ after an incubation period of 20 min. Contrary, the same device presented a random and low analytical signal towards bovine and swine sera at the same concentrations. When exposed to buffered solutions containing real commercial horsemeat, beef and pork, the same trend was observed: the fabricated immunosensor was not sensitive to the heterologous genera. Moreover, with a LOD of only 0.004% w/v, the device proved to be a promising tool for this application, once according to the Food Standards Agency, at concentrations lower than 0.1% w/v, one can assume fraud absence.

In Chapter 7, the increasing variation of R_{ct} indicated that the non-enzymatic faradaic sensor was sensitive exclusively to glucose even at the minimum tested concentration. Other sugars (fructose and sucrose) did not significantly affected the analytical signal of the sensor. The presence of 3-aminophenyl boronic acid as a unit of recognition set this sensor as a competitive technology among several others reported in the current literature. Combined to the low LOD ($8.53 \times 10^{-9} \text{ M}$), the presented sensor possessed as main advantages its simple functionalization and the absence of enzymes, which makes other sensors less stable and more expensive. Besides, the reported results confirmed the robustness of the device, which presented good repeatability and was sensitive to glucose even in the presence of serum, dopamine and NaCl as interfering species. Optimization tests indicated that it is possible to detect the presence of the analyte at 1 Hz in only $4.0 \pm 0.6 \text{ s}$.

Finally, the reusable DMS sensor reported in Chapter 8 was sensitive to the analyte in both faradaic and non-faradaic modes. The higher was the concentration at which DMS (aqueous solution) was in contact with the gold nanoparticles of the functionalized SPCE, the higher was its R_{ct} because of the interactions between sulfur and gold at the electrode, exposing the insulating $-\text{CH}_3$ groups with important steric effect. This sensor presented a LOD equal to $1.50 \times 10^{-9} \text{ M}$, which is compatible to the real application since DMS is usually present in marine environments at nanomolar levels. When DMS was diluted in artificial ocean water, the sensor exhibited non-faradaic response in each 3 min towards this analyte at concentrations varying from 10^{-11} M to 10^{-8} M . Although the impedimetric response

under this last condition was not linear, the reported real-time performance reiterates how amenable this sensor can be for real *in situ* operation.

In future researches, there are some aspects to be further exploited and improved regarding the presented (bio)sensors. In summary, more interfering species representative of each aimed application should be tested in order to ensure the sensors definitely do not suffer non-expected unspecific reactions. The stability along several weeks should be studied in different storage media to make the sensors more amenable for commercialization. In this same direction, since the real market demands more portable and accurate technologies, it would be equally important to undertake more numerous tests in order to evaluate the statistical significance of the analytical responses. Thus, one should consider performing the tests not only at optimal laboratorial atmosphere such as that described in this thesis, but also under different temperature and humidity conditions. Nonetheless, it would be also interesting to make the sensors more automatic by means of the development of algorithms to calculate the R_{ct} or other impedance parameter (extracted from the known equivalents circuits) as a function of the analyte concentration.

Specifically to the horsemeat immunosensor, some tests could be addressed with solutions containing different proportions of different meats. The study of the capability of the device to recognize the target analyte in cooked meat would also represent an important step towards the validation of the technology.

With respect to the glucose sensor, it is relevant to better understand the detailed mechanism of interaction of the 3-aminophenyl boronic molecule with the sugar. Thus, it would be possible to comprehend the precise reason for which the device suffered such a low response towards fructose and to enhance its selectivity in relation to other interfering molecules.

Regarding the DMS sensor, it is worthy notable the necessity to perform selectivity tests with other gases or other several organic compounds present in the same marine environment. The development of a biosensor in this case could be interesting to avoid cross-reactions, diminishing the interference of undesirable species in the device's response. Performing tests with DMS in vapor phase could also contribute to improving the sensor's specificity.

9.2 RESULTADOS DA TESE E SUGESTÕES PARA TRABALHOS FUTUROS

Além dos aspectos teóricos da ciência de sensores com ênfase especial para a EIS como técnica de transdução, várias possibilidades de aplicações dos dispositivos baseados em EICs foram abordadas nesta tese. As principais vantagens dos EICs são suas pequenas dimensões, o custo relativamente baixo devido à facilidade de produção industrial e a facilidade de funcionalização para a obtenção de diversos (bios)sensores. Ainda, os resultados apresentados no Capítulo 2 revelaram que os EICs são aplicáveis ao uso em sensores impedimétricos por causa de suas propriedades eletroquímicas. Apesar da lenta cinética de transferência de elétrons na interface com os eletrólitos, a eletroatividade dos EICs (proveniente das estruturas de grafite dispersas na matriz de tinta de carbono) pôde ser melhorada por meio de um pré-tratamento eletroquímico em solução aquosa de H_2SO_4 . Expostos a eletrólitos que simulam os modos de transdução faradaico e não-faradaico da EIE, os EICs exibiram diferentes mecanismos de corrosão, mas foram eletroquimicamente estáveis sob ambas as condições.

Porque reúnem tão importantes características, os EICs tem encontrado um papel crucial no campo de (bios)sensores. Entre as principais aplicações, as análises de alimentos, os diagnósticos médicos e o monitoramento ambiental merecem particular atenção devido ao crescente número de publicações especialmente nas últimas duas décadas, um reflexo da inquestionável relevância desses temas. Neste contexto, três representativas aplicações foram elucidadas nesta tese: a detecção de fraude alimentar (Capítulo 6) a partir do reconhecimento de soro de cavalo, bem como as detecções de glicose (Capítulo 7) e de DMS (Capítulo 8).

Com diferentes modos de transdução (faradaico e não-faradaico) e mecanismos de funcionalização, todos os (bios)sensores fabricados descritos nesta tese consistiram de um EIC como substrato transdutor e detectaram os analitos de interesse a partir da técnica de EIE. Em comum, os (bios)sensores impedimétricos exibiram alta sensibilidade com baixos LD, boa seletividade diante de seus analitos, respostas lineares e baixos tempos de resposta, corroborando a aplicabilidade de cada dispositivo para seu respectivo campo de interesse.

O imunossensor faradaico produzido para reconhecer adulteração por carne de cavalo foi capaz de detectar a presença de anticorpos equinos em solução tampão em uma faixa de concentrações de 1 pg.mL^{-1} a $1 \text{ } \mu\text{g.mL}^{-1}$ após um período de incubação de 20 min. Contrariamente, o mesmo dispositivo apresentou sinal analítico baixo e aleatório diante de soros bovino e suíno nas mesmas concentrações. Quando exposto às soluções tamponadas de carnes comerciais reais de cavalo, boi e porco, a mesma tendência foi observada: o imunossensor fabricado não foi sensível aos gêneros heterólogos. Além disso, com um LD de apenas 0,004% m/v, o dispositivo provou ser uma ferramenta promissora para essa aplicação, uma vez que de acordo com a *Food Standards Agency*, a concentrações menores que 0,1% m/v, pode-se assumir a ausência de fraude.

No Capítulo 7, a crescente variação da R_{tc} indicou que o sensor faradaico não-enzimático foi sensível exclusivamente a glicose mesmo na menor concentração testada. Outros açúcares (frutose e sacarose) não afetaram significativamente o sinal analítico do sensor. A presença de ácido 3-aminofenil borônico como unidade de reconhecimento colocou o sensor como uma tecnologia competitiva diante de várias outras reportadas na literatura recente. Combinado ao baixo LD ($8,53 \times 10^{-9}$ M), o sensor apresentado possuiu como principais vantagens sua funcionalização simples e a ausência de enzimas, o que torna outros sensores menos estáveis e mais caros. Além disso, os resultados apresentados confirmaram a robustez do dispositivo, que apresentou boa repetibilidade e foi sensível a glicose mesmo na presença de soro, dopamina e NaCl como espécies interferentes. Testes de otimização indicaram que é possível detectar a presença do analito a 1 Hz em apenas $4,0 \pm 0,6$ s.

Finalmente, o sensor reutilizável de DMS apresentado no Capítulo 8 foi sensível ao analito em ambos os modos faradaico e não-faradaico. Quanto maior foi a concentração na qual o DMS (solução aquosa) foi posto em contato com as nano partículas de ouro do EIC funcionalizado, maior foi sua R_{tc} por causa das interações entre enxofre e ouro no eletrodo, expondo os grupos $-\text{CH}_3$ com importante impedimento estérico. O sensor apresentou LD igual a $1,50 \times 10^{-9}$ M, o que é compatível com sua real aplicação uma vez que o DMS está usualmente presente nos ambientes marinhos a concentrações nanomolares. Quando DMS foi diluído em

água do mar artificial, a cada 3 min o sensor exibiu resposta não-faradaica ao seu analito em concentrações variando de 10^{-11} M a 10^{-8} M. Embora a resposta impedimétrica nessa última condição tenha sido não linear, o desempenho apresentado em tempo real reitera quão aplicável esse sensor pode ser para reais aplicações em campo.

Em pesquisas futuras, existem alguns aspectos a serem mais explorados e aprimorados em relação aos (bios)sensores apresentados. Em resumo, mais espécies interferentes representativas de cada aplicação pretendida devem ser testadas para garantir que os sensores definitivamente não sofram reações inespecíficas não esperadas. A estabilidade ao longo de várias semanas deve ser estudada em diferentes meios de armazenamento para tornar os sensores mais aplicáveis à comercialização. Nessa mesma direção, como o mercado real exige tecnologias mais portáteis e precisas, seria igualmente importante realizar mais testes para avaliar a significância estatística das respostas analíticas. Assim, deve-se considerar a realização dos testes não apenas em atmosfera laboratorial ideal, como aquela descrita nesta tese, mas também sob diferentes condições de temperatura e umidade. Não obstante, também seria interessante tornar os sensores mais automáticos por meio do desenvolvimento de algoritmos para calcular a R_{tc} ou outro parâmetro de impedância (extraído dos circuitos equivalentes conhecidos) em função da concentração do analito.

Especificamente para o imunossensor de carne de cavalo, alguns testes podem ser realizados com soluções contendo proporções variadas de diferentes carnes. O estudo da capacidade do dispositivo de reconhecer o analito alvo em carne cozida também representaria um passo importante para a validação da tecnologia.

No que diz respeito ao sensor de glicose, é relevante entender melhor o mecanismo detalhado de interação da molécula de ácido 3-aminofenil borônico com o açúcar. Assim, seria possível compreender a razão exata pela qual o dispositivo sofreu uma resposta tão baixa em relação à frutose e aumentar sua seletividade em relação a outras moléculas interferentes.

No que diz respeito ao sensor de DMS, é notável a necessidade de se realizar testes de seletividade com outros gases ou outros compostos orgânicos presentes no mesmo ambiente marinho. O desenvolvimento de um biossensor nesse caso pode

ser interessante para evitar reações cruzadas, diminuindo a interferência de espécies indesejáveis na resposta do dispositivo. A realização de testes com DMS em fase vapor também pode contribuir para melhorar a especificidade do sensor.